Strål
säkerhets
myndigheten
Swedish Radiation Safety Authority

Author: Lars Olof Jernkvist

2017:12

Computational assessment of LOCA simulation tests on high burnup fuel rods in Halden and Studsvik

Report number: 2017:12 ISSN: 2000-0456
Available at www.stralsakerhetsmyndigheten.se

SSM perspective

Background

Loss of Coolant Accidents (LOCA) are among the most demanding accidents that can happen in a Light Water Reactor (LWR). The lack of cooling and the drop in pressure impose large stresses on the nuclear fuel which would increase the risk of fuel rod damage and the subsequent release of active material. But LOCA is also an accident that the nuclear power plant is designed to withstand with a limited release of radioactivity to the surroundings.

Resent research has shown that nuclear fuel that has been irradiated to high burnup can fail at lower temperatures than prescribed by current design criteria. One benign phenomenon is the fragementation of pellets and axial relocation of fuel fragments. Fuel fragments that move within the rod can accumulate at positions where the cladding is strained and cause an increased load there. Models that describes fuel fragmentation and relocation and enable analysis including those phenomena has been developed by Quantum Technologies AB and implemented in FRAPTRAN-1.5 (see SSM report 2015:37).

Objective

This report describes the validation of the models against tests performed in Halden and in Studsvik, the latter commissioned by NRC. The objective for SSM in this project is to gain insight into the course of events in a LOCA and how these can be implemented in analytical tools.

Results and conclusion

The comparisons between analysis and tests in this report show good agreement and improvement of the calculations when using the fragmentation and relocation models. The results indicate that without modeling fuel relocation there can be a significant underestimation of cladding temperature and local oxidation in case of a cladding damage. This implies that there is a need to include fuel fragmentation in analytical verification of high burnup nuclear fuel in LOCA.

The present work also identifies needs for further development of the analytical tools, for example; failure criteria, fragmentation mechanisms including constraint from the cladding and mechanical effects from fission gases. This development in turn needs further data from tests on nuclear fuel, both for the development and for the validation of the new models.

Project information

Contact person SSM: Anna Alvestav
Reference: SSM2015-3357

Strål
säkerhets
myndigheten
Swedish Radiation Safety Authority

Author: Lars Olof Jernkvist
Quantum Technologies AB, Uppsala Science Park

2017:12

Computational assessment of LOCA simulation tests on high burnup fuel rods in Halden and Studsvik

Date: March 2016
Report number: 2017:12 **ISSN:** 2000-0456
Available at www.stralsakerhetsmyndigheten.se

This report concerns a study which has been conducted for the Swedish Radiation Safety Authority, SSM. The conclusions and viewpoints presented in the report are those of the author/authors and do not necessarily coincide with those of the SSM.

SSM 2017:12

Computational assessment of LOCA simulation tests on high burnup fuel rods in Halden and Studsvik

Report TR15-004, April 15, 2016

Lars Olof Jernkvist

Quantum Technologies AB

SSM 2017:12

Contents

Appendices

Summary

In this work, computer analyses are used to assess five recent loss-of-coolant-accident (LOCA) simulation experiments, carried out in Halden, Norway, and Studsvik, Sweden. The experiments were done on short test rodlets that had been sampled from high burnup fuel rods after discharge from commercial light water reactors. The main objectives of the work are to gain understanding of the thermal-mechanical behaviour of high burnup fuel under LOCA by making interpretations of the test results, to elucidate differences between the Halden and Studsvik experiments with regard to testing conditions, to assess the transferability of the test results to real light water reactor conditions, and to validate newly developed computational models for high burnup fuel fragmentation and axial relocation that have been implemented in an extended version of the FRAP-TRAN-1.5 computer program.

Key results of the experiments, such as cladding tube temperatures and deformations, are reproduced with fair accuracy in the computer simulations, which indicates that most of the involved phenomena are understood and adequately modelled. Important exceptions are the fine fragmentation (pulverization) of the high burnup fuel, with associated release of gaseous fission products, and the restricted axial gas flow within the fuel rods.

The newly developed models for axial fuel relocation successfully reproduce the observed relocation and the thermal effects that it brings about by redistributing the fuel rod heat load. Our simulations suggest that axial fuel relocation takes place concurrently with cladding ballooning and that the thermal feedback effects from the relocation are strong enough to affect the dynamics of cladding ballooning and rupture. For the simulated Halden tests, the axial fuel relocation increases the calculated peak cladding temperature by 25 to 250 K, and high temperature cladding oxidation is aggravated. These aggravating effects of axial fuel relocation are not seen in the Studsvik tests, since they are done without nuclear heating.

The significance of findings from the experiments as well as the computer analyses to the behaviour of full-length fuel rods under conditions expected in light water reactor LOCAs are discussed. Suggestions are also made for future experiments, model improvements and further computational analyses.

Sammanfattning

I detta arbete används datorsimuleringar för att utvärdera fem experiment, avsedda att efterlikna haverifall med kylmedelsförlust (LOCA), vilka nyligen utförts i Halden, Norge, och Studsvik, Sverige. Experimenten utfördes på korta provstavar, vilka tagits från använt högutbränt bränsle från kommersiella lättvattenreaktorer. Arbetets huvudsakliga mål är att skapa fördjupad förståelse för det högutbrända bränslets termomekaniska beteende under LOCA genom att tolka provresultaten, att belysa skillnader i provförhållanden mellan Halden och Studsvik, att bedöma provresultatens överförbarhet till verkliga lättvattenreaktorförhållanden, samt att utvärdera nyligen utvecklade beräkningsmodeller för fragmentering och axiell omflyttning av högutbränt bränsle. Dessa beräkningsmodeller har införts i en utökad version av beräkningsprogrammet FRAPTRAN-1.5.

Nyckelresultat från experimenten, såsom kapslingsrörens temperatur och deformation, reproduceras med godtagbar noggrannhet i datorsimuleringarna, vilket antyder att merparten av de aktiva fenomenen är förstådda och nöjaktigt modellerade. Viktiga undantag utgörs av det högutbrända bränslets fina fragmentering (pulverisering), med tillhörande frigörelse av gasformiga fissionsprodukter, samt begränsningarna i det axiella gasflödet inuti bränslestavarna.

De nyutvecklade modellerna för axiell omflyttning av bränsle reproducerar framgångsrikt den observerade bränsleomflyttningen och de effekter på temperaturen som denna ger upphov till genom att omfördela bränslestavens värmebelastningen. Våra simuleringar antyder att axiell bränsleomflyttning sker samtidigt med att kapslingsrören sväller upp radiellt, och att de termiska återkopplingseffekterna från bränsleomflyttningen är tillräckligt starka för att påverka kapslingsrörens svällnings- och brottförlopp. För de simulerade Haldenproverna medför den axiella bränsleomflyttningen att de beräknade maxtemperaturerna för kapslingen ökar med mellan 25 och 250 K, och att högtemperaturoxidationen av kapslingen förvärras. Dessa försvårande konsekvenser av axiell bränsleomflyttning saknas i Studsvikproverna, då dessa utförs utan nukleär värmning.

Betydelsen av resultaten, såväl från de beaktade experimenten som från datoranalyserna, diskuteras med avseende på beteendet hos hellånga bränslestavar under förhållanden som kan förväntas i lättvattenreaktorer under LOCA. Förslag ges även för framtida experiment, modellförbättringar och fortsatta datoranalyser.

1. Introduction

Loss-of-coolant accidents (LOCAs) in light water reactors (LWRs) may lead to overheating of the fuel rods, which in turn may lead to distension of the internally overpressurized cladding tubes and to loss of cladding ductility by high temperature oxidation of the material. To maintain structural integrity of the fuel and to ensure that the reactor core remains coolable, the cladding temperature and oxidation should not transgress certain limits [1]. These regulatory safety criteria for LOCA are based primarily on experimental studies from the 1970s and 1980s, which were carried out on low burnup fuel of the design and materials of that time. The introduction of new fuel designs, most importantly new cladding materials, and the move to higher discharge burnups have prompted a need to verify that the existing safety criteria remain valid and appropriate. To this end, both separate effect tests and integral LOCA simulation tests have been carried out on modern fuel designs and fuel with high burnup over the last decade. Examples of the latter are the IFA-650 series of in-reactor tests in Halden, Norway [2], the out-of-reactor tests done in Studsvik, Sweden [3], and the recent MIR-LOCA in-reactor test in Dimitrovgrad, Russia [4].

One important finding from these tests is that UO_2 fuel with a pellet average burnup in excess of about 60 MWd(kgU)$^{-1}$ may 'pulverize' into very fine (< 0.2 mm) fragments, when transiently overheated. This kind of very fine fragmentation was not observed in earlier LOCA tests, which were limited to fuel rods with pellet average burnups lower than 35 MWd(kgU)$^{-1}$. The mechanisms responsible for the pulverization are poorly understood, but the prevailing hypothesis is that it occurs by cracking initiated at overpressurized bubbles and pores that contain gaseous fission products [5]. Hence, a critical overpressure in the pores must be reached for pulverization to occur. This means that the material must be sufficiently heated, and that the heating needs to be fairly fast to preclude stress relaxation by creep and slow gas depressurization through connected pathways or re-solution of gas into the material surrounding the pores. Mechanical constraint from the cladding tube, resulting in compressive hydrostatic stress in the fuel pellet, is also known to affect the pulverization [5, 6].

Another conclusion from the aforementioned tests is that the very fine fragments formed by high burnup fuel during LOCA have a higher potential for downward axial relocation within the distending cladding tubes than the fairly large fuel fragments typically observed in early LOCA tests on low to medium burnup fuel. The axial fuel relocation is of safety concern, since it changes the axial distribution of heat load along the fuel rod and also has the potential to increase the amount of fuel material dispersed into the reactor coolant, should the cladding fail [7, 8]. The fuel dispersal is an issue with regard to energetic fuel-coolant interaction, radiological consequences and long-term coolability of the material ejected into the coolant [9].

The increased propensity for fuel fragmentation, relocation and dispersal at high burnup are probably the most important findings from the recent LOCA simulation tests, but some other high burnup effects should also be mentioned. For example, the tests show that release of fission product gases from overheated and pulverized high burnup fuel is extensive, and that the axial flow of gas within the fuel rod may be restricted because of pellet-cladding gap closure that occurs at high burnup. The fission gas behaviour in high burnup fuel rods is thus different than in low burnup rods, and the build-up of axial pressure gradients within high burnup rods may amplify cladding ballooning, axial fuel relocation and fuel dispersal. Another notable high burnup effect is that the oxidation induced embrittlement of the cladding under LOCA is aggravated by hydrogen picked up by the metal during the fuel lifetime [10, 11].

The above findings have prompted revisions of LOCA safety criteria in some countries. At the time of writing, new rules have been proposed in France [12] and in the USA [13]. The rules proposed in the USA are performance based and intended to expand the applicability of the existing safety criteria from fuel designs with uranium dioxide pellets within cylindrical zirconium alloy cladding tubes to any light-water reactor fuel design or cladding material. Experimental programs are running, e.g. within the OECD Halden Reactor Project and phase three of the Studsvik Cladding Integrity Project (SCIP-III), to gain further understanding and to produce quantitative data on the behaviour of high burnup fuel under loss-of-coolant accidents. The Swedish Radiation Safety Authority (SSM) participates in these projects.

Along with the LOCA experiments on high burnup fuel, computational models and computer programs for analyses of LOCA are being modified and refined to capture the experimentally observed phenomena. An example of international cooperation in this field is the IAEA coordinated research project FUMAC – Fuel Modelling in Accident Conditions. This international project, which is running from 2014 to 2017, brings together 27 organisations, including SSM, with a common interest in improving their computational tools [14]. Organisations participating in FUMAC are given access to detailed data on experiments deemed particularly valuable for computer program validation. Another benefit from FUMAC is the possibility to compare models and computational tools used among the participants, and to share knowledge and best practices within the group. A final report on the activities in FUMAC is planned to be issued by the IAEA in 2018. To date, SSM has contributed to the project by developing computational models for axial relocation of fragmented and pulverized fuel pellets in distending fuel rods, including models for the effects on fuel rod heat load that the relocation brings about during LOCA [15-17]. The models have been implemented in an extended version of FRAPTRAN-1.5, a computer program used for fuel rod thermal-mechanical analyses of transients and accidents [18].

To date, the aforementioned models have been validated against a single LOCA test [15]. The test, Halden IFA-650.4, was done on a fuel rodlet with an average fuel burnup of 92.3 MWd(kgU)$^{-1}$ that had been sampled from a pressurized water reactor (PWR) fuel rod after seven operating cycles in a commercial power reactor. The test resulted in cladding ballooning and burst, as well as significant axial fuel relocation and dispersal of pulverized fuel into the coolant. In this report, we apply our newly developed models for fuel fragmentation, pulverization and axial relocation to four additional LOCA simulation tests on high burnup fuel rods. Three of the tests are in-reactor experiments from the Halden IFA-650 series (tests 9, 10 and 14), whereas the fourth test is an out-of-reactor experiment from the NRC-Studsvik series (test 192). Three of these tests, IFA-650.9/10 and NRC-Studsvik-192, belong to the set of experiments considered for model validation in the IAEA coordinated research project FUMAC, which means that all experimental data for these tests have been obtained through this project. It should also be remarked that six other tests in the Halden IFA-650 series have been evaluated by Quantum Technologies in the past [19-21]. These evaluations did not address fuel pulverization or axial relocation. They also differed from the assessment presented here with regard to applied methodology and computer programs.

The primary objective of the work presented in this report is to gain understanding of the thermal-mechanical behaviour of high burnup fuel under LOCA, in particular the axial relocation of fragmented and pulverized fuel and the thermal effects that the relocation may bring about. Another objective is to elucidate differences between the Halden and Studsvik experiments with regard to testing conditions, and how these differences may affect the phenomena observed in the experiments. Understanding of these issues is important, not least for assessing to what extent the experiments are representative of conditions expected in commercial light water reactors under LOCA.

Finally, the work also aims to validate our computational models. The most important computer program used in the assessment, our extended version of FRAPTRAN-1.5, is ultimately intended for safety analyses of LWR fuel under accidents and transients. Validation of the program and its models against experiments of the kind dealt with in this report is a necessary step to qualify the program for such analyses.

The organization of the report is the following:

The LOCA simulation tests in Halden and Studsvik that are assessed in this report are summarized in section 2. Further details on the experimental procedures and the results obtained from the tests and from post-test investigations and analyses are presented in Appendices A and B.

Section 3 deals with the methodology and computer programs that are used for the assessment. In addition to our extended version of FRAPTRAN-1.5, which is used

for simulating the actual LOCA tests, we use the FRAPCON-3.5 program for generating the necessary burnup dependent fuel rod initial conditions. No computer program is used for calculating the transient thermal-hydraulic boundary conditions that are needed for fuel rod analyses with FRAPTRAN-1.5. These boundary conditions are derived from measured temperatures and pressures in the tests, using assumptions and fitting procedures that are presented in Appendices C and D.

In section 4, we present and discuss the results of our computational assessment in light of measured data from the LOCA tests and from results reported from post-test examinations of the fuel rods. Comparisons are also made with data and results from other LOCA testing programs.

Finally, in section 5, we draw some general conclusions from the presented study and make suggestions for further work. We also discuss the transferability of the results, i.e. the relevance of findings from the experiments as well as the computer analyses to the behaviour of prototypical, full-length, fuel rods under conditions expected in light water reactor loss-of-coolant accidents.

2. Considered LOCA simulation test

The LOCA simulation tests considered in our assessment are summarized below. The Halden IFA-650 LOCA tests number 4, 9, 10 and 14 are presented in section 2.1, and section 2.2 deals with the NRC-Studsvik LOCA test number 192. Details on the results of these tests are presented in Appendices A and B.

2.1. The Halden LOCA tests IFA-650.4/9/10/14

The IFA-650 series of tests are conducted since 2003 in the Halden heavy water test reactor, Norway. To date, fifteen tests on short fuel rodlets have been carried out under simulated loss-of-cooling accident conditions. Twelve of the tests have been made on pre-irradiated fuel rods [2, 22]. One of the primary objectives of the tests is to quantify the extent of fuel fragment axial relocation into the ballooned regions of the rods, and to study possible effects of fuel relocation on cladding temperature and oxidation. Several tests have exhibited axial relocation of fuel fragments; the most notable relocation resulted from tests 4 and 9.

2.1.1. Design and operation of the IFA-650 test rig

The design of the IFA-650 test rig is shown in Fig. 1, and a schematic cross-sectional drawing of the heated part of the rig is given in Fig. 2. In each test, a single test rodlet with an active (fuelled) length of 360–480 mm is instrumented and placed in the centre of the rig, which in turn is placed in one of the experimental channels of the test reactor. The rodlet is surrounded by an electrically heated shroud and a pressure flask. The heated shroud is part of a flow separator, which separates the coolant into a central channel adjacent to the fuel rod and an outer annulus. The heated shroud provides boundary conditions that resemble the heating effects of nearby fuel rods with similar power. The temperature of the test rodlet is controlled both by nuclear heating of the rodlet itself and the electrical heating of the shroud. The power for the heated shroud is uniformly distributed along the test section, while the axial power profile for the rodlet is peaked to the rodlet midplane; see Fig. 1. The inner/outer diameters of the heated shroud and pressure flask are 20/26.2 mm and 34/40 mm, respectively.

The pressure flask is connected to a water loop. During the precondition phase before the test, the loop is filled with heavy water at a pressure and temperature of about 7 MPa and 515 K, which is circulated by pumps through the loop. Shortly before the test, the pressure flask is isolated from the loop and the test rodlet is cooled only by natural circulation within the flask. The LOCA simulation test is then initiated by opening valves to a blowdown tank, which causes a sudden pres-

sure drop in the flask. The coolant flashes to steam, which flows to the blowdown tank and condensates. The flashing lowers the temperature of the remaining coolant. At the end of this blowdown phase, the coolant pressure in the flask stabilizes at 0.2–0.3 MPa [22]. The duration of the blowdown phase differs between tests, since some tests are done by evacuating the test rig through flow lines from the bottom part only (referred to as one-sided blowdown), while others are done by evacuating the rig from both the bottom and top (two-sided blowdown). The typical duration of the blowdown phase is 65–70 s for the former case and about 30–35 s for the latter.

After the blowdown phase, the test rodlet heats up with a rate that depends on the predetermined power levels of the rodlet and the electrically heated shroud. In most of the tests, small amounts of water are periodically sprayed into the upper part of the rig during this high temperature phase to maintain a sufficient amount of steam for cladding oxidation, but otherwise, no actions are taken until the test is terminated by switching off the electrical heater and scramming the reactor. The test rod is then left to cool down slowly, without quenching, in order to minimize any disturbances that could influence the fuel fragmentation and relocation that may have occurred during the high temperature phase.

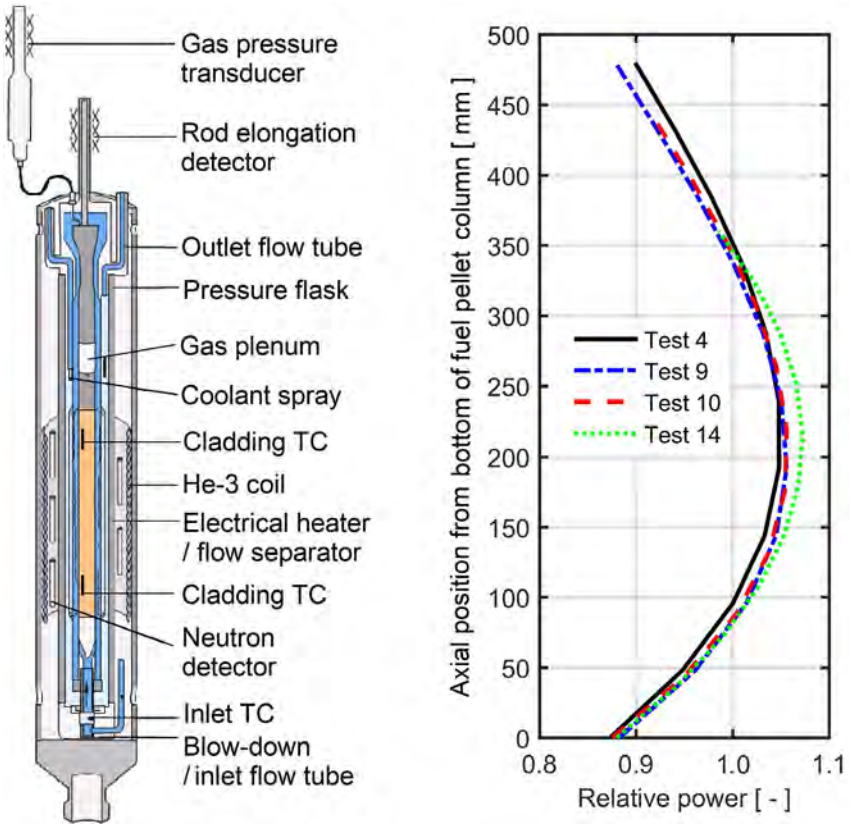

Fig. 1: Design of the IFA-650 test rig (left) and rodlet axial power profiles for the four considered test rodlets in the IFA-650 series (right) [22, 23].

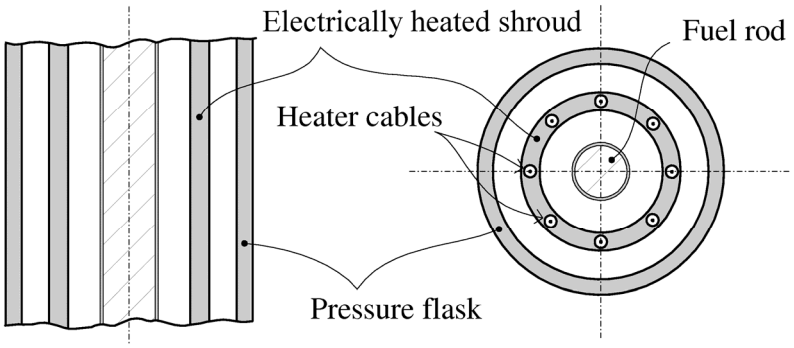

Fig. 2: Schematic drawing of the heated section of the IFA-650 test rig [20].

The general test procedure includes a preconditioning period of 7–8 hours, during which the test rodlet is operated at a linear heat generation rate (LHGR) around 8.5 kWm^{-1}. The reactor and rod power is decreased prior to the test. During the test, the rod power is held nearly constant, typically at 1–3 kWm^{-1}, depending on the target peak cladding temperature. The axial power profile in the rodlet during the test is nearly symmetric, with an axial peak to average power ratio of 1.04–1.08. Fig. 1 shows the axial power profiles for the IFA-650 LOCA tests considered in this report. The variation from one test to another is fairly small.

As indicated in Fig. 1, the IFA-650 test rig instrumentation consists of a fuel rod elongation detector, a fuel rod gas pressure transducer, and coolant thermocouples at the inlet and outlet of the rig. For most tests, there are also 2–4 cladding surface thermocouples, three vanadium neutron detectors and 2–3 heater surface thermocouples. All of these are axially distributed along the rod. Tests 4 and 10 were also equipped with thermocouples at the axial level of the rod gas plenum; the gas plenum is located about 250 mm above the top of the fuel pellet column, away from the heated section.

2.1.2. Test rodlets IFA-650.4, 9 10 and 14

The considered test rodlets were sampled and re-fabricated from full-length light water reactor UO_2 fuel rods that had been operated in commercial power reactors to high burnup. All samples were taken from axial segments between spacer grids, except for the IFA-650.14 rodlet. The length of the samples differed, and the active length of the re-fabricated test rodlets varied between 360 and 480 mm. The design and pre-test material conditions of the considered IFA-650 test rodlets are summarized in Table 1, and the pre-irradiation histories for the re-fabricated short length segments are shown in Fig. 3.

Table 1: Design data and pre-test conditions for the considered IFA-650 test rodlets. Data are compiled from [22, 24-29]. It should be remarked that these sources are not always consistent.

Parameter:		**650.4**	**650.9**	**650.10**	**650.14**
Rodlet active length	[mm]	480	480	440	360
Cold free volume	[cm^3]	21.5	19.0	17.0	1.9
Fill gas pressure at 295 K	[MPa]	4.0	4.0	4.0	2.0
As-fabricated enrichment of ^{235}U	[wt%]	3.5	3.5	4.49	3.71
As-fabricated fuel pellet density	[kgm^{-3}]	10 421	10 443	10 457	10 550
As-fabricated fuel pellet diameter	[mm]	9.13	9.13	8.19	8.19
As-fabricated fuel pellet height	[mm]	11.00 (?)	8.00 (?)	13.78	8.70
As-fabricated dish volume per pellet	[mm^3]	16.0	16.0	11.3	3.8
Pre-test average fuel burnup	[$MWd(kgU)^{-1}$]	92.3	89.9	61.0	70.8
Cladding tube design		Duplex	Duplex	Monotube	Liner
Cladding tube base material		Zircaloy-4	Zircaloy-4	Zircaloy-4	Zircaloy-2
Inner surface liner material		-	-	-	Zr-0.3%Sn
Outer surface liner material		Zr-2.6wt%Nb	Zr-2.6wt%Nb	-	-
Heat treatment		SRA	SRA	SRA	RX
Inner surface liner thickness (nominal)	[µm]	-	-	-	70
Outer surface liner thickness (nominal)	[µm]	100	100	-	-
As-fabricated cladding outer diameter	[mm]	10.75	10.75	9.50	9.62
As-fabricated cladding wall thickness	[mm]	0.725	0.725	0.570	0.630
Pre-test oxide thickness (mean)	[µm]	10	7	27	32
Pre-test oxide thickness (max)	[µm]	11	8	30	40
Pre-test hydrogen concentration	[wppm]	50	30	150-220	180
Pre-test fast neutron fluence (> 1 MeV)	[m^{-2}]	1.52×10^{26}	1.47×10^{26}	1.01×10^{26}	1.18×10^{26}

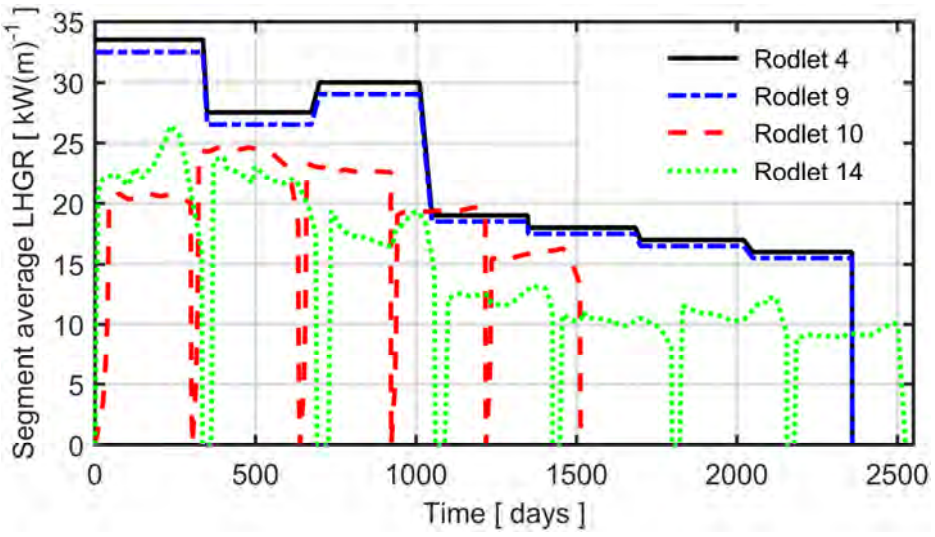

Fig. 3: Pre-irradiation histories for the considered IFA-650 test rodlets.

As part of the re-fabrication process, the test rodlets were filled with a gas mixture consisting of 95 vol% argon and 5 vol% helium to a pressure of either 2 or 4 MPa at room temperature. Argon was used to mimic the low conductivity fission product gases Xe and Kr, while a small amount of helium was needed to leak test the rodlet. Except for the IFA-650.14 rodlet, the gas plenum volume of each rodlet was made large, in order to maintain a stable internal gas pressure until cladding rupture. The IFA-650.14 rodlet, on the other hand, was fabricated with a very small plenum volume, since this test was intended to be interrupted before cladding rupture. The small plenum volume helped to achieve this objective, since it resulted in a declining internal pressure as the cladding tube ballooned.

The test rodlets for IFA-650.4 and IFA-650.9 were re-fabricated from one or two full-length PWR fuel rod(s)[1], manufactured by Framatome ANP and operated in the Gösgen nuclear power plant, Switzerland, to very high burnup [24, 25]. The IFA-650.4 rodlet was sampled from the span between the fifth and sixth spacer grid, whereas the IFA-650.9 rodlet was sampled between the second and the third spacer. The active length of both rodlets was 480 mm, and the sampled sections had reached a burnup of 92.3 and 89.9 MWd(kgU)$^{-1}$, respectively, during seven reactor cycles of operation in the Gösgen reactor. The irradiation histories were very similar, but the IFA-650.4 segment had somewhat higher power than IFA-650.9, as shown in Fig. 3. The mother fuel rod(s) to the IFA-650.4 and 650.9 rodlets had an experimental, Duplex-type Zircaloy-4 stress relieved annealed (SRA) cladding, with an outer layer of Zr-2.6wt%Nb. This cladding had a good corrosion resistance, which explains the low hydrogen concentration and thin oxide layer, in spite of the long operating life of the mother fuel rod. The variation in pre-test oxide layer thickness along the rodlets was insignificant.

The mother rod to the IFA-650.10 rodlet was a 17×17 PWR fuel rod of standard Framatome design; it had UO_2 fuel pellets with fairly high enrichment and standard stress relieved annealed Zircaloy-4 cladding. The mother rod was irradiated in the Gravelines 5 PWR, France, during five reactor cycles [26, 27]. The average burnup of the sampled fuel rod segment was 61.0 MWd(kgU)$^{-1}$, and the irradiation history is shown in Fig. 3.

The IFA-650.14 rodlet was re-fabricated from a boiling water reactor (BWR) mother rod of SVEA-96 design (AEB072-J9), manufactured by Westinghouse Electric Sweden [29, 30]. The cladding material was recrystallized (RX) Zircaloy-2 with an internal zirconium liner with low concentrations of Sn and Fe. The mother fuel rod was irradiated in the Leibstadt BWR, Switzerland, during seven reactor cycles. The average burnup of the sampled fuel rod segment was 70.8 MWd(kgU)$^{-1}$, and the irradiation history is shown in Fig. 3. It should be remarked that the sampled segment contained the fourth spacer grid, and that there were local variations in cladding oxide layer thickness and crud thickness along the part of the segment where the spacer had been positioned [29]. The IFA-

[1] It is not clear from the available documentation wether the rodlets were sampled from the same mother rod, or from two sibling mother rods in the same fuel assembly.

650.14 rodlet differed from the other rodlets also by having a lower fill gas pressure and a much smaller fission gas plenum; see Table 1. The plenum was made small to better control the ballooning of the cladding tube and to make it possible to terminate the test before cladding rupture.

2.1.3. Summary of test conditions and test results

The most important test parameters for the considered Halden IFA-650 LOCA tests are summarized in Table 2. All tests resulted in local ballooning of the cladding tube, and except for IFA-650.14, the cladding tube failed. Gamma emission scanning shortly after each test, as well as later neutron radiography of the rodlets, revealed significant axial fuel relocation in all tests except for IFA-650.10. Further details on the tests and results of post-test examinations are presented in Appendix A.

Table 2: Summary of test parameters for the considered IFA-650 tests [24-26, 28].

Parameter:		**650.4**	**650.9**	**650.10**	**650.14**
Rodlet LHGR	[kWm^{-1}]	0.93	2.60	1.37	0.97
Heater LHGR (initial)	[kWm^{-1}]	1.5	1.6	1.2	1.5
Peak cladding temperature	[K]	1075	1475	1114	1065
Blowdown type (one/two sided)		1	2	1	1
Blowdown duration	[s]	58	35	71	75
Timing of events (after start of blowdown):					
Cladding tube failure	[s]	336	133	249	None
First spraying	[s]	566	149 (175)	261	None
Reactor scram	[s]	617	316	417	274

2.2. The NRC-Studsvik LOCA test 192

A series of six out-of-reactor LOCA simulation tests were performed from 2011 to 2012 by Studsvik Nuclear AB, Sweden, under contract with the U.S. Nuclear Regulatory Commission (U.S. NRC). The tests were done on fuel rodlets that had been sampled from full-length mother rods with average rod burnups ranging from 55 to 72 $MWd(kgU)^{-1}$. All the mother rods were of Westinghouse PWR design and had UO_2 fuel pellets and first generation ZIRLO™ (Zr-1.03Nb-0.98Sn by wt%) cladding. The tests were designed to assess the mechanical performance of ballooned and ruptured high burnup fuel rods under typical LWR LOCA conditions, and they have provided useful information on fuel fragmentation, axial relocation and dispersal [3, 31].

2.2.1. Design and operation of the Studsvik LOCA test rig

The design of the Studsvik LOCA test rig is shown in Fig. 4. A single test rodlet with an active length of about 0.30 m is centred inside a quartz tube and externally heated by infrared radiation from a clamshell furnace. There is no nuclear heating in the tests, and the rig is placed in a hot cell. The rodlet is heated in flowing steam with atmospheric pressure, and the test may be terminated by quenching the rodlet with room temperature water.

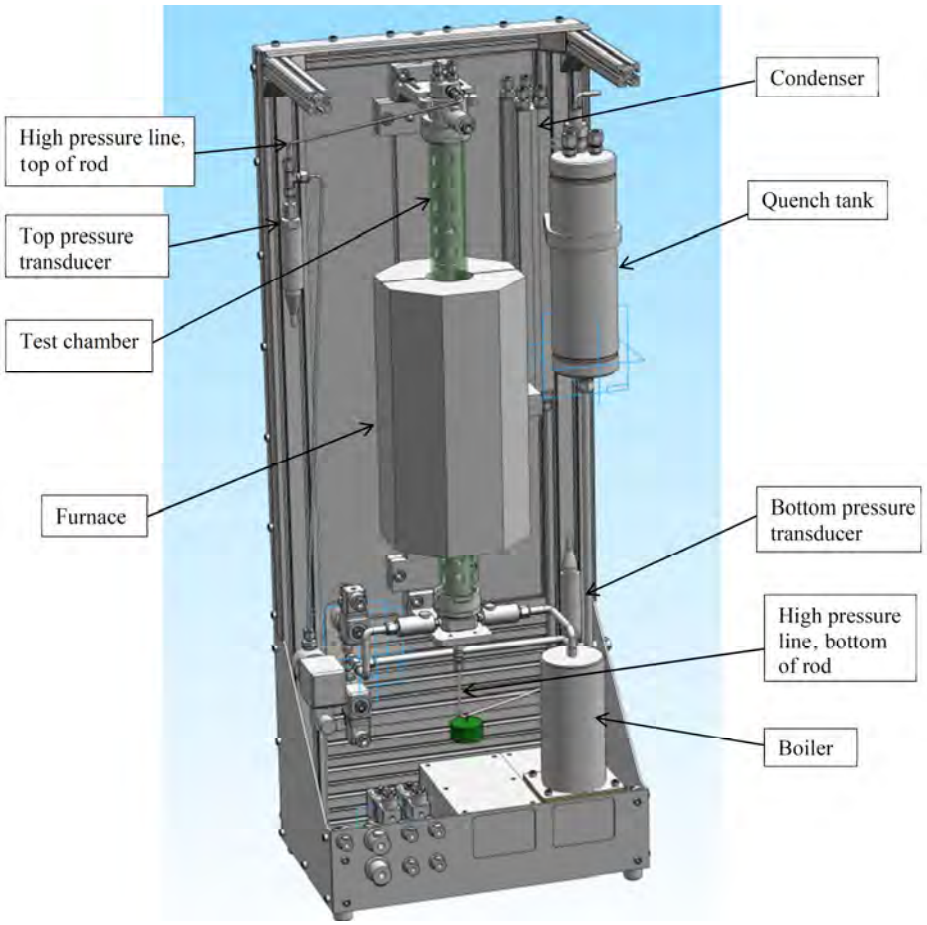

Fig. 4: Design of the Studsvik LOCA test rig [32].

A typical test starts at a temperature of 573 K by heating the rodlet such that a nearly constant heating rate of 5 Ks^{-1} is attained for the cladding tube. The cladding temperature is monitored by a single thermocouple, attached by a metal clamp about 50 mm above the axial midplane of the rodlet. The peak cladding temperature ranged from about 1220 to 1430 K for the six tests, and the rodlets were held at the peak temperature for 0, 5, 25 or 85 s to achieve various degrees of oxidation. Following the high temperature hold, two of the tests (189 and 196) were terminated by switching off the furnace and letting the rodlets cool slowly.

In the other four tests, the rodlets were first cooled with an average rate of -3 Ks^{-1} to 1073 K, after which they were quenched by rapidly filling the quartz tube with room temperature water [3, 32].

The test rodlets were filled with helium to pressures between 8.2 and 11.0 MPa at 573 K. These pressures, which are consistent with high-end end-of-life internal pressures in PWR fuel rods, where chosen to induce cladding ballooning and rupture with hoop rupture strains in the range of 30–50 %. Rupture typically occurred at cladding temperatures around 950–1000 K, i.e. significantly below the peak cladding temperatures reached in the tests.

During the tests, the rod internal pressure was monitored by pressure transducers connected to the top and bottom ends of the rodlet; see Fig. 4. The internal free volume of the pressure lines to the transducers was fairly large; about 7.3 cm^3 in the upper end and about 3.1 cm^3 in the lower end of the test rodlet. Most of this gas volume remained near room temperature during the tests; see section D.2, Appendix D.

After each LOCA simulation test, the rodlet was subject to a four-point bend test at room temperature to measure the residual mechanical strength and ductility of the ballooned and ruptured region. The two broken halves of the rodlet were then inverted and gently shaken to dislodge loose fuel pellet fragments. Mass measurements were made before and after the LOCA simulation test, after the bend test and after the shake test to determine the fuel release at each stage. After the final stage, the size distribution of the dislodged fuel fragments was measured for five of the six rodlets [3, 31].

2.2.2. Test rodlet NRC-Studsvik-192

The rodlet used in the NRC-Studsvik LOCA test 192 was sampled from the middle section of a full-length Westinghouse 17×17 PWR UO_2 fuel rod with first generation ZIRLO™ cladding that had been operated to a rod average burnup of 68.2 $MWd(kgU)^{-1}$ during four reactor cycles at a twin-unit plant in the USA. The first three cycles took place in the first unit from 1987 to 1994 with a two year interruption between the first and second cycle. After the third cycle, the mother fuel rod was extracted from the discharged fuel assembly and inserted into a new assembly, which was operated for an additional reactor cycle in the second unit of the plant from 1999 to 2001. This procedure was applied for altogether ten rods in the original fuel assembly, and some of the sibling high burnup rods have been refabricated into rodlets and used for other tests by Studsvik Nuclear [33, 34]. The design and pre-test material conditions for test rodlet 192 are summarized in Table 3, and the pre-irradiation history for the re-fabricated short length segment in the two PWR units is shown in Fig. 5.

Table 3: Design data and pre-test conditions for the NRC-Studsvik-192 test rodlet [3, 33-35]. Note that data for the rod design are taken from open literature reports on sibling fuel rods that have been used in earlier tests by Studsvik Nuclear AB.

Parameter:		**Value:**
Rodlet active length	[mm]	300
Cold free volume	[cm^3]	10.4
Fill gas pressure at 573 K	[MPa]	8.2
As-fabricated enrichment of ^{235}U	[wt%]	3.99
As-fabricated fuel pellet density	[kgm^{-3}]	10 440
As-fabricated fuel pellet diameter	[mm]	8.192
As-fabricated fuel pellet height	[mm]	9.830
As-fabricated dish volume per pellet	[mm^3]	4.2
Pre-test average fuel burnup	[$MWd(kgU)^{-1}$]	78
Cladding tube design		Monotube
Cladding tube material		ZIRLO™
Heat treatment		SRA
As-fabricated cladding outer diameter	[mm]	9.500
As-fabricated cladding wall thickness	[mm]	0.571
Pre-test oxide thickness (mean)	[µm]	27
Pre-test oxide thickness (max)	[µm]	30
Pre-test hydrogen concentration	[wppm]	235
Pre-test fast neutron fluence (> 1 MeV)	[m^{-2}]	1.31×10^{26}

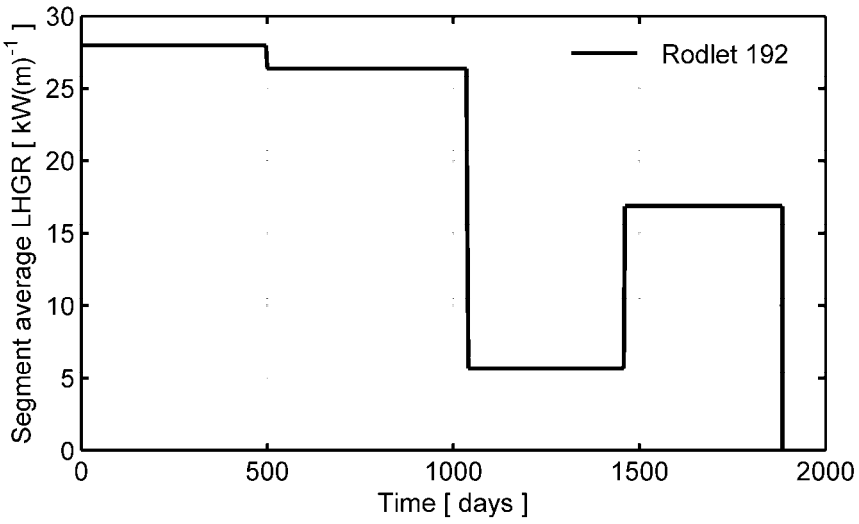

Fig. 5: Pre-irradiation history for the NRC-Studsvik-192 LOCA test rodlet [35].

2.2.3. Summary of test conditions and test results

The most important test parameters for the NRC-Studsvik LOCA test 192 are summarized in Table 4. Further details on the test and the results of post-test examinations are presented in Appendix B.

Table 4: Summary of test parameters for the NRC-Studsvik LOCA test 192 [3, 35].

Parameter:		**Value:**
Initial temperature	[K]	574
Initial rod pressure (at 574 K)	[MPa]	8.21
Cladding temperature at failure	[K]	981
Peak cladding temperature (PCT)	[K]	1446
Hold time at PCT	[s]	5
Steam mass flow	[kgs^{-1}]	1.8×10^{-4}
Timing of events (after start of heating):		
Cladding tube failure	[s]	81
Hold at PCT	[s]	173-178
Quenching	[s]	297

3. Applied methods and computer programs

3.1. Methodology and computer programs

The computer analyses of the considered Halden IFA-650 and NRC-Studsvik LOCA tests were carried out in two steps. In the first step, the pre-irradiation of each fuel rod segment that was later re-fabricated into a test rodlet was modelled by use of FRAPCON-3.5. More precisely, the pre-irradiation in the relevant nuclear power plant was modelled with the standard version of the program [36], as delivered by Pacific Northwest National Laboratory (PNNL), without introducing any modifications or extensions to the program. The procedure is described in section 3.2 below.

Calculated results from FRAPCON-3.5, defining the pre-test conditions for each test fuel rodlet, were used as input to the second analysis step. This step involved simulations of the LOCA test with our extended version of FRAPTRAN-1.5. In addition to models for fuel fragmentation, pulverization and axial relocation [15], this version of FRAPTRAN-1.5 also includes a set of models that treat cladding high temperature metal-water reactions, solid-solid phase transformation, creep and failure in a unified fashion [37, 38]. The applied version is thus different from the standard version of FRAPTRAN-1.5 delivered by PNNL [18], and a number of errors observed in the standard version have also been fixed in our version of the program [39]. Both FRAPCON and FRAPTRAN are best-estimate computational tools, and the presented analyses should be considered as best-estimate; no uncertainty or sensitivity analyses were carried out. However, the analysis of each LOCA test was done twice: with and without the fuel relocation model. Except for this difference, the two calculations were done with identical models and input data.

It should be remarked that no computer program was used for calculating the transient thermal-hydraulic boundary conditions that are needed for fuel rod analyses with FRAPTRAN. These boundary conditions were derived from measured temperatures and pressures in the considered test rigs; the applied methodology and assumptions are described in section 3.3 and Appendices C and D.

3.2. Simulations of pre-irradiation

The pre-irradiation of each fuel rod segment that was later re-fabricated into a test rodlet was simulated by use of the standard version of FRAPCON-3.5 [36]. Input for the simulations, in terms of fuel pellet and cladding design data and power histories, are given in sections 2.1.2 and 2.2.2. The linear heat generation rate dur-

ing the pre-irradiation was assumed to be uniform along each segment. Nominal core average thermal-hydraulic conditions for each PWR were used in the simulations, but the coolant inlet temperature was increased to represent the local conditions at the axial elevation pertinent to the considered segment of the full length mother fuel rod.

Recommended default models and options for FRAPCON-3.5 were used in the calculations. In particular, the thin-shell mechanical model was used for the cladding tube, rather than the finite element based model. The Duplex-type cladding material of the IFA-650.4 and IFA-650.9 rodlets was represented by models for M5® cladding, which are available in FRAPCON-3.5 [36]. These models were selected, since the M5® alloy has similar performance with regard to waterside corrosion as the Zr-2.6wt%Nb surface liner in the Duplex cladding.

In all calculations with FRAPCON-3.5, the fuel rod samples were discretized axially into 20 mm long axial nodes. Hence, the number of axial nodes ranged from 15 to 24, depending on the length of the considered sample. The radial discretisation of the fuel pellet stack consisted of 44 annuli.

3.3. Simulations of LOCA tests

The Halden IFA-650 and NRC-Studsvik LOCA tests were simulated with our extended version of FRAPTRAN-1.5, using previously developed high temperature models for the cladding tube [37] in combination with a slightly modified version of the finite element based mechanical solution module [40]. All tests were simulated twice, with and without consideration of axial fuel relocation, in order to assess the importance of the relocation to the thermal-mechanical behaviour and high temperature degradation of the tested fuel rodlets.

All calculations were done with an axial discretisation consisting of 20 mm long axial segments for the active part of the test rodlet, i.e. the same discretisation as was used for the simulations of the rodlet pre-irradiation with FRAPCON-3.5. Likewise, the radial discretisation comprised 44 annuli in the fuel pellet and one element across the cladding thickness. A constant time step length of 10 ms was used in the calculations, and the simulations covered the heatup phase, the high temperature phase and most part of the cooling phase in each test.

For the Halden IFA-650 tests, the rodlet LHGR was held constant at the values defined in Table 2 until reactor scram, after which the LHGR was reduced to 0.05 kWm^{-1} to simulate decay heating. The axial power profiles used in the simulations of the Halden tests are shown in Fig. 1. No nuclear heating was modelled for the NRC-Studsvik-192 out-of-reactor test.

The NRC-Studsvik-192 test rodlet was filled with helium, whereas the Halden IFA-650 test rodlets were filled with a low-conductivity gas mixture, consisting of

95 vol% argon and 5 vol% helium; see sections 2.1.2 and 2.2.2. These gas compositions were postulated for the calculations with FRAPTRAN. In the calculations, the amount of fill gas in each rodlet was adapted, such that the calculated "hot" pre-test pressure matched the measured value for each test.

Other pre-test conditions of the rodlets were defined by the end-of-life fuel rod conditions after operation in the commercial power reactors, as calculated with FRAPCON-3.5. Calculated results for the permanent deformations of fuel and cladding, cladding oxide layer thickness and hydrogen content, as well as the radial distributions of fuel burnup and power, were imported to FRAPTRAN input from FRAPCON output. Most of these data are presented and discussed in section 4.1. It should be remarked that any axial variation in the pre-test conditions calculated by FRAPCON-3.5, such as the cladding oxide layer thickness, was neglected when using them as input to FRAPTRAN.

Transient fission gas release from the high burnup fuel was not considered in the calculations, except for test Halden IFA-650.14. As mentioned in section 2.1.2, this test was performed on a rodlet with an exceptionally small gas plenum volume, which means that the amount of fill gas was much less than the amount of fission gas released during the test. More precisely, there was 1.56×10^{-3} mole fill gas in the rod before the test, and 4.72×10^{-3} mole gas after the test, as a result of transient fission gas release [41]. The amount of gas released during the test corresponds to about 18 % of the gas produced during the lifetime of the fuel [41].

For reasons described above, modelling of transient fission gas release was necessary for the Halden IFA-650.14 test. The FRAPTRAN-1.5 computer program has no proper model for fission gas release, but the user may prescribe the fractional fission gas release as time dependent input to the program [18]. In our simulations of the IFA-650.14 test, we prescribed the transient fission gas release fraction, x_f, by use of a smooth ramp function with respect to time;

$$x_f(t) = \frac{0.18}{2}\left(1 + \tanh\left(\frac{t - t_c}{t_s}\right)\right). \quad (1)$$

Here, t is the time from start of blowdown in the IFA-650.14 test, while t_c = 225 s and t_s = 50 s are parameters that were empirically fitted so that the calculated and measured time histories of rod internal gas pressure matched. Equation (1) is shown graphically in Fig. 30 and will be further discussed in section 4.2.4.

Possible restrictions of rod internal gas flow during the tests were neglected. Hence, the internal gas was assumed to have uniform pressure and composition along the rod, in the rod plena, and in connected gas-containing systems. For the tests in which transient fission gas release was not modelled, the gas composition remained unchanged until cladding rupture was calculated to occur. By default in FRAPTRAN-1.5, steam is assumed to completely and immediately replace the rod internal gas from the time of cladding rupture [18]. Since the inflowing steam has higher thermal conductivity than argon, cladding rupture resulted in improved

pellet-to-cladding heat transfer and a rapid rise in cladding temperature along the entire rodlet in our simulations of the Halden IFA-650 tests. This rather unrealistic behaviour is further discussed along with the calculated results in section 4.2. The steam entering the fuel rod after cladding rupture is in FRAPTRAN-1.5 assumed to cause oxidation of the cladding inner surface. However, the inner surface oxidation is restricted to axial segments that are within a distance of 3 inches from the cladding breach [18].

All the test rodlets considered in this report had internal gas plena that differed from the typical design of LWR fuel rods. The IFA-650 series of rodlets had a single gas plenum that was located about 200 mm above the top of the fuel pellet column, outside the heated zone. The plenum gas temperature therefore remained fairly low during these tests. In the IFA-650.4 and IFA-650.10 tests, thermocouples were attached to the cladding and shroud at the axial position of the plenum; see Appendix A. Fig. 6 shows the measured temperatures from the IFA-650.4 test, together with the approximation used for the plenum gas temperature in our simulations of the test. During the blowdown phase, the temperature is equal to the saturation temperature of the flashing steam. After blowdown, the gas plenum heats up and approaches a temperature somewhat above the moderator temperature in the Halden reactor (510 K); the temperature difference depends on the combined power of the rodlet and heater. The discontinuity of the measured temperature histories in Fig. 6 is due to the outflow of hot gas upon cladding rupture.

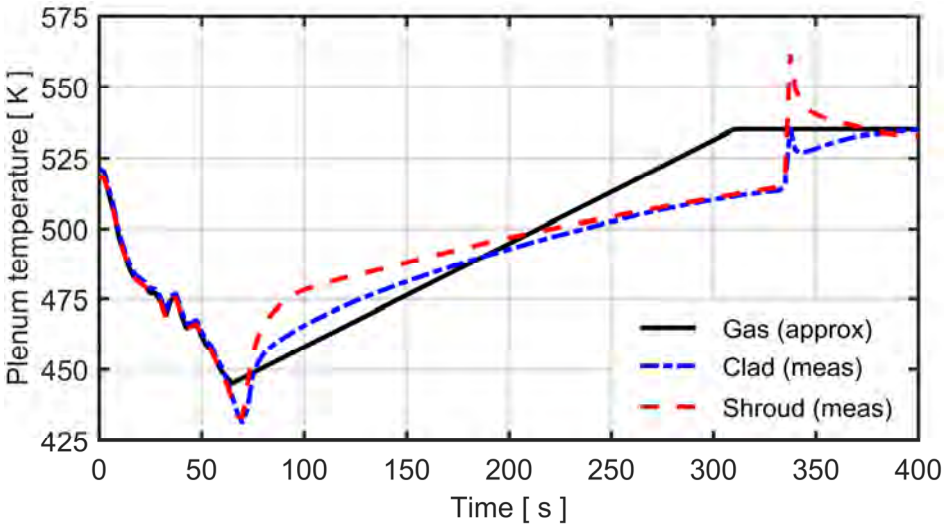

Fig. 6: Measured temperatures at the gas plenum position for the IFA-650.4 rodlet, together with the approximation for plenum gas temperature used in calculations.

In our simulations of the Halden IFA-650 tests, we used approximations to the plenum gas temperature, similar to the one shown in Fig. 6: For each rod, the gas temperature was assumed to follow the steam saturation temperature during the blowdown phase, which was then followed by a phase with linear heat up to a final gas temperature of 515–535 K. As for the NRC-Studsvik-192 test rodlet, it

had a more complex design than the IFA-650 rodlets with regard to internal gas volumes. The modelling of these volumes and their temperature evolution is described in section D.2 of Appendix D.

The time dependent thermal-hydraulic boundary conditions required by FRAPTRAN for calculating the fuel rod behaviour during the LOCA simulation tests were derived from temperatures and pressures measured in different parts of the test rigs. The procedure for deriving the boundary conditions for the Halden IFA-650 tests is fairly complex. It is described in detail in Appendix C.

The thermal-hydraulic boundary conditions for the NRC-Studsvik-192 test were simpler, since the test was performed in steam at atmospheric pressure and the heating was by a furnace that surrounded the rodlet. The boundary conditions for this test were derived from the measured cladding temperature close to the mid-plane of the rodlet, in combination with measured data for the typical axial temperature variation, obtained during conditioning of the test rig [32]. The thermal boundary conditions applied for the NRC-Studsvik 192 test are described in detail in section D.1 of Appendix D.

The NRC-Studsvik-192 test rodlet had ZIRLO™ cladding, in contrast to the Halden IFA-650 rodlets that had Zircaloy cladding. Since our extended version of FRAPTRAN-1.5 lacks specific material models for ZIRLO™, we used generic Zircaloy models also for the NRC-Studsvik-192 rodlet. More precisely, in all calculation presented in this report, we used the Cathcart-Pawel high temperature oxidation model [42], and the Zircaloy-4 high temperature creep model by Rosinger [43, 44]. The latter was used without any specific creep model for the mixed $\alpha+\beta$ phase region.

None of the temperature dependent criteria for cladding high temperature rupture that are available in our version of FRAPTRAN-1.5 [37] worked well for the considered tests. For the IFA-650.4 and IFA-650.9 tests, the calculations resulted in contact between the distending cladding tube and the surrounding heater before cladding rupture was calculated to occur. Once in contact, the heater acted as a die, forcing the cladding balloon to grow in the axial direction until it finally ruptured. Since this behaviour was not observed in the tests, we postulated an ad-hoc threshold for the effective creep strain, at which the cladding was assumed to fail. This threshold effective strain (logarithmic) was set to 0.75 for the IFA-650.4 and IFA-650.9 tests, since this value resulted in cladding failure just before the cladding came into contact with the surrounding heater; see Fig. 10 and Fig. 16. We adopted the same methodology for the IFA-650.10 and the NRC-Studsvik-192 test, for which the threshold effective strain for cladding failure was set to 0.30 and 0.70 respectively.

The cladding creep rate in FRAPTRAN had to be scaled, in order to match the calculated and measured time to cladding rupture. A scale factor of 0.40 was found to give a good match for the considered Halden IFA-650 tests, when fuel

relocation was included in the calculations. To allow meaningful comparisons between tests and also between the calculated cases with and without fuel relocation, this scale factor was used in *all* calculations presented in this report. Except for the scaled creep rate and the ad-hoc rupture criterion described above, models in our extended version of FRAPTRAN-1.5 were not modified or tuned. The model parameters used in our relocation model were those used in earlier work [15], unless otherwise stated; l_p = 0.10 mm, g^{th} = 0.20 mm, g^r = 5.0 µm, x^r = 0.01, ϕ^L = 0.69, and ϕ^S = 0.72.

4. Results and discussion

4.1. Pre-irradiation

Key results of the simulated pre-irradiation of the considered test rodlets with the FRAPCON-3.5 computer program are summarized in Table 5. Measured data are included for comparison, when available. The calculated cladding corrosion (hydrogen pickup and oxide layer thickness) is in fair agreement with measurements. We recall from section 3.2 that the non-standard Duplex-type cladding material of the IFA-650.4 and IFA-650.9 rodlets was represented by models for M5® in our calculations with FRAPCON-3.5 [36], in order to reproduce the corrosion performance.

Table 5: Pre-test conditions of the test rodlets, calculated with the FRAPCON-3.5 computer program. Measured data are given in brackets for comparison.

Parameter		**650.4**	**650.9**	**650.10**	**650.14**	**192**
Rodlet average burnup	[MWd(kgU)$^{-1}$]	91.9 (92.3)	89.5 (89.9)	60.7 (61.0)	70.8 (70.8)	78.4 (78)
Pellet centre burnup	[MWd(kgU)$^{-1}$]	77.9	76.1	54.5	61.6	68.0
Pellet surface burnup	[MWd(kgU)$^{-1}$]	257.0	248.5	128.2	174.6	194.9
Fuel fraction with local BU > 70 MWd(kgU)$^{-1}$		1.0	1.0	0.11	0.32	0.74
Radial power peaking factor	[-]	3.53	3.53	3.06	3.34	3.395
Fuel fragment average size	[mm]	1.87	1.90	2.05	1.93	1.85
Fission gas release	[%]	11.1	7.6	2.5	3.6	11.1
Cladding hydrogen concentration	[wppm]	67–76 (50)	57–65 (30)	172–225 (150–220)	415 (180)	213–256 (176–288)
Cladding outer oxide layer thickness	[µm]	14–16 (6–8)	11–13 (6–8)	20–27 (20–30)	29 (32–35)	22–27 (25–30)

Table 5 includes calculated values for the local fuel burnup at the pellet centre and surface (rim). The calculated distribution of fuel burnup is of interest, since it is used in our version of FRAPTRAN-1.5 to estimate the amount of fuel material that may pulverize when overheated during the LOCA test. More precisely, a local burnup of at least 70 MWd(kgU)$^{-1}$ is required for the fuel to pulverize, according to our model [15]. As can be seen from Table 5, the fuel fraction exceeding this threshold, and thus susceptible to pulverization at high temperature, ranges from 11 to 100 % among the considered test rods.

Fig. 7 shows the distributions of power and burnup across the fuel pellets after pre-irradiation of the IFA-650.4 and IFA-650.10 test rodlets, according to our calculations with FRAPCON-3.5. The radial distributions of power are fairly similar in these two test rods, but the distributions of burnup are much different.

The calculated distributions are assumed to be valid for the entire length of the test rodlets, since the irradiation conditions were fairly uniform along the sampled rod segments.

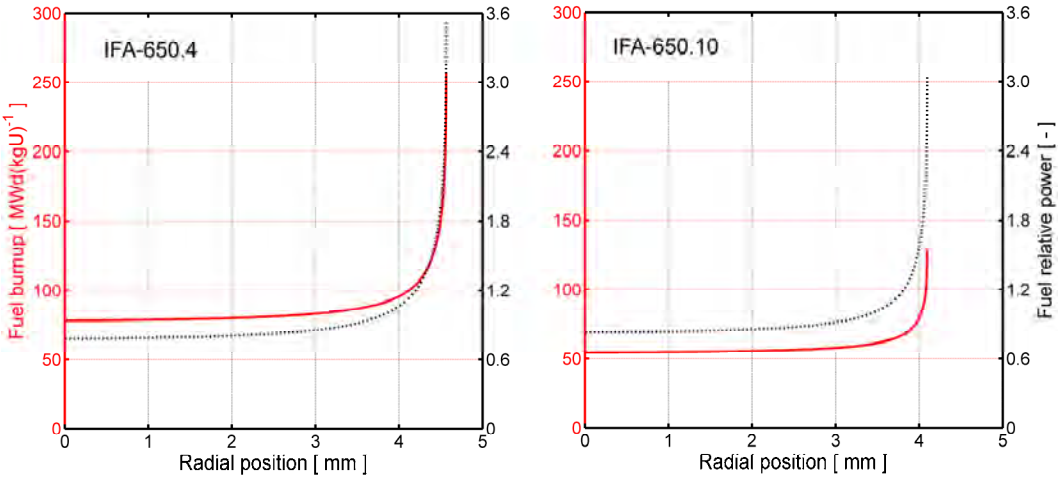

Fig. 7: Calculated distributions of burnup (full red line) and power (dashed black line) across the fuel pellets in the IFA-650.4 and IFA-650.10 test rodlets.

The radial distributions of fuel burnup and power, calculated with FRAPCON-3.5, are used in subsequent analyses of the LOCA simulation tests with our extended version of FRAPTRAN-1.5. It is assumed that the distributions do not change with time during the tests – not even when fuel crumbling and axial fuel relocation occurs [15].

Finally, from Table 5, we note that the estimated average size of fuel fragments in the considered rodlets range from 1.87 to 2.05 mm before the LOCA tests. These fragment sizes are calculated through an empirical model, based on the fuel pellet average burnup and the peak power experienced by the fuel during its lifetime [15].

4.2. Halden IFA-650 LOCA tests

Here, we consider the results of our simulations of the Halden IFA-650 LOCA tests. For each test, calculated results are presented graphically for the cases with and without fuel relocation considered in the analyses with our extended version of FRAPTRAN-1.5. Measured data are included in the graphs for comparison, whenever data are available. Throughout the presentation, time zero refers to the start of the LOCA test, defined by the opening of valves between the in-core pressure flask and the blowdown tank; see section 2.1.1.

4.2.1. IFA-650.4

Fig. 8 shows the calculated and measured evolution of rod internal gas pressure in the upper plenum during the Halden IFA-650.4 test. From section 3.3, we recall that the gas pressure is calculated on the basis of calculated temperatures and deformations along the active length of the rodlet, together with a postulated temperature history for the gas within the rod plenum. We also recall that the initial cold pressure was reduced from its reported value of 4.0 MPa to 3.86 MPa in our calculations, in order to match the calculated "hot" pre-test gas pressure to the measured value (6.95 MPa). The calculated gas pressure is in close agreement with measurements for $t < 290$ s, but overestimated for the remaining 46 seconds preceding cladding rupture. A likely explanation to this deviation is that ballooning of the cladding starts earlier and progresses more gradually than calculated with our version of FRAPTRAN-1.5.

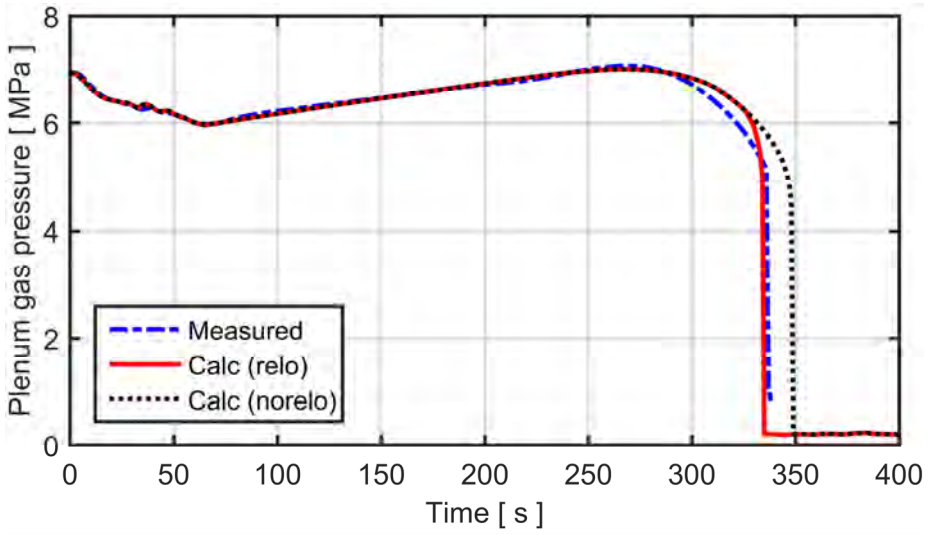

Fig. 8: Calculated evolution of plenum gas pressure in comparison with measurements. Calculations were done with (relo) and without (norelo) assumed axial fuel relocation.

In Fig. 8, the calculated curves for the cases with assumed relocation ("relo") and without relocation ("norelo") coincide up to $t = 326$ s. This is the time at which fuel fragments start to relocate axially, according to our calculations. The calculated time of cladding failure is 334.2 s for the case with fuel relocation and 348.2 s without. These results suggest that cladding ballooning, collapse of the fuel pellet column, and axial relocation of fuel take place in a fairly short (7–8 s) period before cladding rupture, but that the thermal feedback effects are still strong enough to affect the rupture process. For the considered test, the calculated time to rupture was shortened by no less than 14 seconds, as a result of thermal feedback effects from fuel crumbling and relocation. As already mentioned, the deviation between the calculated and measured gas pressure time histories in Fig. 8 suggests that the ballooning and relocation in test IFA-650.4 may actually have

occurred over a longer period than in our calculations. If so, the impact of thermal feedback effects on the rupture process would have been even more important.

Fig. 9 shows the calculated evolution of cladding deformation and axial fuel relocation during the last seven seconds before cladding rupture. The thick red line shows the calculated state at the time of cladding rupture. This is also the state expected after the test is completed, since no further deformation or relocation is supposed to take place after rupture and depressurization of the rodlet. The family of thinner black lines represent the calculated conditions 1, 2, 3,..,7 seconds before cladding rupture. The leftmost curve thus shows the conditions about the time when the balloon starts to grow and fuel starts to relocate.

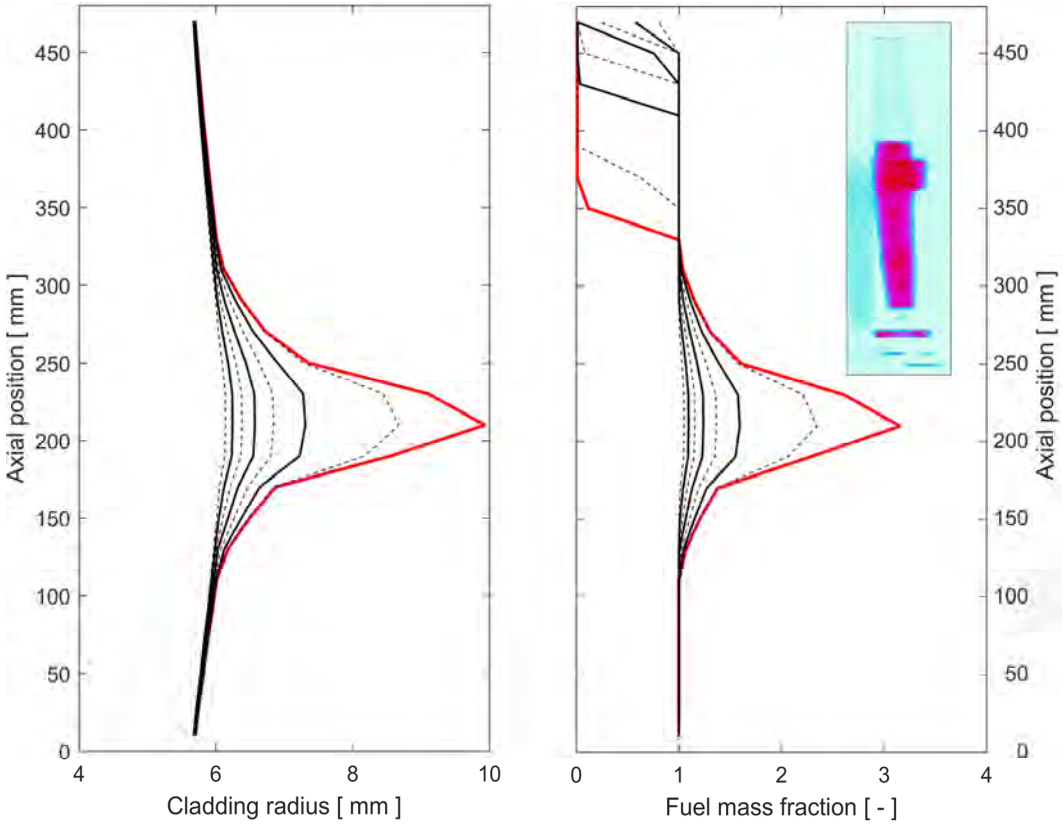

Fig. 9: Calculated evolution of cladding deformation (left) and fuel relocation (right) during the last seven seconds before cladding rupture. The rightmost curve (red) represents the conditions at time of rupture, while the seven curves to the left of it show the calculated state 1, 2,...,7 seconds before rupture. A post-test gamma scan image of the IFA-650.4 test rig is included for comparison [45].

The calculations suggest that the local fuel mass is increased by about a factor of three in the most distended cross section of the test rodlet. The relocated fuel originates from the uppermost, 120 mm long, part of the fuel pellet column, which has disappeared completely. This is well in line with the results reported from the test: Gamma scan (see insert in Fig. 9) as well as ceramography showed that the uppermost part of the fuel pellet column was completely missing after the test; no

remaining fuel fragments were detected. The length of the missing fuel part was 190 mm, which is 70 mm longer than calculated with our model. The difference is understandable, since a significant amount[2] of fuel had been expelled through the cladding breach and was found just above the balloon and at the bottom of the pressure flask after the test [45]. This dispersal of fuel fragments, which is not accounted for by our model, most certainly increased the amount of fuel lost from the upper part of the fuel rod.

Finally, we note that the calculated fuel temperature is in the range of 1100 to 1159 K, when relocation starts at t = 326 s. This means that, according to our model, the entire fuel column has been pulverized into fine (< 0.2 mm) fragments, and that the crumbled fuel has an assumed packing fraction of 0.72 everywhere in the ballooned region; see the description of the applied models for fuel fragmentation and pulverization in [15].

Fig. 10 shows the calculated post-test diameter profile of the IFA-650.4 rodlet in comparison with measurements. The latter were obtained by metallography of thirteen cross sections, for which the cladding tube diameter was measured in two perpendicular directions. Hence, the data also provide some information on the degree of cylindrical symmetry for the deformation. The calculated peak deformation is the same for the two considered cases, since the same failure criterion in terms of a threshold for the local effective strain was used for both of them. However, the calculated deformation profiles differ. As expected, the fuel relocation tends to concentrate, or localize, the cladding deformation. The reason is the concentrated heat load, resulting from fuel crumbling and accumulation of fuel fragments in the ballooned region of the rod.

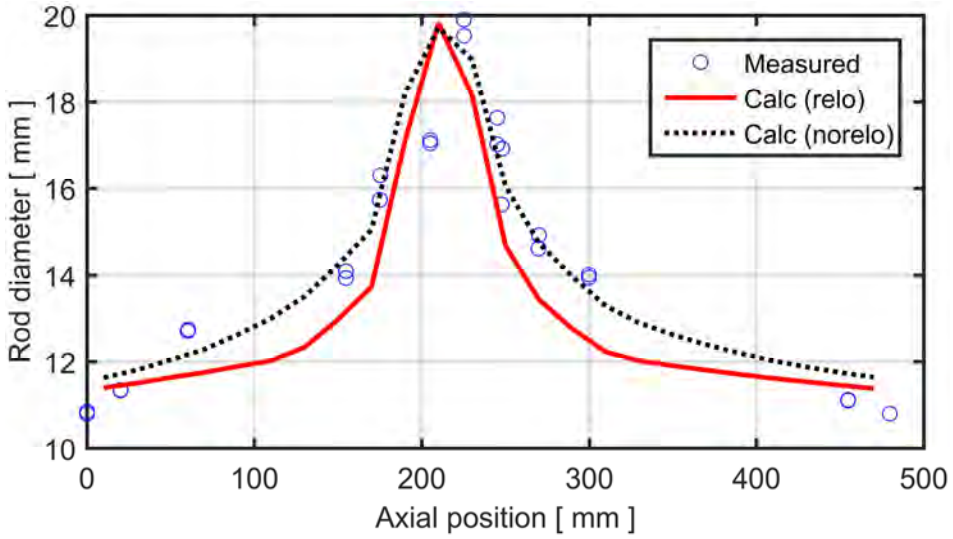

Fig. 10: Calculated and measured post-test diameter profiles for the IFA-650.4 rodlet [45].

[2] The weight of dispersed fuel in the IFA-650 series of tests was not determined. Only qualitative assessments of the dispersal in each test, based on post-test gamma scan results and visual inspections, are available [22, 46].

Consequently, we next consider the thermal effects of fuel relocation and their impact on the cladding failure behaviour. Fig. 11 shows a comparison of the calculated cladding surface temperature with measured data from thermocouples TCC1 and TCC2, which were located 80 mm below the top of the fuel pellet column, i.e. in the part that was completely emptied of fuel upon cladding rupture; see section A.1, Appendix A. The two thermocouples give very similar results, which suggests that the azimuthal temperature difference along the cladding circumference was insignificant at this axial position. It is clear from Fig. 11 that the cladding temperature is slightly underestimated during the heat-up phase ($65 < t < 250$ s): the maximum difference between calculated results and measured data is about 20 K. The most likely explanation to the deviation is our simplified modelling of the clad-to-coolant heat transfer; see Appendix C.

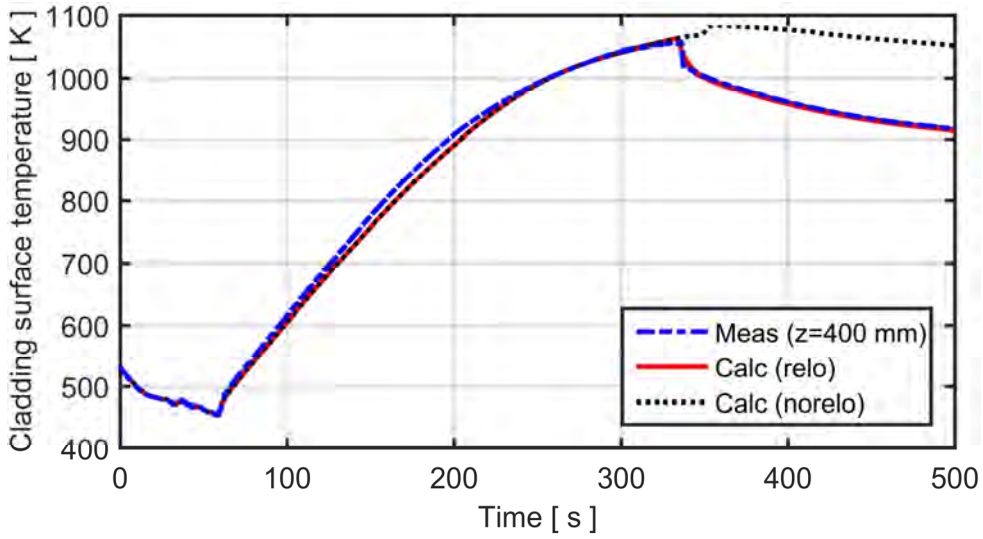

Fig. 11: Calculated and measured cladding surface temperature versus time. The temperature refers to the position of thermocouples TCC1 and TCC2, 400 mm above the bottom of the fuel pellet column; see Table 8.

Fig. 12 is a close-up of Fig. 11, showing the calculated and measured temperature variation about the time of cladding rupture (336 s in experiment, 334 and 348 s in calculations with and without fuel relocation, respectively). The calculated curve for the case with axial fuel relocation is very close to the measured data. This confirms that thermal feedback effects due to the complete fuel loss from the upper part of the rodlet are accurately captured by our model. When the fuel is lost, the cladding temperature approaches that of the surrounding coolant and heater; this is why the calculated and measured curves virtually coincide for $t > 345$ s.

For the calculated case without axial fuel relocation, the cladding temperature increases just after the calculated time of cladding rupture at t = 348 s. The temperature rise is a result of improved pellet-cladding heat transfer, since FRAPTRAN by default models instantaneous and complete ingress of steam from the coolant channel to the pellet-cladding gap upon cladding rupture. The steam has higher thermal conductivity than the initial fill gas, which consisted of 95 vol% argon and 5 vol% helium.

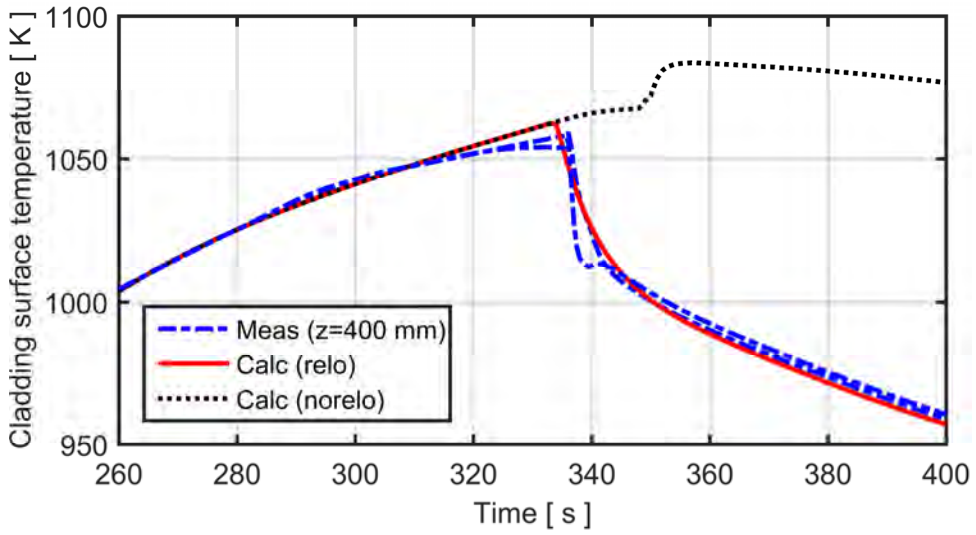

Fig. 12: Calculated and measured cladding surface temperature about the time of cladding rupture (336 s); close-up of Fig. 11.

The long term effect of fuel crumbling and axial relocation on the cladding temperature and oxidation is illustrated by Fig. 13, which shows the calculated cladding outer surface temperature and equivalent cladding reacted (ECR) versus axial position at time t = 500 s. The ECR is a cladding degradation parameter that is widely used in acceptance criteria for emergency core cooling systems. It is defined as the percentage of the cladding thickness that would be oxidized, if all the oxygen from the cladding-water reactions stayed in the oxide layer as ZrO_2. At t = 500 s, transient effects from the collapse of the fuel pellet column into the balloon have decayed and the temperature distribution reflects a quasi-steady condition. It is obvious that the calculated temperature field for the case with axial fuel relocation is governed by the axial distribution of fuel mass and power; compare the right panel of Fig. 9. We note that the case without axial fuel relocation in Fig. 13 shows the opposite trend; the calculated cladding temperature has a minimum in the ballooned region, due to the local increase in coolable surface area. It should be remarked that the case calculated without fuel relocation in Fig. 13 is in fact affected by relocation: the low temperature calculated for the upper part of the fuel rod for the case without relocation is due to the decline in heater temperature, which is caused by the fuel relocation that occurs in the test. The measured space-time variation of the heater temperature is used for defining the thermal-

hydraulic boundary conditions in all calculations with FRAPTRAN, both with and without the relocation model, so this effect is inevitable.

As can be seen from the calculated post-test ECR in the right panel of Fig. 13, the long-term change in temperature distribution caused by the axial fuel relocation has a noticeable effect on the post-failure oxidation of the cladding. The calculated pre-test ECR from low temperature oxidation in Gösgen was about 1.6 %; this pre-test oxidation is included in the curves presented in Fig. 13. From the figure, it is clear that the calculated contribution to the peak post-test ECR from the IFA-650.4 LOCA test is about 70 % larger when axial fuel relocation is considered.

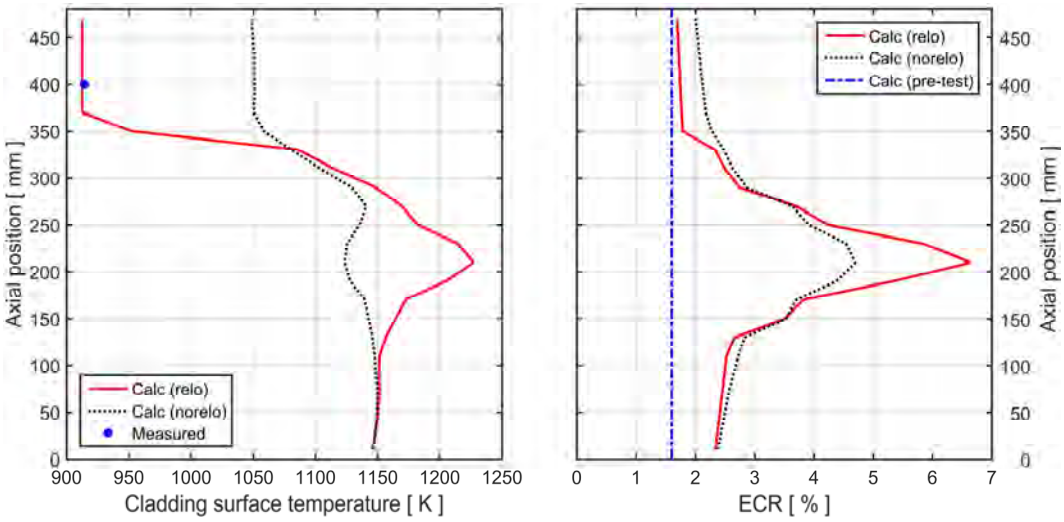

Fig. 13: Calculated cladding outer surface temperature and equivalent cladding reacted (ECR) versus axial position at time t = 500 s, with and without consideration of axial fuel relocation.

The calculated results presented for the ECR in the right panel of Fig. 13 cannot be directly verified against experimental data, since no post-test measurements were made of the axial variation in cladding oxide thickness or metal oxygen concentration. However, the outer surface oxide layer thickness was measured at some positions in the ballooned region after the test. It ranged from about 10 to 13 µm, and the thickest oxide was found at the lower end of the balloon [45]. These results indicate that the peak post-test ECR would be around 3.3 %, i.e. significantly lower than our calculated results for the cases with and without fuel relocation. This is not surprising, considering that fuel fragments were ejected from the failed balloon into the coolant during the test. The fuel ejection, which is not accounted for in our simulations of the test, lowered the fuel fragment packing fraction in the balloon. More precisely, the post-test area fraction covered by fuel fragments was estimated to be no more than 0.4–0.5 in the balloon, based on image analyses [45]. The low fragment packing fraction that resulted from the fuel ejection most certainly limited the thermal feedback effects of axial fuel relocation in the post-failure part of the experiment.

4.2.2. IFA-650.9

The design and pre-irradiation conditions for the IFA-650.9 rodlet were nearly identical to those of the sibling IFA-650.4 rodlet. However, the IFA-650.9 rodlet was tested at much higher power and reached significantly higher temperatures than its sibling IFA-650.4; see section A.2 in Appendix A.

Fig. 14 shows the calculated and measured evolution of rod plenum gas pressure during the Halden IFA-650.9 test. In the calculations, the initial cold pressure was reduced from its reported value of 4.0 MPa to 3.78 MPa, to match the calculated "hot" pre-test gas pressure to the measured value (6.96 MPa). It is clear that the calculated plenum pressure deviates significantly from the measurements in this test, both before and after cladding rupture, which occurred at t = 133 s. The slow equilibration with the external (rig) pressure after cladding rupture suggests that the axial gas flow between the upper plenum and the cladding breach at the bottom part of the rodlet was significantly restricted. This is not captured in the calculations, since axial pressure gradients are neglected by FRAPTRAN-1.5; see section 3.3.

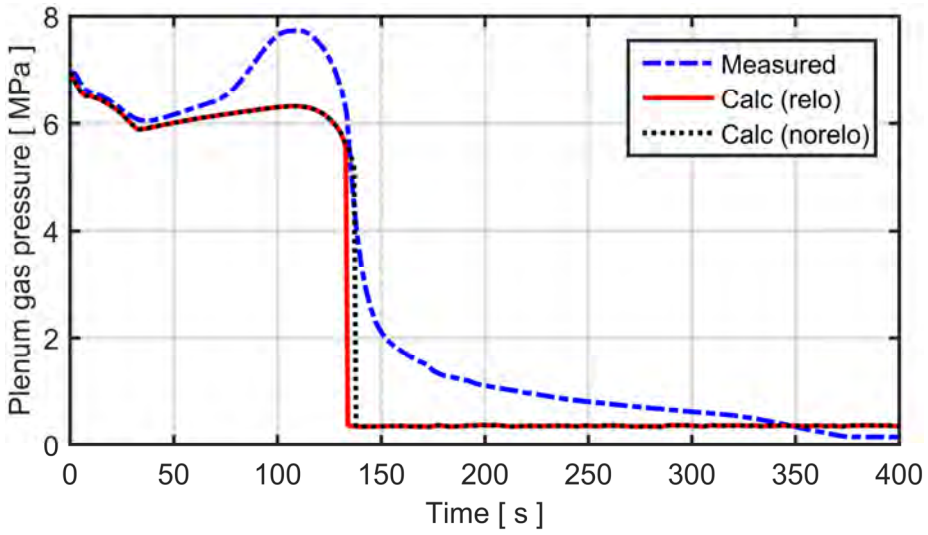

Fig. 14: Calculated evolution of rod plenum gas pressure in comparison with measurements for the IFA-650.9 test rodlet.

Restricted axial gas flow has been observed also in a few other Halden IFA-650 test rodlets (3 and 5), and the behaviour observed in these rodlets has been analysed by use of computer models [47]. The same computer models were then applied to analyse the internal gas flow in a full length PWR fuel rod, having a cladding breach far away from its gas plenum. The results suggest that the flow restrictions in a full length fuel rod are significant, and that the restrictions may de-

lay cladding rupture by limiting the amount of gas available in the ballooned region [47].

In Fig. 14, the calculated curves for the cases with and without assumed fuel relocation coincide up to t = 130 s, which is the time when fuel fragments start to relocate axially, according to our calculations. The calculated time of cladding failure is 133.5 s for the case with fuel relocation and 137.8 s without. These results suggest that cladding ballooning, collapse of the fuel pellet column, and axial relocation of fuel take place within 3–4 s before cladding rupture.

Fig. 15 shows the calculated evolution of cladding deformation and axial fuel relocation during the last four seconds before cladding rupture. The thick red line shows the calculated state at the time of cladding rupture, and the leftmost curve shows the conditions about the time when the balloon starts to grow and fuel starts to relocate.

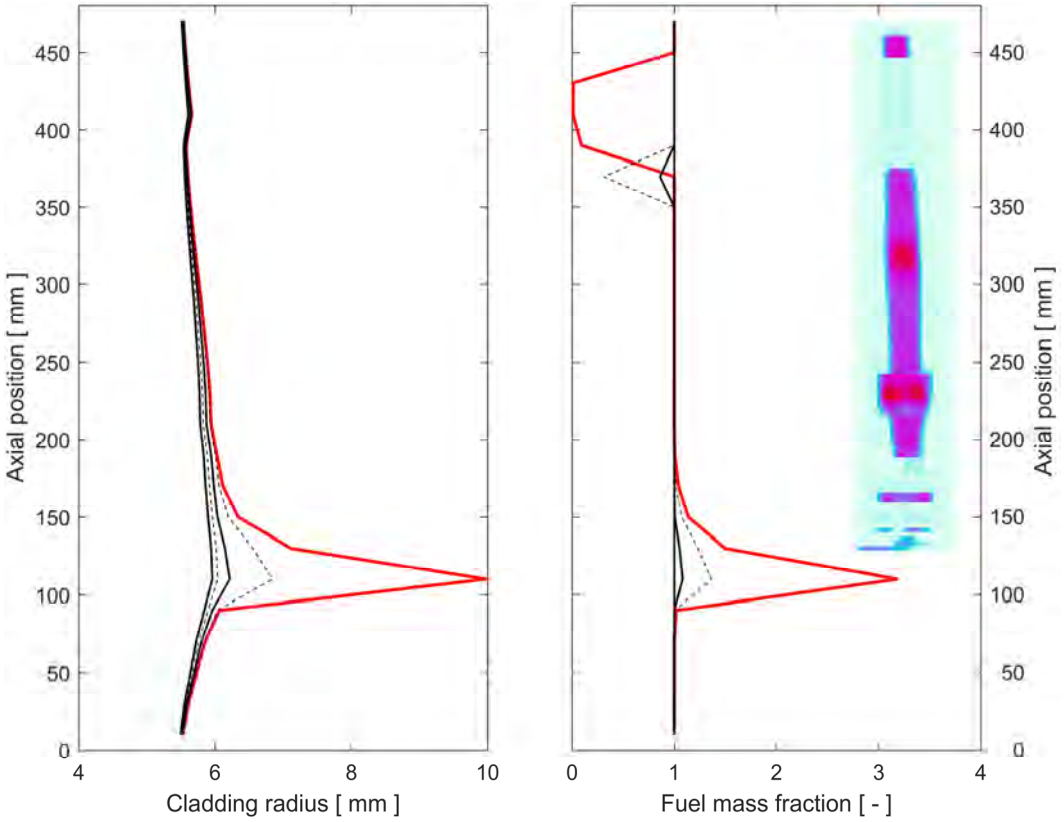

Fig. 15: Calculated evolution of cladding deformation (left) and fuel relocation (right) during the last four seconds before cladding rupture. The rightmost curve (red) represents the conditions at time of rupture, while the four curves to the left of it show the calculated state 1, 2, 3 and 4 seconds before rupture. A post-test gamma scan image of the IFA-650.9 test rig is included for comparison [25].

The calculations suggest that the local fuel mass is increased by a factor of 3.2 in the most distended cross section of the test rodlet. The relocated fuel originates

from a 50 mm long part of the fuel pellet column, which has disappeared completely. Above this emptied part, there is a “plug” of remaining fuel pellets at the very top of the fuel pellet column. This is well in line with the results reported from the test: Gamma scan (see insert in Fig. 15) showed that there were in fact a few remaining fuel pellets above the missing part of the fuel pellet column after the test. The length of the missing fuel part was 120–130 mm, which is about 70 mm longer than calculated with our model. Similar to the IFA-650.4 test, a significant amount of fuel had been expelled through the cladding breach and was found at the bottom of the pressure flask after the test [25, 48]. This dispersal of fuel fragments, which is not accounted for by our model, most certainly increased the amount of fuel lost from the upper part of the IFA.650.9 rodlet. The gamma scan results also show that there is a secondary hot spot, caused by fuel accumulation about the axial midplane of the rodlet. This is not captured by our model, since the secondary balloon is not reproduced; see below.

According to our calculations, the entire fuel column had been pulverized into fine (< 0.2 mm) fragments at time of cladding rupture, which means that the crumbled and relocated fuel had an assumed packing fraction of 0.72 everywhere in the ballooned region; see the description of the applied models for fuel fragmentation and pulverization in [15].

Fig. 16 shows the calculated post-test diameter profile of the IFA-650.9 rodlet, in comparison with data that were obtained by analysing visual inspection photos [48]. The calculated results differ from the measurements in two respects: the position of the primary balloon at the bottom part of the rod is a little bit too high, and the secondary balloon at the midplane of the rodlet is not captured at all. As with the IFA-650.4 test, the calculations suggest that axial relocation of hot fuel tends to localize the cladding deformation to the primary balloon.

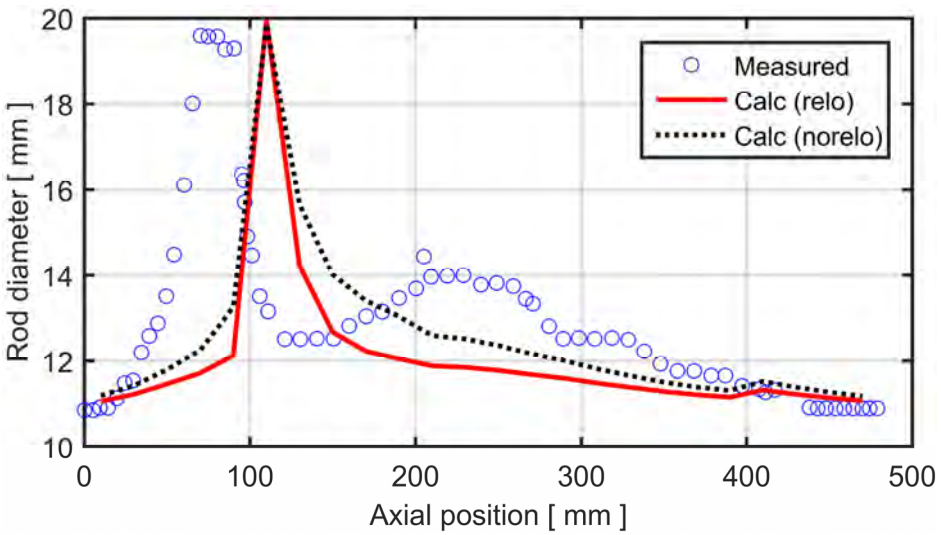

Fig. 16: Calculated and measured post-test diameter profiles for the IFA-650.9 rodlet [48].

Fig. 17 and Fig. 18 show comparisons of the calculated cladding surface temperature with measured data at different axial positions of the IFA-650.9 rodlet. The measured data clearly show that, at time of cladding rupture, the cladding temperature suddenly increases in the lower part of the rodlet, whereas it decreases in the upper part. This is a consequence of axial fuel relocation, and our calculations with the relocation model activated captures the observed thermal feedback effects fairly well. Fig. 19 and Fig. 20 are close-ups, showing the calculated and measured temperature variations about the time of cladding rupture (133 s in experiment, 133.5 and 137.8 s in calculations with and without fuel relocation, respectively).

We note from Fig. 17 and Fig. 19 that the cladding temperature at the primary balloon is overestimated after cladding rupture, when fuel relocation is considered in the calculations. This difference may be due to fuel ejection, possibly leading to a lower fuel fragment packing fraction and cladding temperature in the balloon than in our calculations, where fuel ejection into the coolant is not considered.

Two comments should also be made on Fig. 18 and Fig. 20: Firstly, the temperatures measured by TCC2 and TCC3 differ by up to 30 K after cladding rupture. This azimuthal temperature difference is probably due to bending of the rodlet [25, 48]. Secondly, the temperature drop caused by the fuel loss from the upper part of the rodlet is overestimated by our model. This may be explained either by the fact that axial heat conduction in the cladding tube is not considered in FRAPTRAN-1.5, or by the fact that some fuel actually remained in the upper part of the rodlet for some time after cladding rupture.

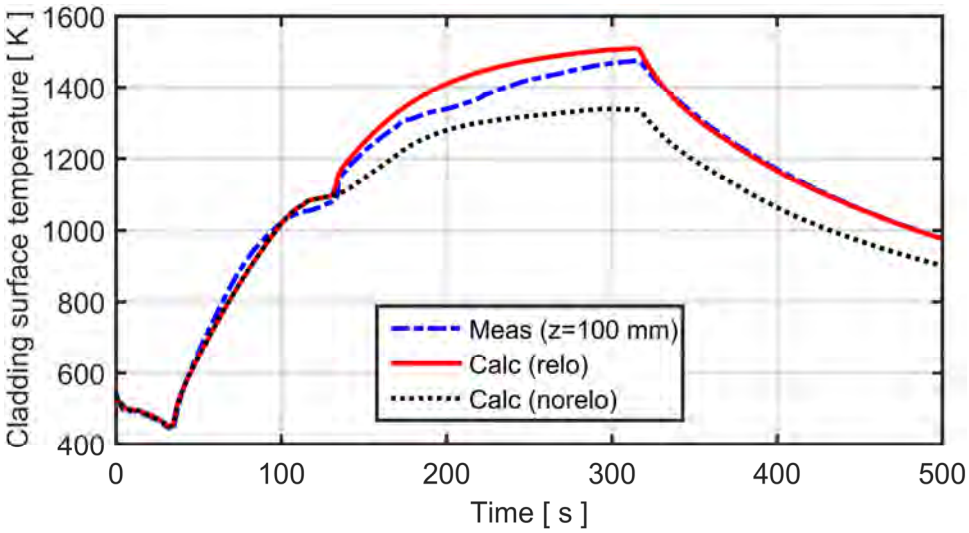

Fig. 17: Calculated and measured cladding surface temperature versus time. The presented temperature refers to the position of thermocouple TCC1, 100 mm above the bottom of the fuel pellet column; see Table 9.

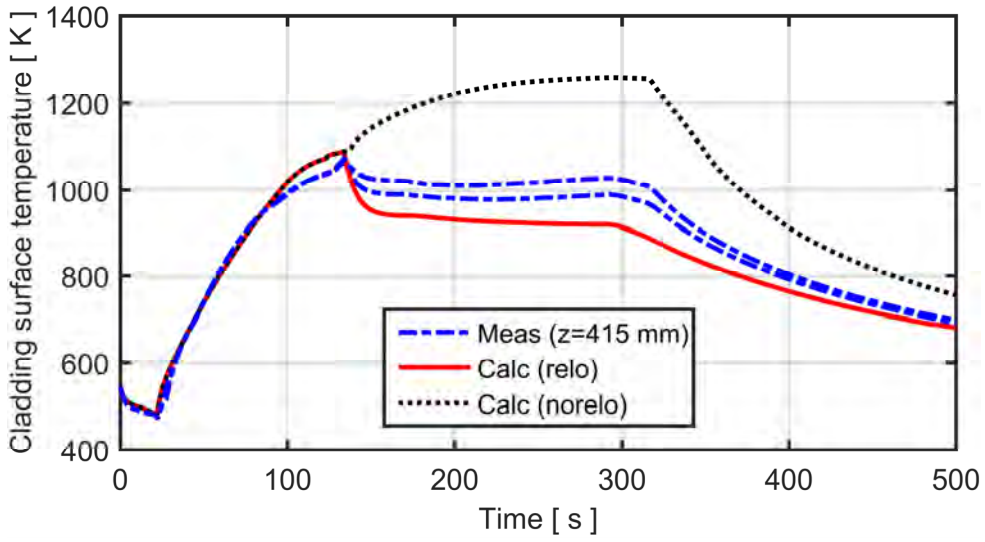

Fig. 18: Calculated and measured cladding surface temperature versus time. The temperature refers to the position of thermocouples TCC2 and TCC3, 415 mm above the bottom of the fuel pellet column; see Table 9.

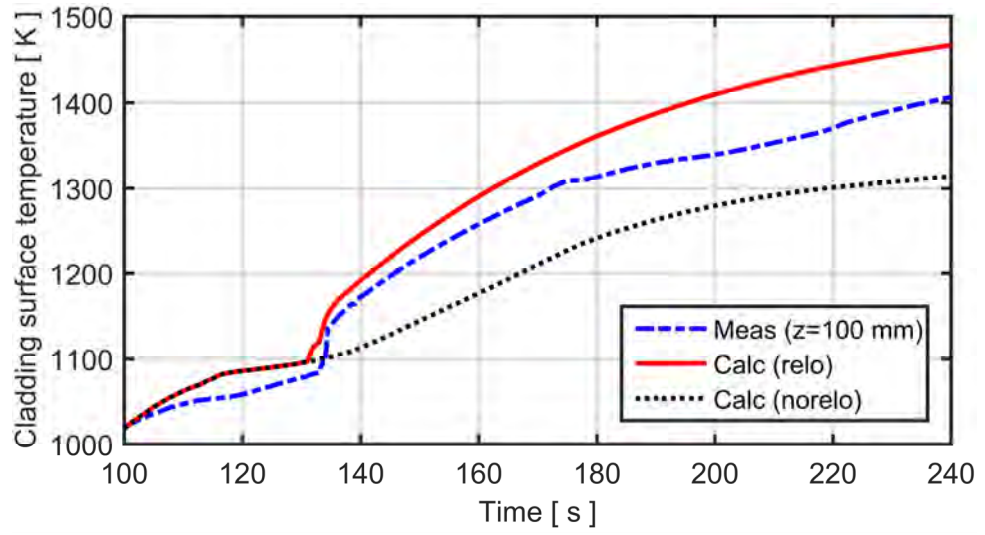

Fig. 19: Calculated and measured cladding surface temperature about the time of cladding rupture (133 s); close-up of Fig. 17.

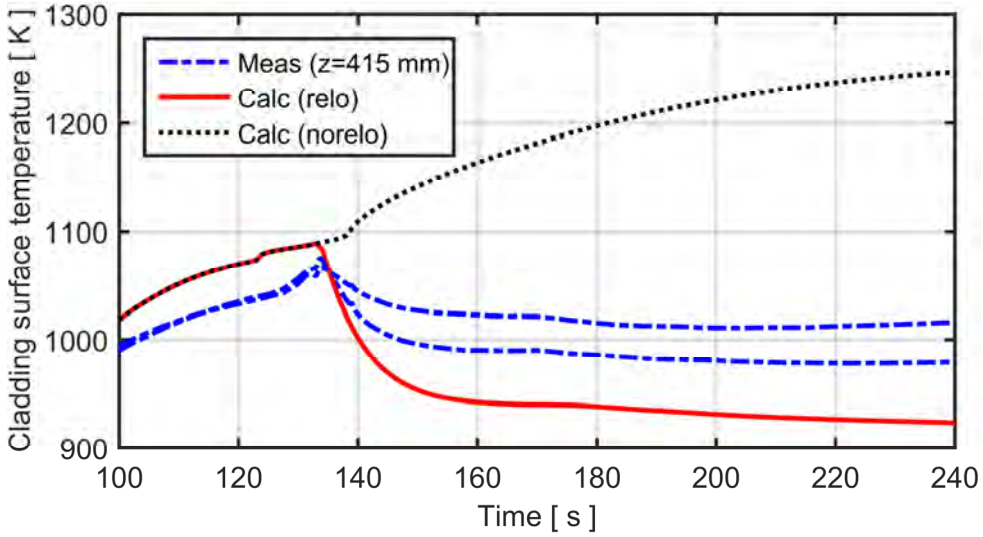

Fig. 20: Calculated and measured cladding surface temperature about the time of cladding rupture (133 s); close-up of Fig. 18.

The long term effect of fuel crumbling and axial relocation on the cladding temperature and oxidation for the IFA-650.9 test is illustrated by Fig. 21, which shows the calculated cladding outer surface temperature and equivalent cladding reacted versus axial position at time t = 500 s. As with the IFA-650.4 test, it is obvious that the calculated temperature field for the case with axial fuel relocation is governed by the axial distribution of fuel mass and power; compare the right panel of Fig. 15. The measured cladding surface temperatures are in perfect agreement with the calculated results for the case with fuel relocation.

As can be seen from the calculated post-test ECR in the right panel of Fig. 21, the long-term change in temperature distribution caused by the axial fuel relocation has a very strong effect on the post-failure oxidation of the cladding for test IFA-650.9. The reason is that the cladding was exposed to high temperature for a fairly long time, following axial fuel relocation and cladding rupture. The calculated pre-test ECR from low temperature oxidation in Gösgen was about 1.3 %; this pre-test oxidation is included in the curves presented in Fig. 21.

Since no systematic post-test measurements were made of the axial variation in cladding oxide thickness or metal oxygen concentration, the calculated axial distribution presented for the ECR in the right panel of Fig. 21 cannot be assessed against experimental data. However, metallography was carried out on three cross sections of the cladding tube, two of which were directly at the failed (primary) balloon in the lower end of the rodlet [48]. The thickness of the outer and inner oxide layer at the balloon was about 20 and 5 µm, respectively [48]. The corresponding values calculated with the Cathcart-Pawel oxidation model in FRAPTRAN-1.5 are 78 and 66 µm, respectively.

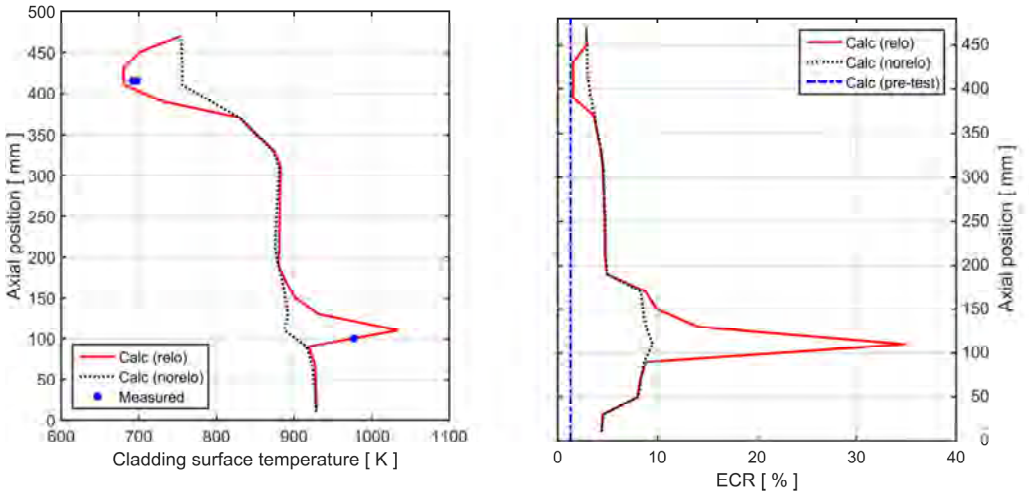

Fig. 21: Calculated cladding outer surface temperature and equivalent cladding reacted (ECR) versus axial position at time t = 500 s, with and without consideration of axial fuel relocation.

These large differences between calculated and measured oxide layer thicknesses cannot be explained by differences between calculated and measured cladding temperatures: as shown by Fig. 17, the local temperature at the primary balloon is fairly well reproduced by our extended version of FRAPTRAN. The only reasonable explanation to the differences is that local oxidation in the lower part of the fuel rod was limited by steam starvation, i.e. the cladding oxidation may have reduced the partial pressure of oxygen and created a gas enriched in hydrogen. This hypothesis is supported by the very high post-test hydrogen concentration, 1570 ±600 wppm, which was measured in the ballooned region of the cladding tube [48].

4.2.3. IFA-650.10

Fig. 22 shows the calculated and measured evolution of rod plenum gas pressure during the Halden IFA-650.10 test. In the calculations, the initial cold pressure was reduced from its reported value of 4.0 MPa to 3.98 MPa, to match the calculated "hot" pre-test gas pressure to the measured value (7.15 MPa). The calculated gas pressure is in close agreement with measurements for t < 160 s, but underestimated for the remaining period up to cladding rupture, which occurred at t = 249 s in this test. We also note that, upon cladding failure, the measured plenum pressure dropped instantaneously to about 1.2 MPa, according to Fig. 22. In reality, the gas pressure fell to that of the coolant (0.3–0.4 MPa), but mechanical constraints in the pressure transducer limited the measuring range.

In Fig. 22, the calculated curves for the cases with and without assumed fuel relocation coincide up to t = 247 s, which is the time when fuel fragments start to relocate axially, according to our calculations. The calculated time of cladding fail-

ure is 249.9 s for the case with fuel relocation and 259.1 s without. These results suggest that cladding ballooning, collapse of the fuel pellet column, and axial relocation of fuel take place within three seconds before cladding rupture.

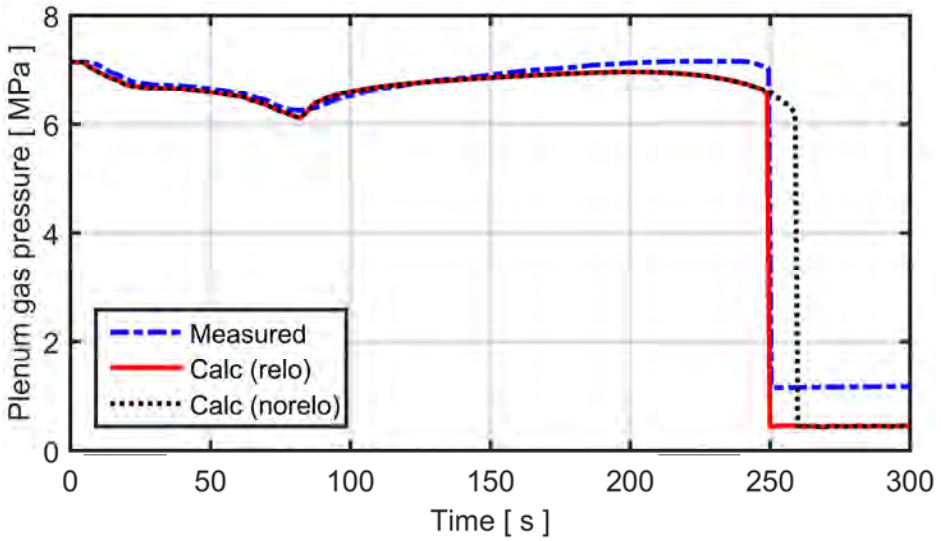

Fig. 22: Calculated evolution of rod plenum gas pressure in comparison with measurements [26] for the IFA-650.10 test rodlet.

Fig. 23 shows the calculated evolution of cladding deformation and axial fuel relocation during these last three seconds before cladding rupture. The thick red line shows the calculated state at the time of cladding rupture, and the leftmost curve shows the conditions about the time when the balloon starts to grow and fuel starts to relocate. The calculations suggest that the local fuel mass is increased by a factor of 1.3 in the most distended cross section of the test rodlet. The relocated fuel originates from the upper part of the balloon and the region just above the balloon. Hence, our relocation model does not calculate any long range axial fuel relocation in the upper part of the rodlet, in contrast to the other IFA-650 tests considered in this report. As can be seen from the inserted gamma scan image in Fig. 23, this result agrees with the relocation pattern observed in the test [49]. Axial fuel relocation was observed only within the ballooned region of the rodlet, where fuel fragments were missing from the upper part. As seen from the inserted gamma scan image in Fig. 23, a small quantity of fuel had been ejected through the rupture opening and was found at the bottom of the test rig after the test [49].

The IFA-650.10 rodlet had an average fuel burnup of 61 MWd(kgU)$^{-1}$, which is significantly lower than other test rods considered in this report. As can be seen from Table 5, only 11 % of the fuel had a calculated local burnup in excess of 70 MWd(kgU)$^{-1}$, which is a necessary condition for fuel pulverization in the applied models for fuel fragmentation and pulverization [15]. Consequently, according to our calculations, 11 % of the fuel in the region where cladding ballooning and fuel relocation took place had been pulverized into fine (< 0.2 mm) fragments at time

of cladding rupture. This result seems to agree qualitatively with findings from the post-test examinations [49], but the post-test fuel fragment size distribution was unfortunately not measured for this test. The calculated mixture of large and small fuel fragments leads to an estimated packing fraction of 0.77 everywhere in the ballooned region [15]. This packing fraction is slightly higher than that calculated for the IFA-650.4 and IFA-650.9 rodlets (0.72), in which the entire fuel inventory was assumed to pulverize during the tests.

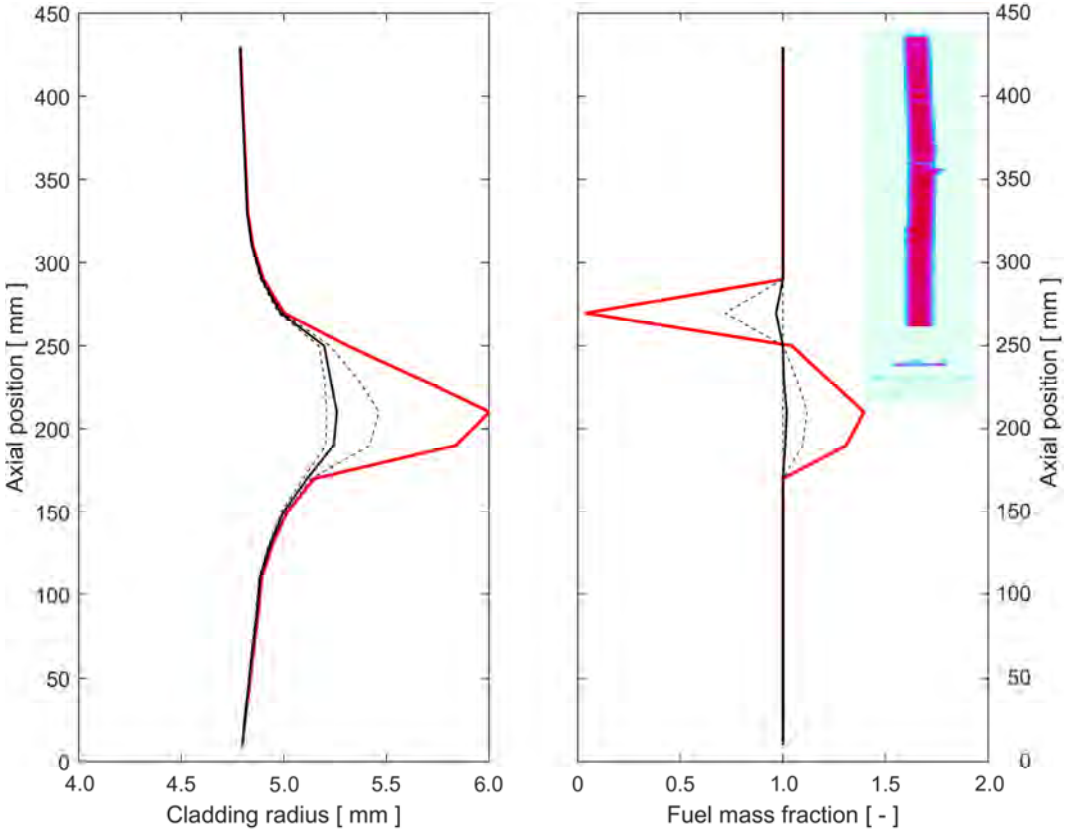

Fig. 23: Calculated evolution of cladding deformation (left) and fuel relocation (right) during the last three seconds before cladding rupture. The rightmost curve (red) represents the conditions at time of rupture, while the three curves to the left of it show the calculated state 1, 2 and 3 seconds before rupture. A post-test gamma scan image of the IFA-650.10 rig is included for comparison [49].

Fig. 24 shows the calculated post-test diameter profile of the IFA-650.10 rodlet in comparison with data that were obtained by analysing visual inspection photos and neutron radiographs [49]. It is clear from Fig. 24 that the length of the ballooned region is overestimated, and the calculated axial position of the balloon is slightly lower than actually observed. As seen also for the other IFA-650 tests in this report, the calculated results presented in Fig. 24 suggest that axial relocation of hot fuel tends to localize the cladding deformation to the balloon.

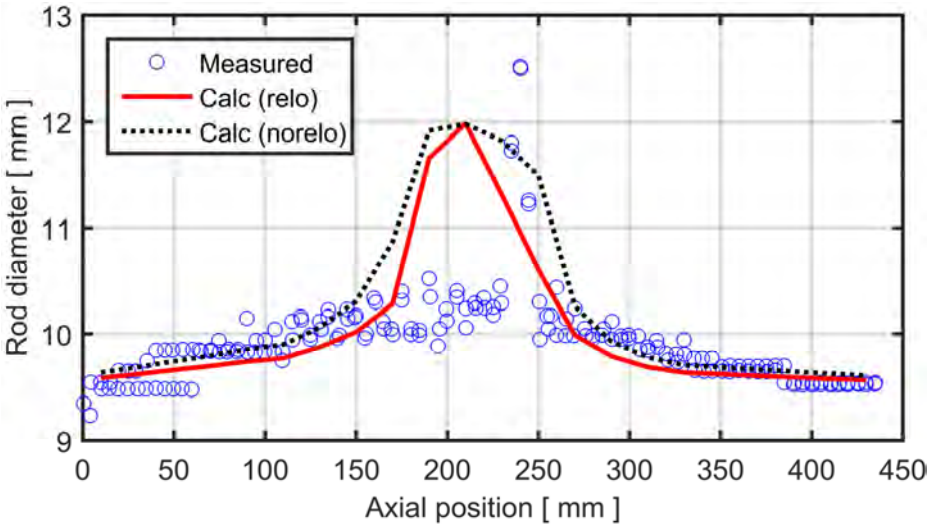

Fig. 24: Calculated and measured post-test diameter profiles for the IFA-650.10 rod [49].

Fig. 25 and Fig. 26 show comparisons of the calculated cladding surface temperature with measured data at different axial positions of the IFA-650.10 rodlet. In addition, Fig. 27 and Fig. 28 are close-ups, showing the calculated and measured temperature variations about the time of cladding rupture (249 s in experiment, 249.9 and 259.1 s in calculations with and without fuel relocation, respectively). The measured data show that, at time of cladding failure, the cladding temperature dropped temporarily for a few seconds in the upper part of the rodlet. This is attributed to cooling from the rod internal gas, which flowed from the relatively cool gas plenum towards the cladding breach [26]. As shown by the data in Fig. 22, the axial gas flow from the plenum was fast in the IFA-650.10 rodlet.

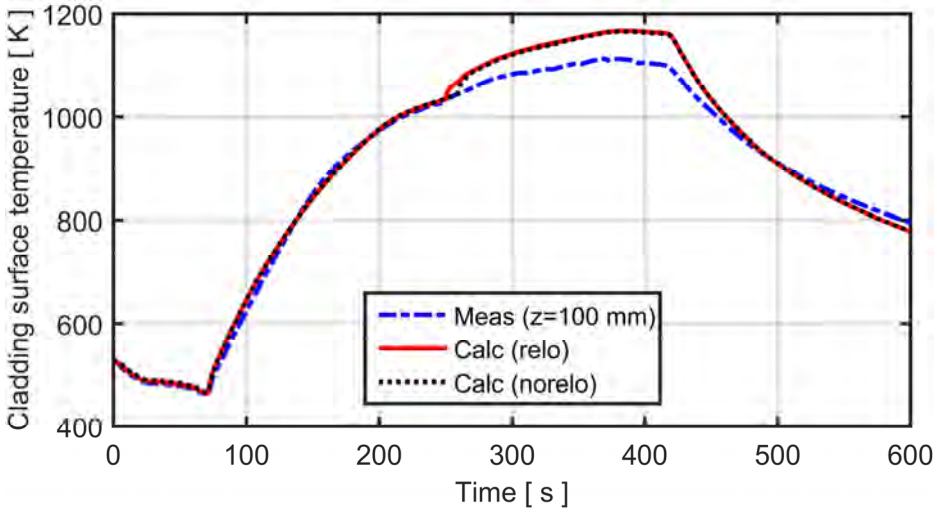

Fig. 25: Calculated and measured cladding surface temperature versus time. The presented temperature refers to the position of thermocouple TCC1, 100 mm above the bottom of the fuel pellet column; see Table 10.

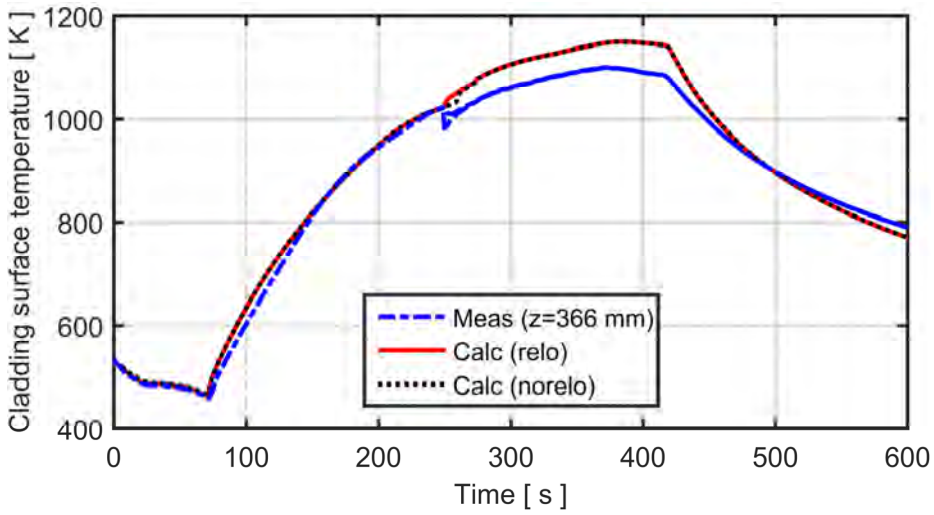

Fig. 26: Calculated and measured cladding surface temperature versus time. The temperature refers to the position of thermocouples TCC2 and TCC3, 366 mm above the bottom of the fuel pellet column; see Table 10.

Effects of cooling from flowing gas in the pellet-cladding gap are not considered in FRAPTRAN-1.5 [18], and the temperature dip measured by TCC2 and TCC3 is therefore not captured in our calculations. The calculations in fact suggest that the cladding temperature increases by 10–15 K immediately upon cladding failure. This calculated temperature rise is an artificial effect, caused by the assumption made in FRAPTRAN-1.5 that steam completely and immediately replaces the rod internal gas from the time of cladding rupture [18].

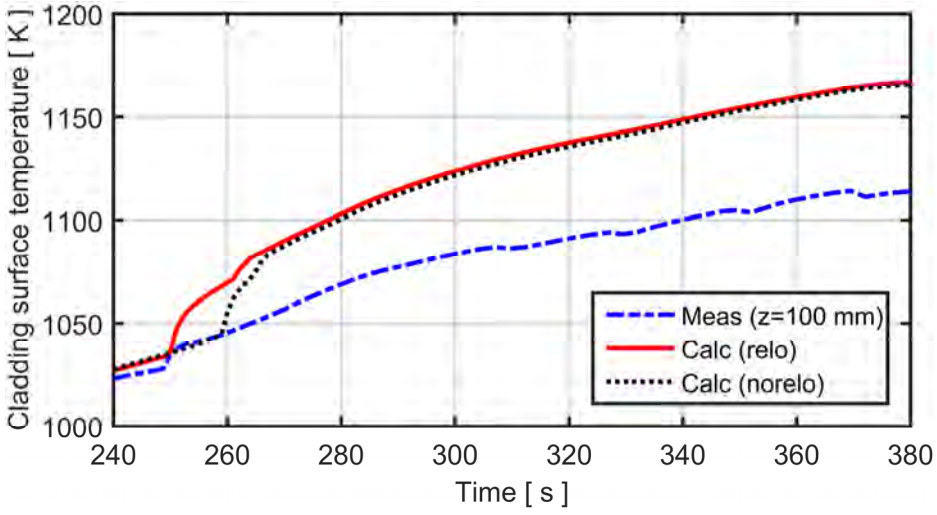

Fig. 27: Calculated and measured cladding surface temperature about the time of cladding rupture (249 s); close-up of Fig. 25.

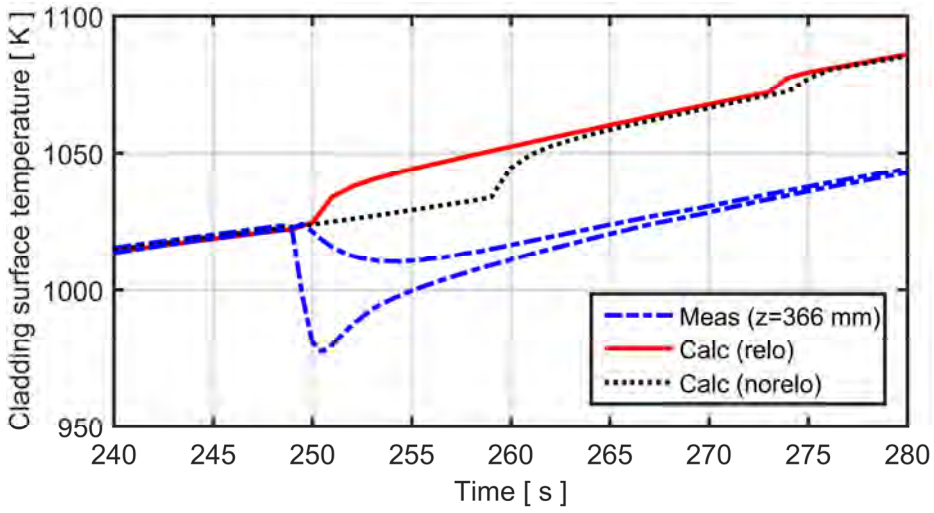

Fig. 28: Calculated and measured cladding surface temperature about the time of cladding rupture (249 s); close-up of Fig. 26.

From Fig. 25 and Fig. 26, it is clear that the cladding surface temperature is overestimated by 40–50 K at both ends of the IFA-650.10 rodlet after cladding failure. The difference is larger than observed for the other IFA-650 tests considered in this report, and the reason is unclear. A possible explanation is that the water spraying cooled the cladding to a larger extent than in the other considered IFA-650 tests; see section A.3, Appendix A. Direct cooling effects from water spraying would not be captured in our calculations, since they are not addressed by the applied thermal-hydraulic boundary conditions; see Appendix C.

Fig. 29 shows the calculated cladding outer surface temperature and equivalent cladding reacted versus axial position at time t = 600 s. Similar to the results presented previously for IFA-650.4 and IFA-650.9, the calculated temperature field for the case with axial fuel relocation is governed by the axial distribution of fuel mass and power. However, the calculated temperature changes caused by the relocated fuel are moderate. The reason is that the calculated amount of relocated fuel is fairly small in the IFA-650.10 test; compare the right panel of Fig. 23. The cladding surface temperature at t = 600 s is underestimated by about 20 K, which is more than for the IFA-650.4 and IFA-650.9 tests.

As can be seen from the calculated post-test ECR in the right panel of Fig. 29, the long-term change in temperature distribution caused by the axial fuel relocation has a moderate effect on the post-failure oxidation of the IFA-650.10 cladding. The calculated pre-test ECR from low temperature oxidation in Gravelines 5 was about 3 %; this pre-test oxidation is included in the curves presented in Fig. 29.

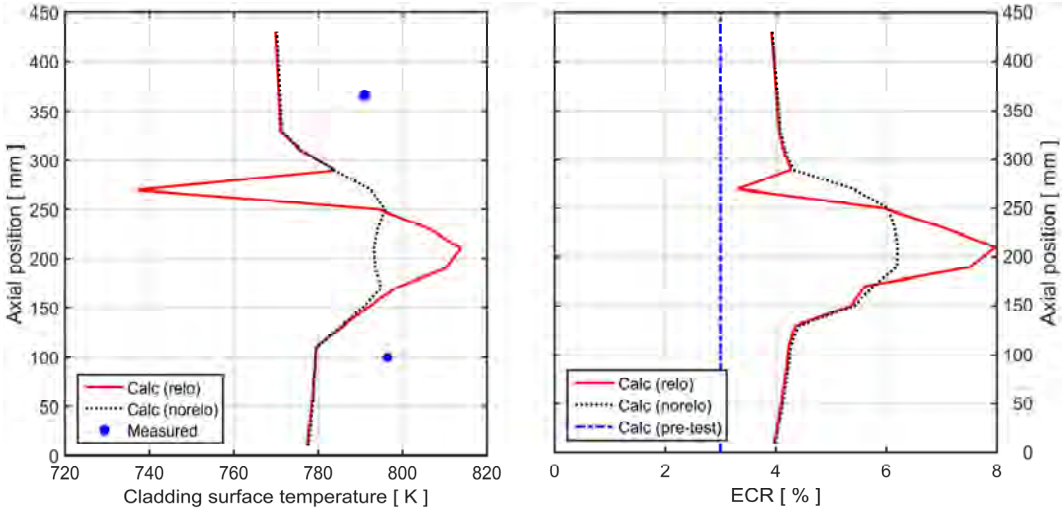

Fig. 29: Calculated cladding outer surface temperature and equivalent cladding reacted (ECR) versus axial position at time t = 600 s, with and without consideration of axial fuel relocation.

The thickness of the oxide layer at the cladding inner and outer surfaces was measured in post-test metallographic investigations [49]. Measurements were made over a 120 mm long section of the cladding, which was centred at the failed balloon. Mean values of the inner surface oxide thickness at various axial positions were in the range of 9–15 µm, while the outer surface oxide was 34–39 µm thick [49]. The calculated results from our extended version of FRAPTRAN-1.5 agree very well with these measurements: the best-estimate peak values for the post-test inner and outer surface oxide layer thickness in the balloon were 12.6 and 35.9 µm when fuel relocation was considered in the calculations, and 8.6 and 31.8 µm when the relocation model was deactivated. The cladding high temperature oxidation is thus accurately reproduced for the IFA-650.10 test, in contrast to the IFA-650.4 and IFA-650.9 tests. This suggests that the water spraying in the IFA-650.10 test was sufficient to maintain cladding oxidation (no steam starvation as suspected for the IFA-650.9 test). The cladding temperature, and thus the oxidation rate, was fairly low in the IFA-650.10 test.

4.2.4. IFA-650.14

The IFA-650.14 test rodlet had an average fuel burnup of 70.8 MWd(kgU)$^{-1}$. According to our calculations, about 32 % of the fuel reached a local burnup above 70 MWd(kgU)$^{-1}$, which is a necessary condition for fuel pulverization in our applied model for fuel fragmentation and pulverization [15]. However, since the fuel temperatures remained low in the test, only 22 % of the fuel pulverized, according to our simulations. The resulting mixture of small and large fuel fragments that relocated into the ballooned region of the cladding tube had a calculated packing fraction of 0.84, which is much higher than for the other tests considered in this report.

The calculated fraction of pulverized fuel, 22 %, disagrees with the results from post-test sifting of the fragmented fuel [41]. According to these measurements, only 0.6 % of the dislodged fuel fragments were smaller than 0.25 mm; see section A.4 in Appendix A. Because of the large difference between calculated and measured fractions of pulverized fuel for the IFA-650.14 test, we used the measured rather than the calculated fraction in calculations with our relocation model. More precisely, we postulated that the maximum value for the fuel fragment packing fraction of crumbled fuel, ϕ_m, is 0.69. This value is based on measured data from LOCA tests on low-burnup fuel, in which no fuel pulverization was observed [15]. In addition, we also considered a case with ϕ_m = 0.72, which corresponds to the fuel fragment packing fraction used for analyses of the IFA-650.4 and IFA-650.9 rodlets in this report. The purpose was to illustrate the sensitivity of the calculated results to the packing fraction assumed for the crumbled fuel.

In addition, we considered transient fission gas release in our analyses of the Halden IFA-650.14 test. As mentioned in section 3.3, the transient fission gas release must be modelled for this test, since it resulted in a threefold increase of the amount of free gas within the rodlet. For lack of a transient fission gas release model in FRAPTRAN-1.5, we postulated a smooth ramp function for the fission gas release, as defined by eq. (1) in section 3.3. This function is shown in Fig. 30, together with the calculated evolution of fuel pellet temperature at the peak power axial position of the rodlet. It is clear that significant transient fission gas release is assumed to occur at fuel temperatures above 900 K.

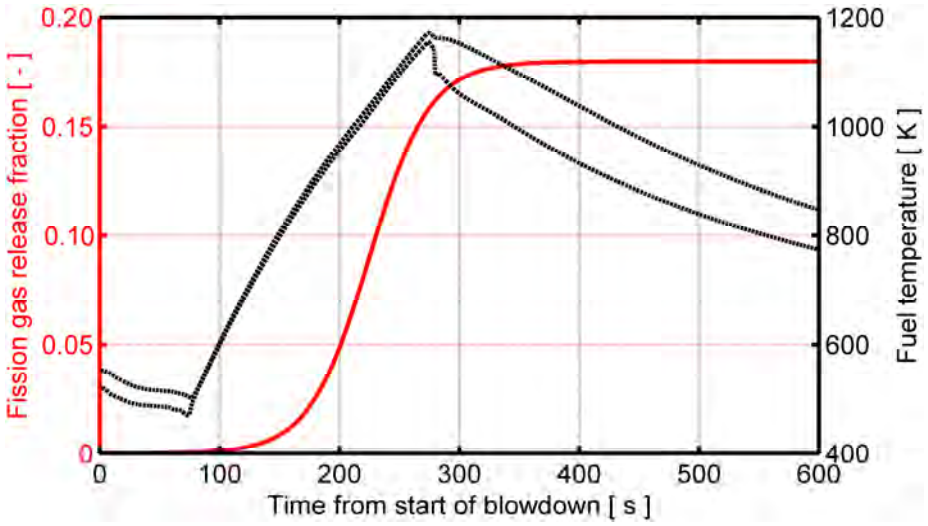

Fig. 30: The red full line shows the assumed time history for the transient fission gas release; see eq. (1). The black dashed lines show the calculated fuel temperatures for the pellet centre and surface at the peak power axial position of the IFA-650.14 test rodlet.

Fig. 31 shows the calculated and measured evolution of rod plenum gas pressure during the Halden IFA-650.14 test. In the calculations, the initial cold pressure was reduced from its reported value of 2.0 MPa to 1.66 MPa, to match the calcu-

lated “hot” pre-test gas pressure to the measured value (3.49 MPa). The calculated gas pressure is in close agreement with measurements throughout the test. The best agreement is obtained for the case with ϕ_m = 0.72, but the influence of axial fuel relocation and assumed fuel fragment packing fraction is moderate.

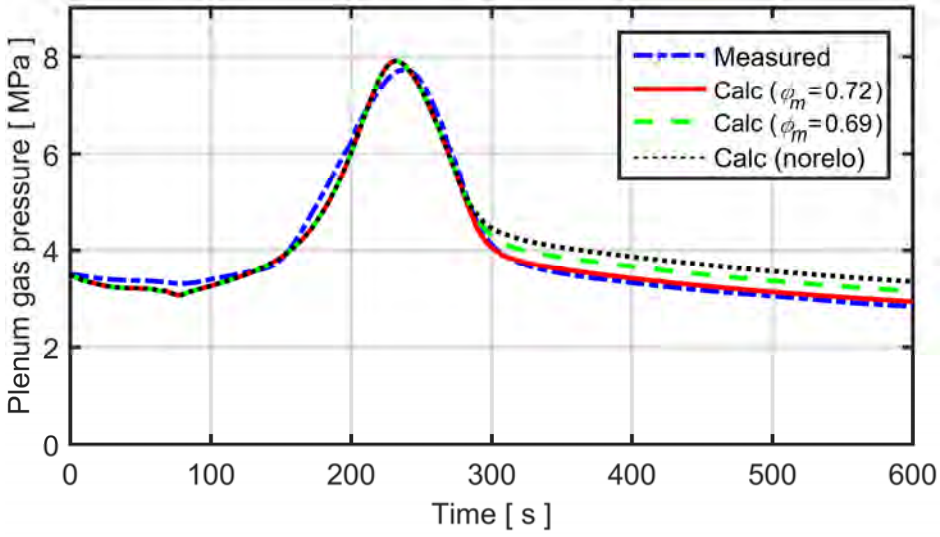

Fig. 31: Calculated evolution of rod plenum gas pressure in comparison with measurements [28] for the IFA-650.14 test rodlet. Here, ϕ_m is the postulated max value for the fuel fragment packing fraction in the relocation model.

Fig. 32 and Fig. 33 show the evolution of cladding deformation and axial fuel relocation, calculated with ϕ_m = 0.72 and ϕ_m = 0.69, respectively. The results pertain to the time interval from 280 to 340 s, in which a cladding balloon is calculated to form just above the axial midplane of the rodlet. The calculations suggest that the local fuel mass is increased by a factor of 1.50 or 1.25 in the most distended cross section of the test rodlet, depending on the value assumed for the fuel fragment packing fraction in the balloon. The relocated fuel originates from the very top of the fuel pellet column, according to our calculations. This is not fully consistent with results reported from post-test neutron radiography of the rodlet, which showed that a 35 mm long section (“plug”) of the fuel pellet column remained at the very top [41].

It is interesting to compare the fairly long (~60 s) period under which the balloon develops in the IFA-650.14 test with the very much shorter ballooning times calculated for the other IFA-650 tests in this report. The difference is caused by the exceptionally small free internal gas volume in the IFA-650.14 rodlet; see Table 1. This effect of internal gas volume is significant to the expected rupture behaviour of full-length LWR fuel rods under LOCA; see section 5.2.

Fig. 34 shows the calculated post-test diameter profile for the IFA-650.14 rodlet in comparison with data that were obtained by contact profilometry [41]. The position of the primary balloon is accurately reproduced, but the local cladding de-

formation at the balloon is underestimated. The calculated peak deformation depends strongly on the assumed packing fraction of the fuel fragments.

Fig. 35 and Fig. 36 show comparisons of the calculated cladding surface temperature with measured data at different axial positions of the IFA-650.14 rodlet. In addition, Fig. 37 and Fig. 38 are close-ups, showing the calculated and measured temperature variations about the time of reactor scram (275 s). It is clear that the cladding surface temperature is reproduced quite well by our extended version of FRAPTRAN-1.5, both in the lower and upper part of the rodlet. The largest differences between calculated and measured temperatures, about 20 K, are found in the upper part of the rodlet, following reactor scram.

There is no evidence of axial fuel relocation in the measured histories for the cladding surface temperature in IFA-650.14. From Fig. 37, it is clear that the calculated cladding surface temperature at z = 100 mm is increased by a few kelvin as a result of calculated fuel relocation. As can be seen from Fig. 32 and Fig. 33, the fuel mass fraction at z = 100 mm is somewhat increased by fuel relocation, according to our calculations.

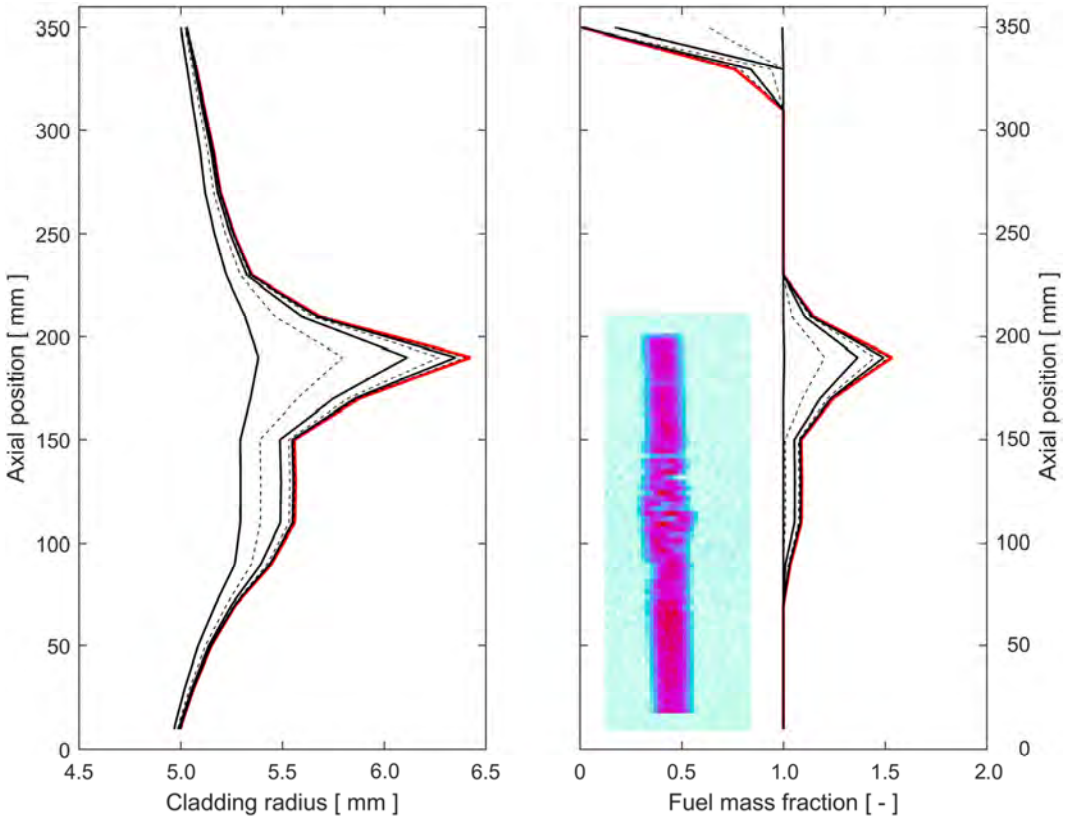

Fig. 32: Calculated evolution of cladding deformation (left) and fuel relocation (right) during the time interval from 280 to 340 s. The calculations were done with a postulated max fuel fragment packing fraction (ϕ_m) of 0.72. A post-test gamma scan image of the IFA-650.14 rodlet is included for comparison [28].

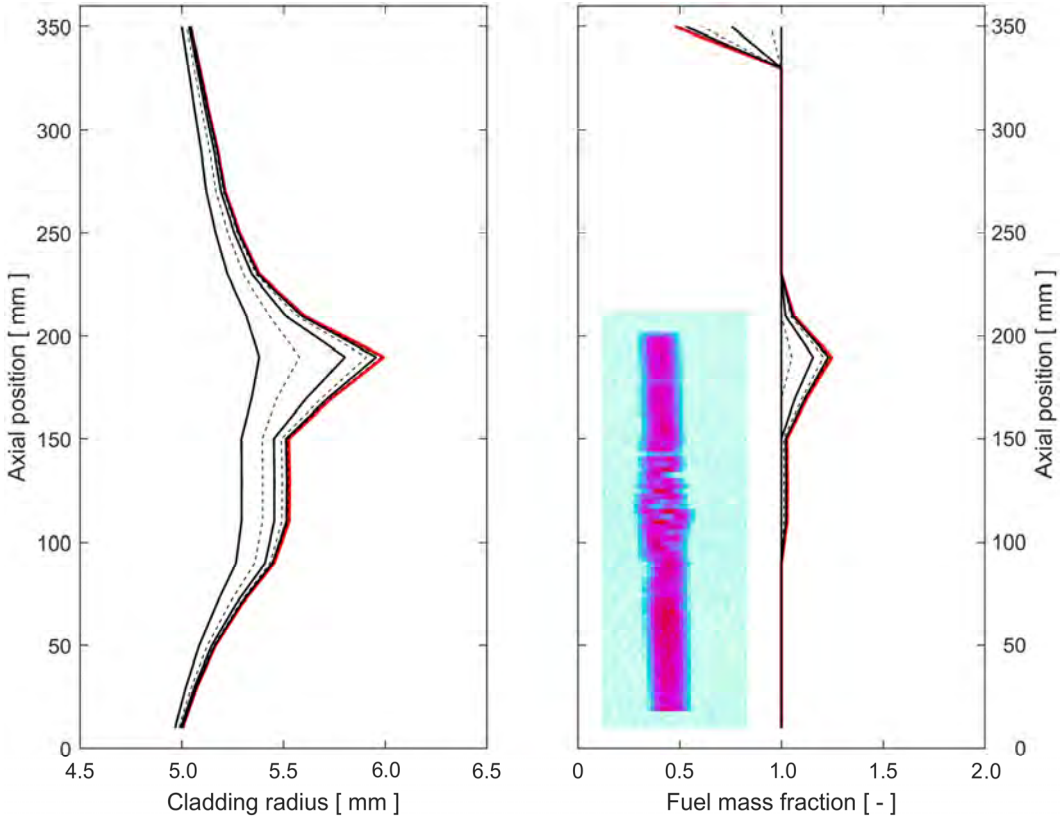

Fig. 33: Calculated evolution of cladding deformation (left) and fuel relocation (right) during the time interval from 280 to 340 s. The calculations were done with a postulated max fuel fragment packing fraction (ϕ_m) of 0.69. A post-test gamma scan image of the IFA-650.14 rodlet is included for comparison [28].

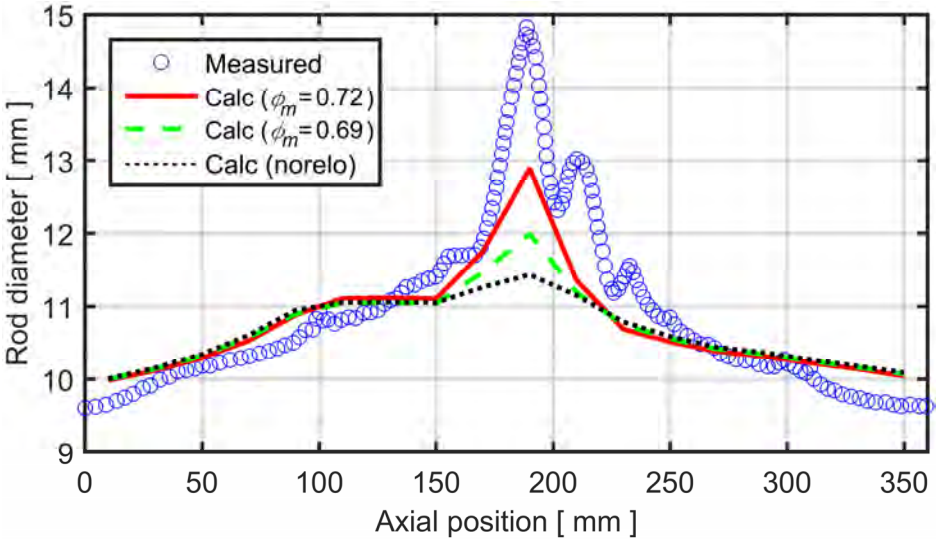

Fig. 34: Calculated and measured post-test diameter profiles for the IFA-650.14 rod [41].

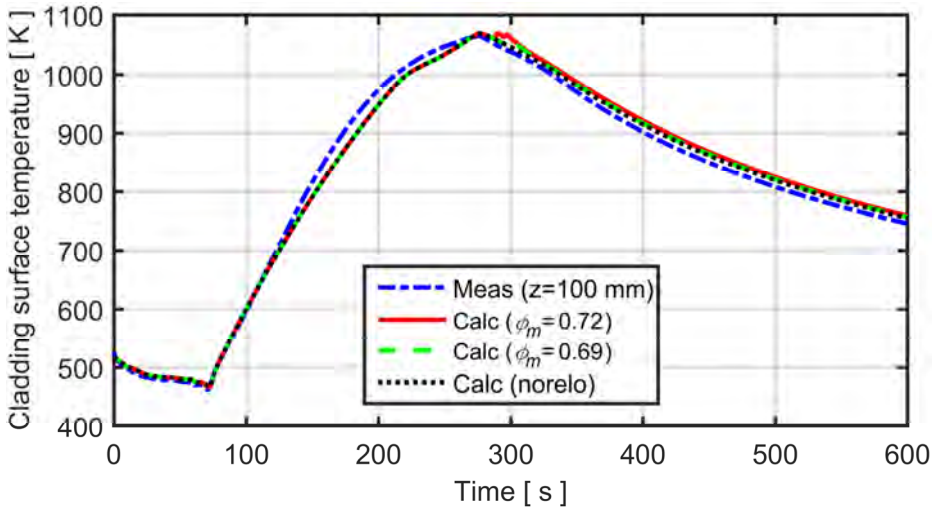

Fig. 35: Calculated and measured cladding surface temperature versus time. The temperature refers to the position of thermocouple TCC1, 100 mm above the bottom of the fuel pellet column; see Table 11.

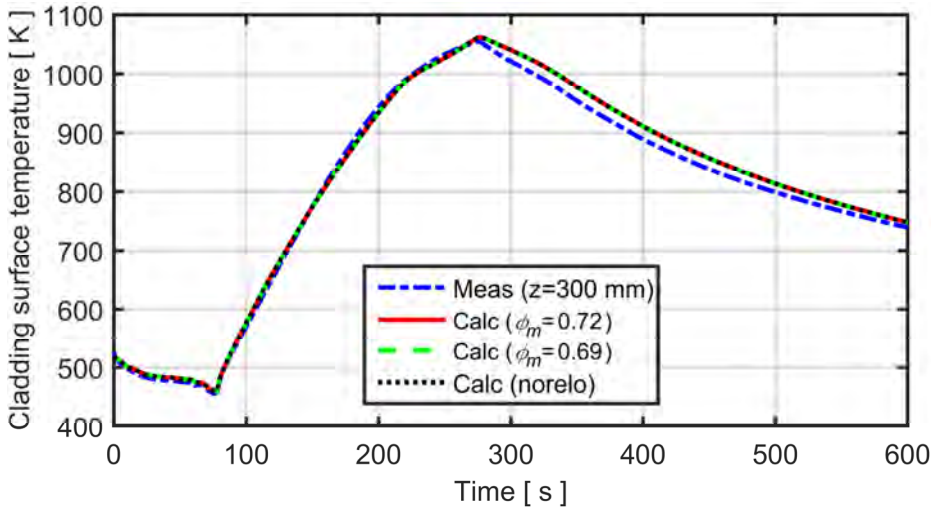

Fig. 36: Calculated and measured cladding surface temperature versus time. The temperature refers to the position of thermocouple TCC2, 300 mm above the bottom of the fuel pellet column; see Table 11.

The calculated effect of the relocation on cladding surface temperature is transitional; as can be seen from Fig. 37, the calculated temperature increase drops from 10–15 K just after the relocation has occurred to less than 5 K within about 30 s. The temperature increase depends on the packing fraction assumed for the fuel fragments.

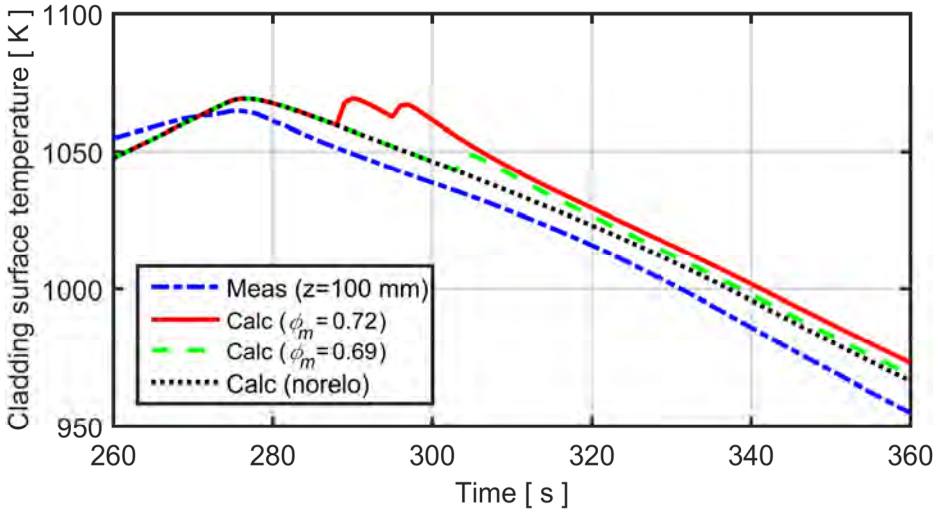

Fig. 37: Calculated and measured cladding surface temperature about the time of reactor scram (275 s); close-up of Fig. 35.

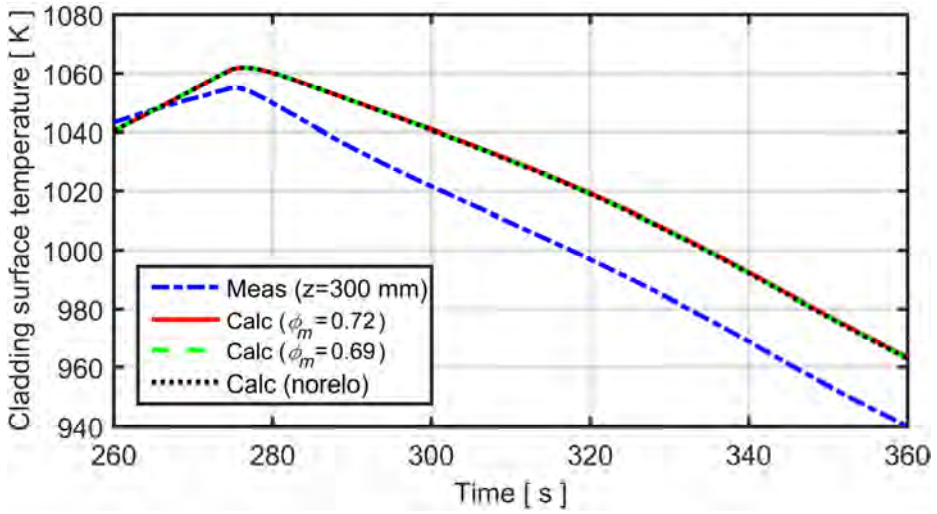

Fig. 38: Calculated and measured cladding surface temperature about the time of reactor scram (275 s); close-up of Fig. 36.

Fig. 39 shows the calculated cladding outer surface temperature and equivalent cladding reacted versus axial position at time t = 600 s. Similar to the calculated results for other tests in the Halden IFA-650 series, the calculated temperature fields for the cases with axial fuel relocation are governed by the axial distribution of fuel mass and power. However, the temperature increase in the ballooned region, caused by the relocated fuel, is less than 25 K. The reason is that the calculated amount of relocated fuel is small in the IFA-650.14 test.

As can be seen from the calculated post-test ECR in the right panel of Fig. 39, the long-term change in temperature distribution caused by the axial fuel relocation has a moderate effect on the post-failure oxidation of the IFA-650.14 cladding. The calculated pre-test ECR from low temperature oxidation in Leibstadt was about 3.2 %; this pre-test oxidation is included in the curves presented in Fig. 39.

It should be remarked that the calculated post-test ECR in the uppermost part of the IFA-650.14 rodlet is apparently not affected by the temperature drop caused by the fuel loss. This peculiarity is due to the fact that FRAPTRAN-1.5 uses a cut-off temperature of 1073 K for the cladding metal-water reactions [18]. In the late part of the test, when fuel relocation occurred, the calculated cladding temperature in the upper part of the rodlet was below this temperature, which means that further cladding oxidation was neglected.

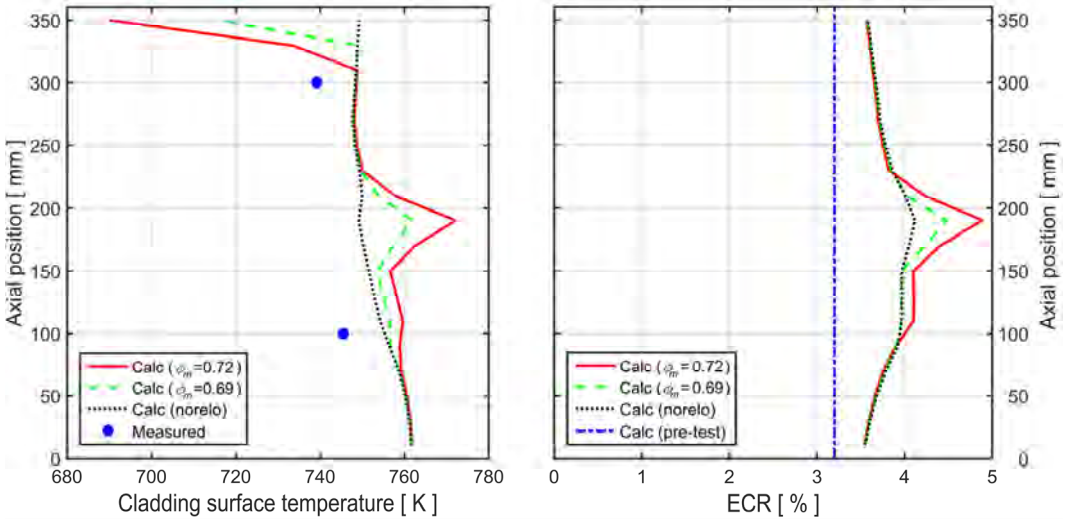

Fig. 39: Calculated cladding outer surface temperature and equivalent cladding reacted (ECR) versus axial position at time t = 600 s, with and without consideration of axial fuel relocation.

4.3. NRC-Studsvik-192 test

A major difference between the NRC-Studsvik LOCA simulation tests and the Halden IFA-650 tests is that the former are done out-of-reactor, i.e. without nuclear heating of the test rodlets. This means that effects of axial fuel relocation on the concentration of heat load to ballooned regions of the rodlets are negligible in the NRC-Studsvik tests: For example, our simulations of test 192 show that axial relocation of the cold fuel delays cladding rupture by 0.13 s, since the cladding tube is slightly cooled by the relocated and crumbled fuel in the balloon. This delay is practically insignificant, and so are all other calculated differences between the cases with and without axial fuel relocation for the NRC-Studsvik tests. In the

following, we therefore present calculated results only for the case with fuel relocation considered in the simulations.

Fig. 40 shows the calculated evolution of rod internal gas pressure in comparison with data from the pressure transducers connected to the lower and upper ends of the NRC-Studsvik-192 test rodlet. Henceforth, time zero refers to the beginning of heating from the initial temperature of 573 K; see section 2.2.3. From section 3.3, we recall that the gas pressure is calculated on the basis of calculated temperatures and deformations along the active length of the rodlet, together with an estimated temperature history for the gas within rod plena and connected gas lines; see section D.2 in Appendix D. The initial amount of free gas in the rodlet and its connected gas lines was adjusted in the calculations, such that a good match was obtained between the calculated and measured initial gas pressures.

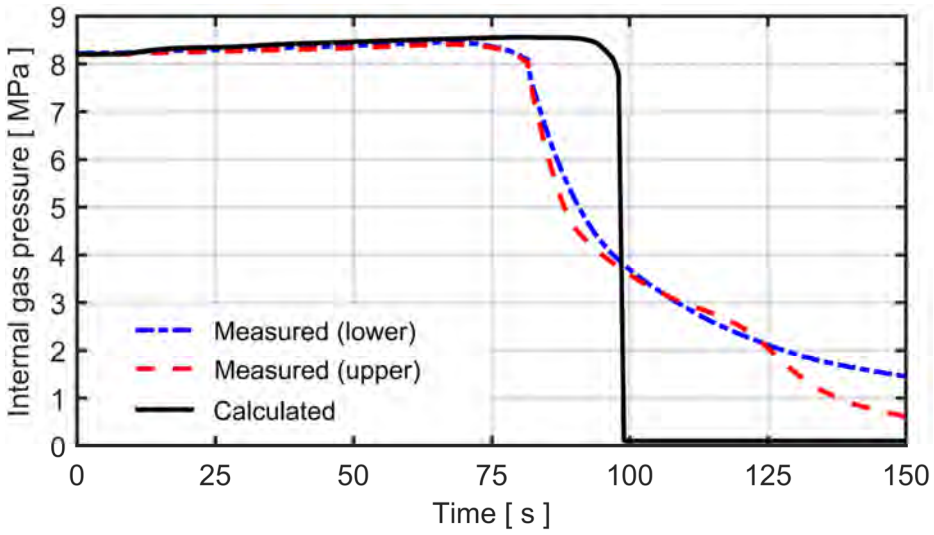

Fig. 40: Calculated evolution of rod internal gas pressure in comparison with data from the upper and lower end pressure transducer in the NRC-Studsvik-192 test rodlet [35].

It is clear from Fig. 40 that the internal gas pressure is fairly constant up to the point of cladding rupture. This is due to the large (12.58 cm^3) gas volume, and that most of the gas (10.60 cm^3) is held at nearly constant temperature during the test; see section D.2 in Appendix D. The two pressure transducers record a significant pressure drop, starting at t = 81 s, which is indicative of cladding rupture. Depressurization of the failed rodlet is fairly slow; the time constant for the pressure equilibration is about 20 s, which indicates that the flow path for the gas is restricted. This conclusion is supported by post-test examinations of the rodlet, which showed that about 48 % of the fuel pellet inventory remained within the cladding tube, even though the rodlet was broken in two halves and gently shaken to dislodge as much fuel as possible [3]. The fuel pellets at both ends of the rodlet thus remained in firm contact with the cladding tube. This explains the restricted flow path for the gas towards the cladding breach, which was slightly above the axial midplane of the rodlet.

From Fig. 40, it is also clear that the time to cladding rupture is overestimated; the calculated rupture time is 98.1 s, while the reported value is 81 s. This is a large difference, considering that the calculated rupture times for the three Halden IFA-650 tests are within seconds of the measured values; see sections 4.2.1 to 4.2.3. The most important reason for the large difference between the measured and calculated rupture time for the NRC-Studsvik test is that generic high-temperature material models for Zircaloy were used to represent the ZIRLO™ cladding in the calculations with our extended version of FRAPTRAN-1.5. This conclusion is based on a recent assessment of the aforementioned models against a large number of high temperature burst tests and LOCA simulation tests, which comprised both Zircaloy and ZIRLO™ cladding [50]. This assessment showed that the models reproduce rupture times for tests on Zircaloy cladding without bias, while rupture times for tests on ZIRLO™ cladding are systematically overestimated; see Figs. 25 and 27 in [50].

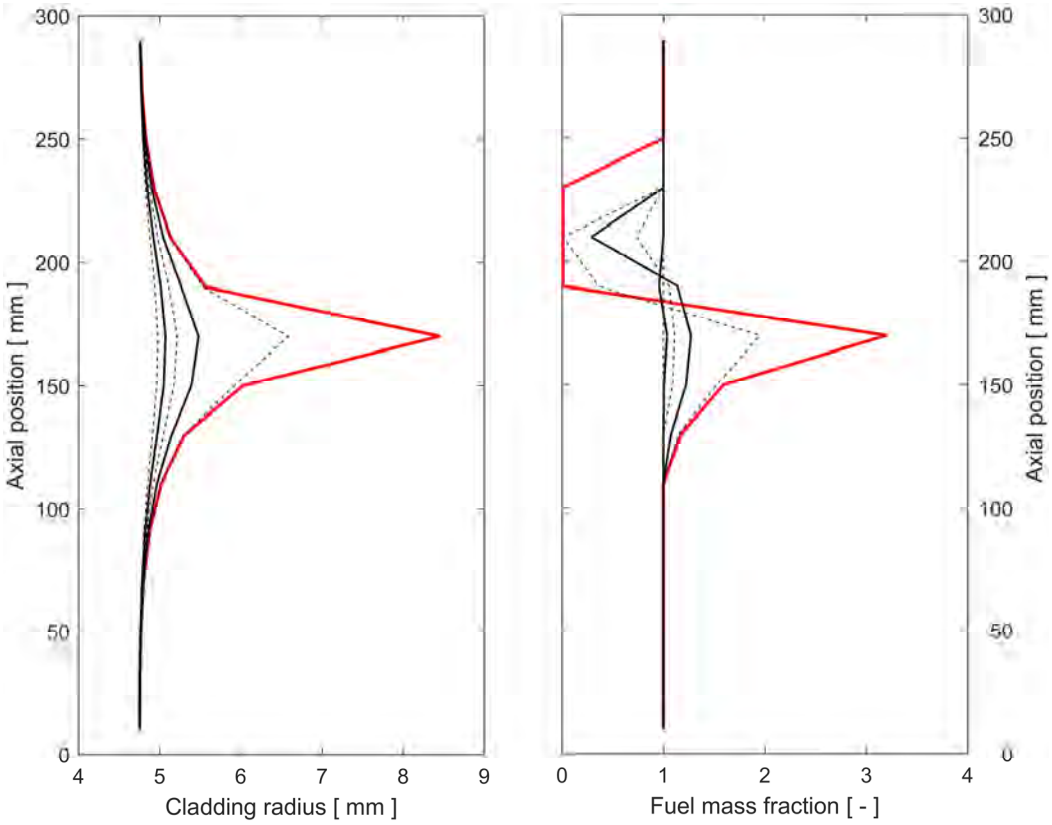

Fig. 41: Calculated evolution of cladding deformation (left) and fuel relocation (right) during the last five seconds before cladding rupture. The rightmost curve (red) represents the conditions at time of rupture, while the five curves to the left of it show the calculated state 1, 2, 3, 4 and 5 seconds before rupture.

Fig. 41 shows the calculated evolution of cladding deformation and axial fuel relocation during the last five seconds before cladding rupture. The thick red line shows the calculated state at the time of cladding rupture, and the leftmost curve shows the conditions about the time when the balloon starts to grow and fuel starts

to relocate. The calculations suggest that the local fuel mass is increased by a factor of 3.2 in the most distended cross section of the test rodlet. This value is comparable to the calculated results for the Halden IFA-650.4 and IFA-650.9 tests; see sections 4.2.1 and 4.2.2. The relocated fuel originates from the upper part of the balloon and the region just above the balloon, where a ~50 mm long section is completely emptied of fuel. Above this emptied section, there is a 60 mm long "plug" of remaining fuel pellets at the very top of the fuel pellet column. This is well in line with the results reported from the test: Wire probe measurements through the cladding breach just after the LOCA simulation test showed that fuel was missing from a 110 mm long segment of the rodlet. The missing part started about 120 mm and ended about 230 mm above the bottom of the fuel pellet column [3]. Later wire probe measurements and axial gamma scans, which were carried out after breaking and shaking the rodlet, revealed further fuel loss, mostly from the lower end [3].

According to our calculations, about 22 % of the fuel within the hot, central, part of the test rodlet had been pulverized into fine (< 0.2 mm) fragments at time of cladding rupture. The calculated degree of pulverization at the ends of the rodlet, where the temperature is significantly lower, was 11–14 %; see the description of applied models for fuel fragmentation and pulverization in [15]. After cladding rupture, the fuel temperature continued to increase, which according to our model led to further pulverization of the fuel. The calculated post-test mass fraction of pulverized fuel was 73 %. This value can be compared with results from post-test size distribution measurements, carried out by sifting of recovered fuel fragments [3]. These measurements showed that about 43 weight% of the fuel fragments collected from the NRC-Studsvik-192 rodlet were smaller than 0.25 mm. Hence, our model overestimates the fuel pulverization also for this test; compare with the similar results obtained for the IFA-650.14 test in section 4.2.4.

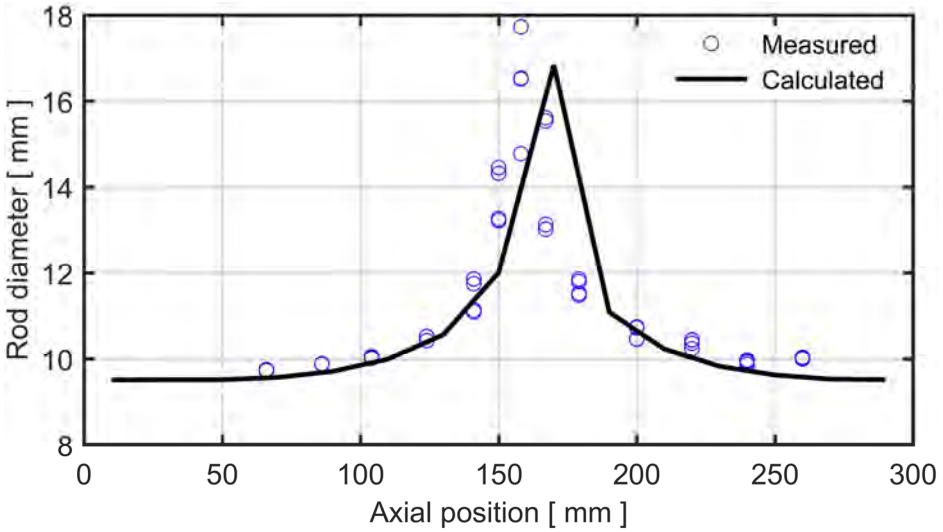

Fig. 42: Calculated and measured post-test diameter profiles for the NRC-Studsvik-192 test rodlet [35].

Fig. 42 shows the calculated post-test diameter profile of the NRC-Studsvik-192 test rodlet in comparison with measured data. The latter were obtained at thirteen axial positions, where the cladding tube diameter was measured in two perpendicular directions. This means that the data also provide some information on the degree of cylindrical symmetry for the deformation. It is clear from Fig. 42 that the calculated position of the cladding balloon is about 10 mm above the observed position. This is an acceptable difference, considering that the calculations were done with an axial discretization consisting of 20 mm long segments (nodes); see section 3.3. It is likely that a closer match would be obtained with a finer axial discretization. We also note that the cladding deformation outside the ballooned region is reproduced with fair accuracy. Very limited cladding deformation is obtained towards the ends of the rodlet, due to the axial temperature gradient in the test; see section D.1 in Appendix D, and Fig. 44 below.

Temperature gradients exist both in the radial and axial direction of the NRC-Studsvik-192 test rodlet. The radial temperature gradient, calculated at an axial position of 170 mm above the bottom of the fuel pellet column and at four different times during the test, is illustrated in Fig. 43. The considered times correspond to the conditions just after cladding rupture (99 s), attainment of peak cladding temperature (173 s), start of final quenching (297 s) and thirty seconds into the quenching (327 s). The results suggest that significant temperature gradients exist across the crumbled fuel in the balloon, particularly during quenching. It should be remarked that the calculations were done without considering possible cooling effects of water entering into the balloon through the cladding breach; the modelled heat removal was only by cooling at the cladding outer surface.

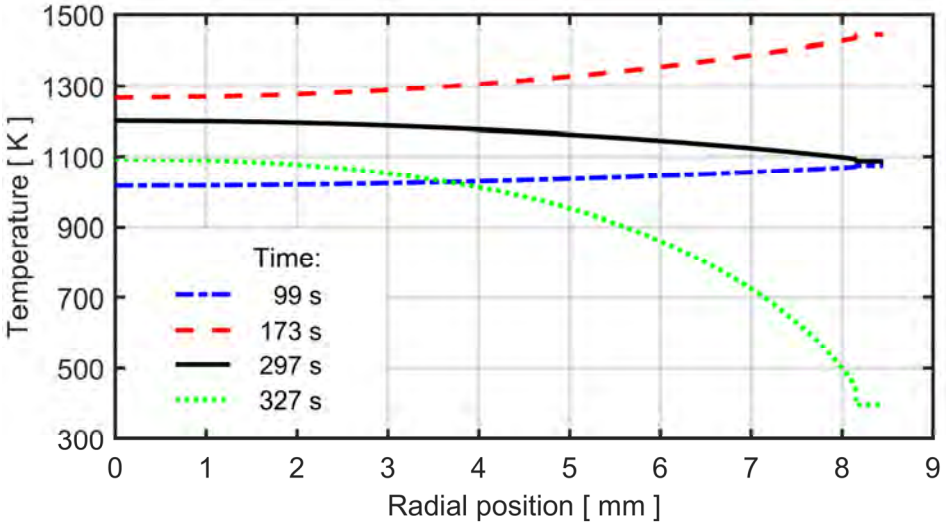

Fig. 43: Radial temperature distributions, calculated at an axial position 170 mm above the bottom of the fuel pellet column for four stages of the NRC-Studsvik-192 test.

The calculated axial temperature gradient, evaluated at the cladding outer surface, is shown in the left panel of Fig. 44. The difference between the peak temperature

position and the lower end of the rodlet is nearly 250 K, when the peak cladding temperature is attained (t = 173 s); see section D.1 in Appendix D. The axial temperature gradient leads to large differences in the cladding oxidation rate, which is illustrated by the post-test ECR in the right panel of Fig. 44. The marked peak at z = 170 mm is a result not only of the temperature peak, but also of substantial thinning of the cladding wall at the rupture position.

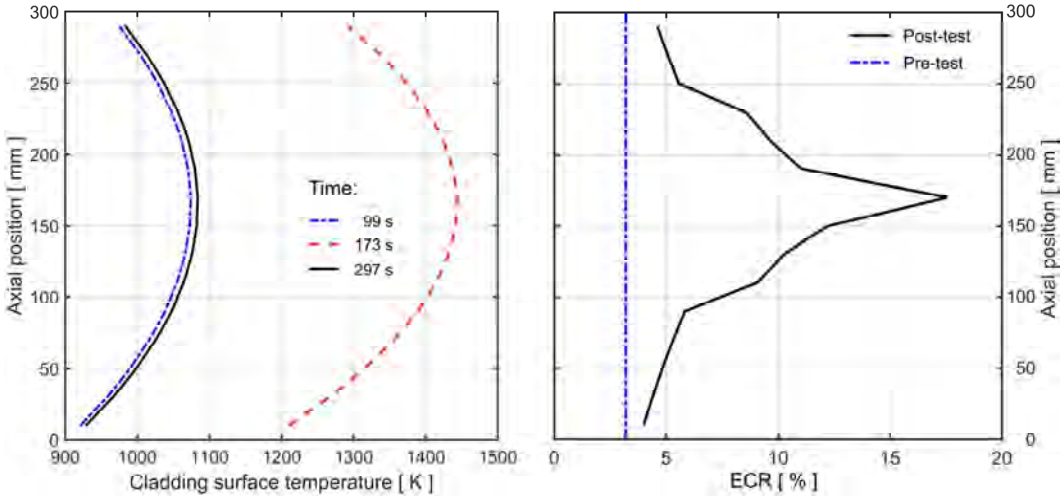

Fig. 44: Calculated cladding outer surface temperature at different times during the NRC-Studsvik-192 test (left) and calculated equivalent cladding reacted (right).

The calculated post-test ECR presented in the right panel of Fig. 44 can unfortunately not be compared with measurements, since no quantitative data regarding the ECR or the cladding inner and outer oxide layer thicknesses are reported for the NRC-Studsvik LOCA test rods. However, metallographic examinations of the oxidized cladding were done at a few axial positions of the rodlets, and quantitative information in the form of micrographs is available [3].

5. Concluding remarks

5.1. Summary and interpretation of results

The reported assessment of Halden and Studsvik LOCA simulation tests was done by best-estimate computational analyses of the experiments, using an extended version of FRAPTRAN-1.5. Since the objective was partly to validate this computer program, we deliberately refrained from matching the calculated and measured results by tuning model parameters. The only exceptions are the cladding creep rate, for which we used a constant scaling factor of 0.40 in all calculations, and the ad-hoc criteria for cladding rupture; see section 3.3. It should also be remarked that the thermal-hydraulic boundary conditions used in the analyses were approximations, based on measured data for each test, simplifying assumptions regarding the heat transfer, and fitting procedures; see Appendices C and D.

Let us first examine the agreement/disagreement between measured and calculated results for key properties: Disagreements indicate that the involved phenomena are inadequately modelled, and possibly, poorly understood. In summary, we get good or even very good agreement between measured and calculated results for the cladding temperature and the time to cladding rupture for the Halden IFA-650 tests. In particular, the calculations seem to capture the thermal effects of axial fuel relocation well. Poor agreement between measured and calculated results is on the other hand seen for the time to cladding rupture in the NRC-Studsvik-192 test, and in some of the considered tests, for the dynamics of gas depressurization after rupture. In addition, the degree of fuel pellet fine fragmentation ("pulverization") is overestimated for the tests where the fragment size distribution has been reported.

The disagreement between calculated and measured time to cladding rupture for the NRC-Studsvik-192 test is due to the lack of high temperature models for ZIRLO™ cladding in our extended version of FRAPTRAN-1.5; as explained in section 3.3, generic models for Zircaloy were used in simulations of all the tests. A recent assessment of these models against a large number of high temperature burst tests and LOCA simulation tests shows that they reproduce rupture times for tests on Zircaloy cladding without bias, while rupture times for tests on ZIRLO™ cladding are systematically overestimated [50].

The slowly decreasing internal gas pressure after cladding rupture in the IFA-650.9 and the NRC-Studsvik-192 tests gives evidence of impeded axial gas flow, and a few other tests in the same series exhibit similar behaviour [3, 22]. This phenomenon, which is seen in high burnup fuel rods that usually have a tightly closed pellet-cladding gap, is not modelled by our extended version of

FRAPTRAN-1.5, where unrestricted gas flow and mixing are assumed in all internal cavities. Impeded axial gas flow will reduce the driving force for cladding ballooning, burst and subsequent ejection of fuel fragments through the cladding breach. More precisely, the gas inventory in fuel rod plena becomes less important for driving the local deformation in the ballooning region, whereas transient fission gas release in the same region becomes relatively more important [47]. In this context, we recall from section 4.2.2 that the IFA-650.9 test rodlet exhibited not one, but two balloons, which were separated by a ~40 mm long axial section with fairly small cladding distension. The fact that this deformation pattern occurs in a short rodlet with fairly peaked power and temperature profiles suggests that growth of multiple balloons, controlled by local fission gas release, is likely in full-length fuel rods where the axial gradients are moderate; see section 5.2.

The importance of transient fission gas release to the internal pressure loading in high burnup fuel rods is also illustrated by the IFA-650.14 test rodlet, which had an exceptionally small gas plenum. Transient fission gas release therefore accounted for most (67 %) of the post-test internal free gas in this rodlet, and in contrast to the other tests considered in this report, the IFA-650.14 test could not be reproduced without considering transient gas release in the computer simulations; see sections 3.3 and 4.2.4. The calculated results and the experimental data for test IFA-650.14 suggest that the cladding ballooned gradually for more than a minute, concurrent with fission gas release caused by the increasing fuel temperature. This is much different from the other IFA-650 tests, where the cladding ballooned rapidly, typically within 3–5 s, and failed by plastic instability. This difference has importance to the transferability of the test results to LWR LOCA conditions; see section 5.2.

The post-test size distribution of fuel pellet fragments was determined by sifting all dislodged fragments in two of the considered tests. The measured mass fractions of small (< 0.25 mm) fragments in these tests are compared with our calculated results in Table 6. The table also includes information on differences between the two tests and the test rods, which may explain the fairly large difference in their fragmentation behaviour.

Table 6: Measured and calculated mass fractions of small (< 0.25 mm) fuel fragments, collected after LOCA simulation test IFA-650.14 [41] and NRC-Studsvik-192 [3].

Parameter:		**Halden IFA-650.14**	**NRC-Studsvik 192**
Measured mass fraction of small fragments	[wt%]	0.6	43
Calculated mass fraction of small fragments	[wt%]	22	73
Fuel pellet average burnup	[$MWd(kgU)^{-1}$]	70.8	78
Average LHGR during final operating cycle	[kWm^{-1}]	9	17
Peak fuel temperature during LOCA test	[K]	1180	1430
Final quenching of test rodlet		No	Yes

In summary, the NRC-Studsvik-192 test was performed on a rodlet with higher burnup, the fuel had been operated at higher power during end of life, it reached higher temperature during the test, and after the test, the rodlet was rapidly cooled by quenching. All these factors are known to promote fine fragmentation (pulverization) of the fuel [5, 6]. However, our computational model for the pulverization accounts only for two of these factors: burnup and peak fuel temperature [15]. The measured post-test mass fraction of small fragments for the IFA-650.14 test rodlet is surprisingly small, considering that the transient fission gas release measured in the test was no less than 18 % [41]. Such a high release fraction is difficult to reach within minutes, unless virtually all fuel grain boundaries are broken and all gas residing in grain boundary pores is released [51]. The grain boundary rupture, if it occurred, did in any case not lead to much observable fuel pulverization in the IFA-650.14 test.

The fact that our model for fuel pulverization seems to overestimate the fraction of small fuel fragments is problematic, since the calculated fraction is used for estimating the packing fraction of crumbled fuel. The packing fraction, which is a key parameter in our relocation model [15], has a very limited data base. Some data for the packing fraction of crumbled fuel with burnup below 16 MWd(kgU)$^{-1}$ are available [52, 53], while data for higher burnup fuel are unavailable. However, recent post-test investigations of the latest rodlet tested in the Halden IFA-650 series, with a burnup around 64 MWd(kgU)$^{-1}$, provide valuable information on this matter [54]. More precisely, high resolution gamma emission scans along the rodlet show that the fuel mass increased locally by a factor 2.7–2.8 in the most distended part of the rodlet, as a consequence of axial fuel relocation [54]. This value is marginally lower than the calculated results from our simulations of the IFA-650.4 and IFA-650.9 tests, where 0.72 was used as an approximation for the fuel fragment packing fraction in the ballooned regions; see Fig. 9 and Fig. 15. Hence, we conclude that fragment packing fractions around 0.7 are realistic, and that the best-estimate value of 0.69, presented more than thirty years ago by Siefken [52], is relevant also for high burnup fuel. It should be remarked that a cursory sensitivity analysis with regard to the fuel fragment packing fraction was done for the IFA-650.14 test in section 4.2.4. The analysis shows that a slight variation of the packing fraction, from 0.69 to 0.72, has a fairly large impact on some parameters, such as the peak cladding deformation and oxidation.

Our simulations of tests 4, 9 and 10 in the Halden IFA-650 series suggest that ballooning of the cladding, and the fuel relocation that resulted from it, occurred over a short (3–5 s) period, just before cladding rupture. The close agreement between the calculated and measured changes in cladding temperature that suddenly occurred in the IFA-650.4 and IFA-650.9 rodlets just before cladding rupture corroborates that the time of fuel relocation is accurately reproduced by the model. The results are interesting, and it should be remarked that there has been some dispute in the past as to whether axial fuel relocation during LOCA occurs before or after cladding rupture. Today, there is clear experimental evidence from two in-reactor LOCA tests that fuel relocation may precede cladding rupture. These are

test E5, conducted in the German FR2 reactor [53], and the Halden IFA-650.14 test [28, 41]. The cladding did not rupture in either of these tests, but post-test neutron radiography revealed that extensive axial relocation had nevertheless taken place inside the ballooned cladding during the tests.

Our simulations also suggest that thermal feedback effects from fuel relocation are strong enough to influence the dynamics of cladding ballooning and rupture, notwithstanding the short duration of these processes. As shown in Table 7, the calculated time to cladding rupture in the considered IFA-650 tests was shortened by 4–14 seconds, as a result of thermal feedback effects from the fuel relocation. According to our calculations, the most important thermal feedback effect during the short period from onset of axial fuel relocation to cladding rupture is caused by the collapse of the fuel pellet column, which makes hot fuel fragments come into direct contact with the expanding cladding. The local increase of fuel mass in ballooned regions results in minor thermal feedback effects *before* cladding rupture, but as can be seen from Table 7, it has significant effects on the local cladding temperature and oxidation rate *after* rupture. These results are interesting with regard to LOCA licensing analyses, since they indicate that conservative assumptions have to be made in the analyses, unless fuel relocation and its consequences to cladding local temperature and oxidation are accounted for in the computational evaluation models.

Table 7: Calculated impact of axial fuel relocation on key parameters in the considered Halden IFA-650 LOCA simulation tests.

Parameter (calculated results)		**650.4**	**650.9**	**650.10**	**650.14**
Peak cladding temperature [K]	With relocation	1230	1646	1244	1095
	Without relocation	1149	1400	1180	1071
	Difference	81	246	64	24
Peak post-test ECR [%]	With relocation	6.64	35.0	7.97	4.89
	Without relocation	4.69	9.55	6.21	4.12
	Difference	1.95	25.4	1.76	0.77
Time to cladding rupture [s]	With relocation	334.2	133.5	249.9	-
	Without relocation	348.2	137.8	259.1	-
	Difference	-14.0	-4.3	-9.2	-

5.2. Transferability of test results to LWR LOCA conditions

As shown in Table 7, most of the Halden IFA-650 tests considered in this report give evidence of strong thermal feedback effects from the axial fuel relocation. However, it should be borne in mind that the tests were deliberately designed to amplify axial fuel relocation, and they are therefore not fully representative of actual conditions under LOCA in commercial power reactors [7].

The most important differences in design and operating conditions between the considered test rodlets and typical LWR fuel are:

- The fuel burnup of the rodlets is higher than today's typical discharge burnup of commercial fuel.
- The cladding distension is not limited by contact with neighbouring fuel rods, as it would be in a real fuel assembly.
- Except for the IFA-650.14 rodlet, the ratio of the gas plenum volume to the rod active length is an order of magnitude larger than in commercial LWR fuel designs.
- The axial gradients in fuel rod power and/or temperature are larger than those expected in the high temperature phase of an LWR LOCA.

These differences accentuate fuel fragmentation and localized cladding deformation in the test rodlets, and thus, they contribute to the axial fuel relocation.

Based on these observations and the results of parametric studies in the Halden IFA-650 tests, the NRC-Studsvik tests and similar LOCA test programs [4, 53, 55], it is reasonable to expect that the fuel behaviour in an LWR LOCA will be somewhat different than observed in the aforementioned tests. For example:

- The local increase in fuel mass caused by axial fuel relocation within the fuel rods will most likely be lower, since cladding ballooning is limited by contact with neighbouring fuel rods, and since the fuel fragment packing fraction is supposedly lower for the lower-burnup fuel.
- Once a fuel rod fails, fuel fragments ejected through the cladding breach may accumulate at the spacer grid below and contribute to the local heat load of neighbouring, yet unfailed, rods. The possibility of thermal feedback from axial fuel fragment relocation *outside* the fuel rods is currently unexplored.
- The cladding ballooning is expected to be slower, since it will be controlled mainly by the rate of transient fission gas release, as in the IFA-650.14 test.
- In fuel rods with high burnup, impeded axial gas flow will make the occurrence of multiple balloons likely. Multiple balloons, separated by spacer grids, have been observed in LOCA simulation tests on longer test rods than those used in Halden and Studsvik [4, 55]. It is also expected that the axial positions at which the balloons develop will be difficult to predict by computational models, since these positions will depend on local pellet-cladding gap conditions and transient fission gas release. Also, the aforementioned possibility of axial fuel relocation of dispersed fuel to lower spacer grid positions will contribute to the complexity.

Further experiments, model development and computational analyses are needed to elucidate the fuel behaviour under more realistic LWR LOCA conditions. Of particular concern is the behaviour of high burnup fuel rods, for which the database is restricted to single-rod LOCA simulation tests on short rodlets.

5.3. Suggestions for further work

5.3.1. Model development

The results presented in this report indicate that there are certain models in our extended version of FRAPTRAN-1.5 that could be improved. Firstly, the fact that we needed to scale the cladding high temperature creep rate by a factor of 0.40 in all calculations and use ad-hoc criteria for cladding rupture (see section 3.3) suggests that the current creep models and failure criteria can be improved. The same conclusion was reached in a recent assessment of these models against a large database of high temperature burst tests and LOCA simulation tests [50]. The models also need to be adapted to ZIRLO™ cladding, since they are not calibrated against this material.

Secondly, the mass fraction of fine fuel fragments is currently calculated by use of an empirical threshold for pulverization of high burnup fuel during temperature excursions [5, 56, 57]. The results put forth in Table 6 show that this empirical model significantly overestimated the degree of fuel pulverization for two of the considered tests. The threshold should therefore be replaced with a refined, mechanistically based, model for fuel pulverization, which accounts for more parameters than just the fuel local burnup and temperature. Of particular interest is the impact of mechanical constraint from the cladding and effects of pre-LOCA operating history for the fuel. Models of this kind, which link pulverization to the local fuel porosity and distribution of gaseous fission products in the fuel, are currently being studied by Quantum Technologies in a separate research project for SSM [58, 59]. Ongoing and planned separate effect tests on high burnup fuel in the third phase of the Studsvik Cladding Integrity Project (SCIP-III) will provide useful data for setting up an improved pulverization model.

Thirdly, the model used for estimating the fuel fragment packing fraction from the calculated state of fuel fragmentation and pulverization predicts very high packing fractions for fuel that contains about 30 wt% fine (< 0.2 mm) fragments [15]. According to the aforementioned threshold for fuel pulverization, this mass fraction of fine fragments is typically obtained when overheating fuel pellets with an average burnup around 70–75 $MWd(kgU)^{-1}$. In this burnup range, the packing fraction predicted by the model may exceed 0.80–0.85. At present, there are no experimental data for UO_2 fuel that directly support such high values, but supporting data exist for other granular materials with binary size distributions [15]. This is further discussed in section 5.3.3 below.

The lack of models for transient fission gas release and restricted axial gas flow in our extended version of FRAPTRAN-1.5 is clearly one of the main reasons for the observed differences between calculated and measured results in this work.

Transient fission gas release and restricted axial gas flow within the rod are phenomena with importance to the internal pressure loading of high burnup fuel rods. As already mentioned in section 5.2, the phenomena are expected to be more important for full-length LWR fuel rods than for the short rodlets typically used in LOCA simulation tests. Models for transient fission gas release from high burnup fuel in LOCA conditions are currently being studied by Quantum Technologies in the aforementioned research project on fuel pulverization, since pulverization and transient fission gas release are related phenomena. The aim is to formulate a combined model for pulverization and transient gas release, suitable for implementation in FRAPTRAN-1.5. For completeness, a model for axial gas flow is also needed, in particular for analysing full-length fuel rods.

Finally, we note that local mesh refinement is necessary for analyses of cladding ballooning and burst in full-length fuel rods with our extended version of FRAPTRAN-1.5. In the calculations presented in this report, we used a fixed axial discretisation, consisting of 20 mm long axial segments (nodes), along the entire active length of the rodlets. To carry out analyses of a full length (3.6 m) LWR fuel rod with such a discretisation is impracticable. Computer programs used for analyses of ballooning must therefore allow local refinement of the discretisation at axial positions of particular interest. FRAPTRAN-1.5 has this capacity [18], but the program would be significantly improved if the refinement could be done adaptively, i.e. automatically in the course of the calculation.

5.3.2. Computational analyses

As already mentioned, the fuel behaviour observed in LOCA simulation tests on single test rods with an active length of 0.3–0.5 m may depart from that of real full-length fuel rods in a commercial fuel assembly under LWR LOCA conditions. Some of the expected differences were discussed in section 5.2, where it was also stated that further experiments, model development and computational analyses are needed to elucidate these differences.

Computational analyses of the thermal-mechanical behaviour of full-length fuel rods under conditions expected in LWR LOCAs with our extended version of FRAPTRAN-1.5 are therefore recommended. The current version of the program is adequate for analyses of low to medium burnup fuel; analyses of high burnup fuel should preferably wait until the model improvements proposed in section 5.3.1 have been made. Of particular importance are the models for restricted axial gas flow, fuel pulverization and transient fission gas release.

The calculations carried out so far with our model for axial fuel relocation suggest that the results are sensitive to two model parameters, namely the fuel fragment packing fraction, ϕ, and the minimum pellet-cladding gap size needed for fuel fragments to detach from their original, close-packed configuration and relocate

downwards, g^{th}. These parameters, as well as the experimental data base in support of the values used for them, are presented in [15].

A cursory sensitivity study for the fuel fragment packing fraction, pertinent to the IFA-650.14 test, is presented in section 4.2.4 of this report. A more comprehensive sensitivity study, including both ϕ and g^{th}, is desirable. Any of the IFA-650 tests considered in this report would be a suitable baseline case for such a study.

5.3.3. Tests and experiments

Computer analyses presented here and elsewhere [60-62] suggest that the effects of axial fuel relocation on peak cladding temperature and ECR under a loss-of-coolant accident would depend strongly on the fuel fragment packing fraction in the ballooned region of the fuel rod. As already mentioned, some data on the packing fraction exist for fuel with low (< 16 MWd(kgU)$^{-1}$) burnup [52, 53], but there are currently no open literature data at all for higher burnup fuel. Such data can be produced by combining high resolution gamma scans, carried out on the rodlets shortly after the LOCA tests, with axial scans of the cladding radial deformation. A first step in this direction has been taken in Halden [54], and similar experimental techniques will be used in the third phase of the Studsvik Cladding Integrity Project (SCIP-III).

The model used for estimating the fuel fragment packing fraction in our calculations predicts particularly high packing fractions for fuel that contains about 30 wt% fine (< 0.2 mm) fragments [15]. Unfortunately, there are currently no measured data on the fuel fragment packing fraction versus mass fraction of fine fragments that can confirm or refute this modelling result. Such data can be produced in connection with post-test sifting of collected fuel fragments from failed test rods, simply by measuring the mass and bulk (effective) volume of the fragments. Although these measured packing fractions would not be representative of fuel accumulated within the balloon of a distended fuel rod, they would still be valuable for identifying and determining possible relationships between the packing fraction and the fragment size distribution.

Finally, we suggest some modifications of the LOCA testing procedures in Halden and Studsvik, in order to ease the interpretation of the tests. With regard to the Halden IFA-650 tests, we suggest that water spraying into the upper part of the test rig is conducted with constant flow instead of intermittent pulses: When liquid water is injected into the rig, the water flashes to steam and expands by a factor ~550. The volume expansion forces much of the steam out of the test rig, into the evacuation line to the blowdown tank; see section 2.1.1. Hence, only part of the injected water remains in the rig to feed the zirconium-water reactions. This amount was obviously insufficient for the IFA-650.9 test; as mentioned in section 4.2.2, there is clear evidence that the local cladding oxidation in the lower part of the IFA-650.9 rodlet was limited by steam starvation. The pulse-wise flow

caused by the intermittent spray procedure is difficult to model, which leads to large uncertainties regarding the actual amount of water locally available in the rig for oxidation of the cladding. A constant water spray would be easier to model, and thus, reduce some of this uncertainty.

As for the LOCA simulation tests in Studsvik, we request that more than one thermocouple should be used for measuring the cladding temperature during the test, in order to reduce the uncertainty that currently exists regarding axial temperature gradients. One thermocouple at each end of the active length, in addition to the more centrally placed thermocouple, would provide the information needed. If possible, the heated zone of the rig should also be lengthened, to reduce the unrealistically steep axial gradients in cladding temperature.

It would also be interesting to carry out a pair of tests to investigate the effect of final quenching on fuel pulverization. Early investigations on fresh UO_2 fuel suggest that the thermal shock experienced by the fuel during quenching leads to formation of micro cracks [63]. The response of high burnup fuel is unclear, since open literature reports on this issue are unavailable. Ideally, two identical rodlets with high burnup fuel should be tested under identical conditions, except for the final cooling, i.e. quench or no quench. Two of the six tests in the NRC-Studsvik series were done without quenching, but unfortunately, the fuel burnup and/or peak temperature in these two tests were such that comparisons with the other four tests become inconclusive [3].

Acknowledgements

Thanks are due to the OECD Halden Reactor Project for the generous decision to allow publication of results from the four Halden IFA-650 LOCA tests considered in this report. We are also indebted to the U.S. Nuclear Regulatory Commission and Studsvik Nuclear AB, who kindly placed experimental data for the NRC-Studsvik LOCA test 192 at our disposal.

6. References

1. *Nuclear fuel behaviour in loss-of-coolant accident (LOCA) conditions: State-of-the-art report,* 2009, Report NEA No. 6846, OECD Nuclear Energy Agency, Paris, France.
2. Kolstad, E., et al. *High burn-up fuel behaviour under LOCA conditions as observed in Halden experiments,* 2011. In: IAEA Technical Meeting on Fuel Behaviour and Modelling under Severe Transient and Loss-of-Coolant Accident (LOCA) Conditions, October 18-21, 2011, Mito, Japan: International Atomic Energy Agency, IAEA-TECDOC-CD-1709.
3. Flanagan, M., et al., *Post-test examination results from integral, high-burnup, fueled LOCA tests at Studsvik Nuclear Laboratory,* 2013, Report NUREG-2160, U.S. Nuclear Regulatory Commission, Washington, DC, USA.
4. Fedotov, P.V., et al. *LOCA test with high burnup VVER fuel in the MIR reactor*, 2015. In: Reactor Fuel Performance 2015 (TopFuel-2015), September 13-17, 2015, Zürich, Switzerland: European Nuclear Society, pp. 335-344.
5. Turnbull, J.A., et al., *An assessment of the fuel pulverization threshold during LOCA-type temperature transients.* Nuclear Science and Engineering, 2015. 179: pp. 477-485.
6. Bianco, A., et al., *Experimental investigation on the causes for pellet fragmentation under LOCA conditions.* Journal of Nuclear Materials, 2015. 465: pp. 260-267.
7. Wiesenack, W., *Safety significance of the Halden IFA-650 LOCA test results,* 2010, Report NEA/CSNI/R(2010)5, OECD Nuclear Energy Agency, Paris, France.
8. Raynaud, P.A.C., *Fuel fragmentation, relocation and dispersal during the loss-of-coolant accident,* 2012, Report NUREG-2121, U.S. Nuclear Regulatory Commission, Washington, DC, USA.
9. *Report on fuel fragmentation, relocation and dispersal,* 2016, Report NEA/CSNI/R(2016)16, OECD Nuclear Energy Agency, Paris, France.
10. Brachet, J.C., et al., *Hydrogen content, preoxidation, and cooling scenario effects on post-quench microstructure and mechanical properties of Zircaloy-4 and M5 alloys in LOCA conditions.* Journal of ASTM International, 2008. 5(5): pp. 1-28.
11. Desquines, J., et al., *Embrittlement of pre-hydrided Zircaloy-4 by steam oxidation under simulated LOCA transients.* Journal of Nuclear Materials, 2016. 469: pp. 20-31.
12. Boutine, S. and S. Graff. *A new LOCA safety demonstration in France,* 2015. In: Reactor Fuel Performance 2015 (TopFuel-2015), September 13-17, 2015, Zürich, Switzerland: European Nuclear Society, pp. 384-393.
13. *Nuclear Regulatory Commission: 10 CFR Parts 50 and 52: Performance-based emergency core cooling systems cladding acceptance criteria - Proposed rule.* Federal Register, 2014. 79(56): pp. 16106-16146.

14. Killeen, J.C. *Status of the FUMAC and ACTOF CRPs*, 2015. In: Meeting of the IAEA Technical Working Group on Fuel Performance and Technology, April 22-24, 2015, Vienna, Austria: International Atomic Energy Agency.

15. Jernkvist, L.O. and A.R. Massih, *Models for axial relocation of fragmented and pulverized fuel pellets in distending fuel rods and its effects on fuel rod heat load*, 2015, Report SSM 2015:37, Swedish Radiation Safety Authority, Stockholm, Sweden.

16. Jernkvist, L.O. and A.R. Massih. *Modelling axial relocation of fragmented fuel pellets inside ballooned cladding tubes and its effects on LWR fuel rod failure behaviour during LOCA*, 2015. In: 23rd International Conference on Structural Mechanics in Reactor Technology (SMiRT-23), August 10-14, 2015, Manchester, UK.

17. Jernkvist, L.O., et al. *Axial relocation of fragmented and pulverized fuel and its effects on fuel rod heat load during LOCAs*, 2015. In: Reactor Fuel Performance 2015 (TopFuel-2105), September 13-17, 2015, Zürich, Switzerland: European Nuclear Society, pp. 401-410.

18. Geelhood, K.J., et al., *FRAPTRAN-1.5: A computer code for the transient analysis of oxide fuel rods*, 2014, Report NUREG/CR-7023, Vol. 1, Rev. 1, Pacific Northwest National Laboratory, Richland, WA, USA.

19. Manngård, T., et al. *Evaluation of Halden IFA-650 loss-of-coolant accident experiments 2, 3, 4, 5, 6 and 7*, 2013. In: Enlarged Halden Programme Group Meeting, March 10-15, 2013, Storefjell, Norway: OECD Halden Reactor Project, Halden, Norway.

20. Manngård, T., et al., *Evaluation of the Halden IFA-650 loss-of-coolant accident experiments 2, 3 and 4*, 2014, Report SSM 2014:18, Swedish Radiation Safety Authority, Stockholm, Sweden.

21. Manngård, T. and J.-O. Stengård, *Evaluation of the Halden IFA-650 loss-of-coolant accident experiments 5, 6 and 7*, 2014, Report SSM 2014:19, Swedish Radiation Safety Authority, Stockholm, Sweden.

22. Wiesenack, W., *Summary of the Halden Reactor Project LOCA test series IFA-650*, 2013, Report HPR-380, OECD Halden Reactor Project, Halden, Norway.

23. Kolstad, E. *LOCA experiments with high burnup fuel in the Halden programme*, 2010. In: Swedish Radiation Safety Autority Research Seminar on Reactor Safety, April 22-23, 2010, Stockholm, Sweden.

24. Kekkonen, L., *LOCA testing at Halden: The fourth experiment - IFA-650.4*, 2007, Report HWR-838, OECD Halden Reactor Project, Halden, Norway.

25. Bole du Chomont, F., *LOCA testing at Halden: The ninth experiment IFA-650.9*, 2009, Report HWR-917, OECD Halden Reactor Project, Halden, Norway.

26. Lavoil, A., *LOCA testing at Halden: The tenth experiment IFA-650.10*, 2010, Report HWR-974, OECD Halden Reactor Project, Halden, Norway.

27. Nishi, M. and B.-H. Lee, *Summary of pre-irradiation data on fuel segments supplied by EDF/Framatome and tested in IFA-610, 629 and 648*, 2001, Report HWR-664, OECD Halden Reactor Project, Halden, Norway.

28. Tradotti, R., *LOCA testing at Halden: The BWR fuel experiment IFA-650.14*, 2014, Report HWR-1084, OECD Halden Reactor Project, Halden, Norway.

29. Ledergerber, G., *Characterisation of KKL BWR fuel for test series in IFA-610, IFA-629 and IFA-650,* 2014, Report HWR-1033 Rev. 1, OECD Halden Reactor Project, Halden, Norway.

30. Ledergerber, G., et al., *Characterization of high burnup fuel for safety related fuel testing.* Journal of Nuclear Science and Technology, 2006. 43(9): pp. 1006-1014.

31. Flanagan, M. and P. Askeljung. *Observations of fuel fragmentation, mobility and release in integral high-burnup, fueled LOCA tests*, 2012. In: OECD Halden Reactor Project LOCA Workshop, May 29-30, 2012, Lyon, France: OECD Halden Reactor Project, Halden, Norway.

32. Helin, M. and J. Flygare, *NRC LOCA tests at Studsvik: Design and construction of test train device and tests with unirradiated cladding material*, 2012, Report STUDSVIK/N-11/130, Studsvik Nuclear AB, Studsvik, Sweden.

33. Zwicky, H.-U., *Re-fabrication of ramp rodlet Z-3 from Westinghouse father rod irradiated in North Anna,* 2006, Report N-05/131 Rev. 1, Studsvik Nuclear AB, Nyköping, Sweden.

34. Zwicky, H.-U., *Re-fabrication of ramp rodlet Z-4 from Westinghouse father rod irradiated in North Anna,* 2006, Report N-05/133 Rev. 1, Studsvik Nuclear AB, Nyköping, Sweden.

35. Raynaud, P.A.C., *NRC Studsvik LOCA test 192*, 2014, MS Excel data file contributed to the IAEA CRP FUMAC on December 8, 2014, U.S. Nuclear Regulatory Commission, Washington, DC, USA.

36. Geelhood, K.J. and W.G. Luscher, *FRAPCON-3.5: A computer code for the calculation of steady-state, thermal-mechanical behavior of oxide fuel rods for high burnup,* 2014, Report NUREG/CR-7022, Vol. 1, Rev. 1, Pacific Northwest National Laboratory, Richland, WA, USA.

37. Jernkvist, L.O., *Implementation of models for cladding high temperature metal-water reactions, phase transformation, creep and failure in the FRAPTRAN-1.4 computer program,* 2012, Report TR10-005V2, Quantum Technologies AB, Uppsala, Sweden.

38. Manngård, T. and A.R. Massih, *Modelling and simulation of reactor fuel cladding under loss-of-coolant accident conditions.* Journal of Nuclear Science and Technology, 2011. 48(1): pp. 39-49.

39. Jernkvist, L.O., *Observed and corrected errors in source code and algorithms of FRAPTRAN-1.5,* 2015, Report TR15-002, Quantum Technologies AB, Uppsala, Sweden.

40. Knuutila, A., *Improvements on FRAPCON3/FRAPTRAN mechanical modelling,* 2006, Research report VTT-R-11337-06, VTT Technical Research Centre of Finland, Helsinki, Finland.

41. Oberländer, B.C. and H.K. Jenssen, *PIE on the rod from the LOCA test IFA-650.14 on high burn-up BWR fuel,* 2014, Report HWR-1096, OECD Halden Reactor Project, Halden, Norway.

42. Cathcart, J.V., et al., *Zirconium metal-water oxidation kinetics, IV: reaction rate studies,* 1977, Report ORNL/NUREG-17, Oak Ridge National Laboratory, Oak Ridge, TN, USA.

43. Rosinger, H.E., *A model to predict the failure of Zircaloy-4 fuel sheating during postulated LOCA conditions.* Journal of Nuclear Materials, 1984. 120: pp. 41-54.

44. Rosinger, H.E., et al., *The steady-state creep of Zircaloy-4 fuel cladding from 940 to 1873 K*, 1978, Report AECL-6193, Atomic Energy of Canada, Pinawa, MB, Canada.

45. Oberländer, B.C., et al. *PIE results from the high burnup (92 MWd/kgU) PWR segment after LOCA testing in IFA 650-4*, 2008. In: Enlarged Halden Programme Group Meeting, May 18-23, 2008, Loen, Norway: OECD Halden Reactor Project

46. Oberländer, B.C. and W. Wiesenack, *Overview of Halden reactor LOCA experiments (with emphasis on fuel fragmentation) and plans*, 2014, Report IFE/KR/E-2014/001, Institute for Energy Technology, Kjeller, Norway.

47. Khvostov, G., et al., *Some insights into the role of axial gas flow in fuel rod behaviour during the LOCA, based on Halden tests and calculations with the FALCON-PSI code.* Nuclear Engineering and Design, 2011. 241: pp. 1500-1507.

48. Oberländer, B.C. and H.K. Jenssen. *LOCA IFA-650.9: PIE of the 90 MWd/kgU PWR rod subjected to a high temperature transient*, 2010. In: Enlarged Halden Programme Group Meeting, March 14-19, 2010, Storefjell, Norway: OECD Halden Reactor Project.

49. Oberländer, B.C. and H.K. Jenssen. *LOCA IFA-650.10: PIE of a PWR rod with a burn-up of 61 MWd/kgU after LOCA testing in the HBWR*, 2011. In: Enlarged Halden Programme Group Meeting, October 3-6, 2011, Sandefjord, Norway: OECD Halden Reactor Project.

50. Massih, A.R. and L.O. Jernkvist, *Assessment of data and criteria for cladding burst in loss-of-coolant accidents*, 2015, Report SSM-2015:46, Swedish Radiation Safety Authority, Stockholm, Sweden.

51. Guerin, Y. *In-pile and out-of-pile burst release of fission gases*, 2012. In: Enlarged Halden Programme Group Meeting, September 8-13, 2002, Storefjell, Norway: OECD Halden Reactor Project.

52. Siefken, L.J. *Axial fuel relocation in ballooning fuel rods*, 1983. In: 7th International Conference on Structural Mechanics in Reactor Technology (SMiRT-7), August 22-26, 1983, Chicago, IL, USA.

53. Karb, E.H., et al., *LWR fuel rod behavior in the FR2 in-pile tests, simulating the heatup phase of a LOCA*, 1983, Report KfK-3346, Kernforschungszentrum Karlsruhe, Karlsruhe, Germany.

54. Andersson, P., et al., *Inspection of LOCA test rod IFA-650.15 using gamma emission tomography*, 2016, Report HWR-1164, OECD Halden Reactor Project, Halden, Norway.

55. Freshley, M.D. and G.M. Hesson, *Summary results of the LOCA simulation program conducted in NRU,* 1983, Conference paper presented at the Eleventh NRC Water Reactor Safety Meeting, Gaithersburg, MD, USA, October 14-28, 1983, Report PNL-SA-11536, Pacific Northwest Laboratory, Richland, WA, USA.

56. Turnbull, J.A., et al. *An investigation into fuel pulverization with specific reference to high burnup LOCA*, 2014. In: Enlarged Halden Programme Group Meeting, September 7-12, 2014, Røros, Norway: OECD Halden Reactor Project, Halden, Norway.

57. Yagnik, S., et al. *An investigation into fuel pulverization with specific reference to high-burnup LOCA*, 2014. In: 2014 Water Reactor Fuel Performance Meeting (WRFPM 2014), September 14-17, 2014, Sendai, Japan.

58. *Utveckling av modeller för fissionsgasinducerad fragmentering av högutbränt kärnbränsle*, 2015, Research project agreement SSM-2015-4050-2, (In Swedish), Swedish Radiation Safety Authority, Stockholm, Sweden.

59. *Utveckling av modeller för fissionsgasinducerad fragmentering av högutbränt kärnbränsle, fortsättning*, 2016, Research project agreement SSM2016-3944-2, (In Swedish), Swedish Radiation Safety Authority, Stockholm, Sweden.

60. Bergquist, P., *A parameter study concerning the impact on the calculated peak clad temperature of a redistribution of the fuel after cladding swelling and rupture*, 1979, Report FV-79-0017/2, AB Fjärrvärme, Trosa, Sweden.

61. Routledge, K.T., et al. *Calculations of the effects of fuel pellet fragment axial relocation on the peak clad temperature during a loss-of-coolant accident in a pressurized water reactor*, 1988. In: Second UK National Conference on Heat Transfer, September 14-16, 1988, Glasgow, UK: Institution of Mechanical Engineers, Mechanical Engineering Publications, London, UK, 2, pp. 1531-1540.

62. Grandjean, C., et al. *High burnup UO_2 fuel LOCA calculations to evaluate the possible impact of fuel relocation after burst*, 2001. In: OECD Topical Meeting on LOCA Fuel Safety Criteria, March 22-23, 2001, Aix-en-Provence: OECD Nuclear Energy Agency, Committee on the Safety of Nuclear Installations, Report NEA/CSNI/R(2001)18, Paris, France, pp. 239-266.

63. Oguma, M., *Integrity degradation of UO_2 pellets subjected to thermal shock.* Journal of Nuclear Materials, 1985. 127: pp. 67-76.

64. Aounallah, Y., et al. *Simulations of the Halden IFA-650.3/.4 high burnup LOCA tests with TRACE and FALCON; A preliminary study on axial relocation*, 2006. In: 2006 International Meeting on LWR Fuel Performance (TopFuel 2006), October 22-26, 2006, Salamanca, Spain: European Nuclear Society, pp. 305-311.

65. Khvostov, G., et al. *Modeling the effects of axial fuel relocation in the IFA-650.4 LOCA test*, 2007. In: Enlarged Halden Programme Group Meeting, March 12-15, 2007, Storefjell, Norway: OECD Halden Reactor Project, Halden, Norway.

66. Tofino, Y., et al. *Evaluation of ECR and PCT in balloon region under LOCA conditions of the Halden IFA 650 tests (single rod tests)*, 2009. In: Water Reactor Fuel Performance Meeting 2009 (TopFuel 2009), September 6-10, 2009, Paris, France: European Nuclear Society, pp. 573-580.

67. Govers, K. and M. Verwerft. *Simulation of ballooning and relocation in the Halden LOCA tests with FRAPTRAN*, 2014. In: Enlarged Halden Programme Group Meeting, September 7-12, 2014, Røros, Norway: OECD Halden Reactor Project, Halden, Norway

68. Sonnenburg, H.G., et al., *Development of methods for the analysis of the fuel rod behaviour under loss of coolant and reactivity initiated accidents*, 2010, Report GRS-A-3519, Gesellschaft für Anlagen und Reaktorsicherheit (GRS) mbH, Garching, Germany.

69. Bestion, D. *System code models and capabilities*, 2008. In: OECD-NEA/UNIPI Seminar on the Transfer of Competence, Knowledge and Experience Gained through CSNI Activities in the Field of Thermal Hydraulics (THICKET 2008), May 5-9, 2008, Pisa, Italy: OECD Nuclear Energy Agency, pp. 81-106.

70. Modest, M.F., *Radiative Heat Transfer*. 3rd ed. 2013, Oxford, UK: Academic Press.

71. Stuckert, J., et al., *On the thermo-physical properties of Zircaloy-4 and ZrO_2 at high temperature*, 2002, Report FZKA 6739, Forschungszentrum Karlsruhe, Karlsruhe, Germany.

72. Karlsson, J., *Studsvik LOCA test machine data sheet*, 2016, MS Excel data file contributed to the IAEA CRP FUMAC on March 24, 2016, Studsvik Nuclear AB, Nyköping, Sweden.

Appendix A:
The Halden IFA-650.4/9/10/14 LOCA tests

A.1. IFA-650.4

The fourth test in the Halden IFA-650 LOCA test series was conducted in April 2006, using a test rodlet with an average fuel burnup of 92.3 MWd(kgU)$^{-1}$. The rodlet was sampled from a full-length mother fuel rod that had been operated for seven reactor cycles in the Gösgen PWR, Switzerland. The test resulted in cladding ballooning and burst, as well as significant axial fuel relocation and dispersal of pulverized fuel into the coolant. The fact that this happened at a cladding temperature more than 400 K below the allowable peak temperature postulated in existing acceptance criteria for LOCA, caused concern about the applicability of these criteria to high burnup fuel [7]. Consequently, the IFA-650.4 test has been analysed with a number of computer programs and models to better understand the mechanisms behind the unexpectedly large fuel dispersal observed in the test [19, 20, 47, 64-68]. Fuel pulverization and axial relocation of the fine fragments have been identified as important mechanisms that ease the fuel dispersal.

Fig. 45 presents temperature measurements from eight different thermocouples, the positions of which are defined in Table 8. Time t = 0 refers to the time at which the test was initiated by opening the valves to the blowdown tank. It should be remarked that cladding thermocouples were attached only at the upper end of the IFA-650.4 test rodlet. This was done to ensure that the cladding was not weakened in the centre and lower end of the rodlet, where cladding ballooning and burst were expected.

Table 8: Thermocouple (TC) positions in the IFA-650.4 LOCA simulation test [68]. The axial position z refers to the height above the bottom of the fuel pellet column.

TC	Position and measured property	z [mm]
TCC1	Cladding surface (upper part of active length)	400
TCC2	Cladding surface (upper part of active length)	400
TCC3	Cladding surface (gas plenum position)	678
TCC4	Inner flow channel (upper part)	670
TCH1	Heater surface (mid position)	205
TCH2	Heater surface (top part)	380
TIA	Coolant inlet (average signal from 2 TCs)	-
TOA	Coolant outlet (average signal from 2 TCs)	-

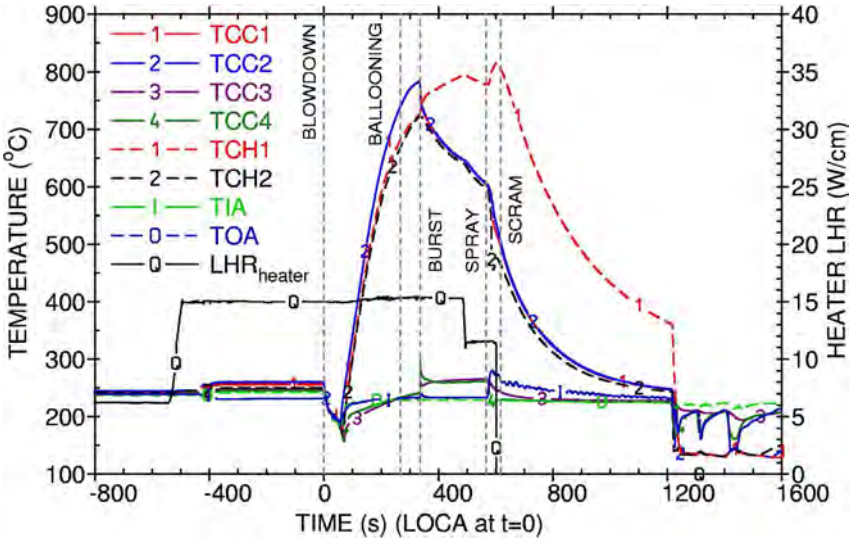

Fig. 45: Measured temperatures during the IFA-650.4 LOCA simulation test [23]. See Table 8 for definition of the thermocouples listed in the legend.

Fig. 46 presents the recorded rod internal gas pressure in the upper plenum, rod elongation and the gamma activity in the pipeline to the blowdown tank. From these recordings, it is clear that the cladding ruptured at t = 336 s. The plenum pressure dropped instantaneously to about 0.8 MPa, according to Fig. 46. In reality, the gas pressure fell to that of the coolant (0.3–0.4 MPa), but mechanical constraints in the pressure transducer limited the measuring range.

From Fig. 45, it is evident that the cladding temperature at the upper part of the fuel pellet column started to decrease significantly, approximately at time of cladding rupture. This is a consequence of axial fuel relocation, which emptied the cladding tube at the thermocouple locations (TCC1 and TCC2). At the same time, the heater temperature at the rodlet mid position (TCH1) started to increase. This is a result of fuel accumulation in the ballooned cladding at this position, together with a much reduced gap between the ballooned cladding and the heater. Water spraying was started at t = 566 s and the reactor was scrammed at t = 617 s, i.e. more than 10 minutes after start of blowdown.

The entire pressure flask was gamma scanned 105–115 days after the test. The flask was then filled with epoxy and sent to the hot cell laboratory for ceramographic and metallographic examinations of the test rodlet. The epoxy was intended to stabilize the fuel relocation that had occurred during the test. However, the impregnation failed below the balloon, which was located slightly below the axial midplane of the rodlet. The balloon filled the entire cross section, and the cladding was in contact with the inner surface of the heated shroud.

A detailed presentation of the results from gamma scanning, ceramography and metallography of the IFA-650.4 rodlet can be found in [45], and selected data from the investigations are compared with our calculated results in section 4.2.1.

With regard to fuel fragmentation and axial relocation, the post-test characterization of the rodlet showed that about 190 mm of the fuel pellet column was missing from the upper part of the rod. This fuel had relocated axially to the balloon, and some of it had been expelled through the cladding breach and had accumulated above the balloon and at the bottom of the pressure flask. Ceramography revealed extensive fragmentation and pulverization of the fuel in the balloon and its vicinity, where mechanical restraint from the cladding had disappeared [45]. The pulverization had occurred across the entire cross section of the pellet, and was not confined to the high burnup structure at the pellet rim. The fuel fragment size distribution was determined by image analysis of two cross sections, both located within the ballooned and ruptured region of the rodlet. Most of the fuel fragments were less than 200 µm in size [2].

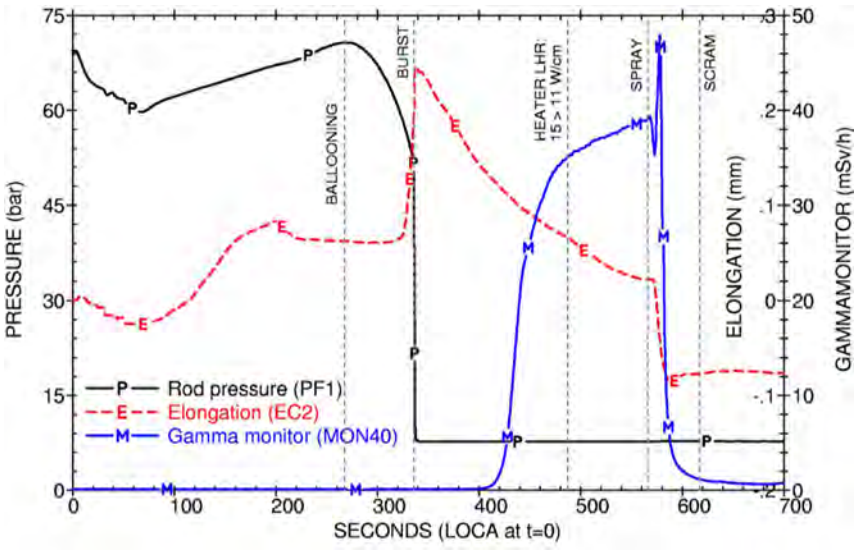

Fig. 46: Measured rod elongation, rod plenum gas pressure and coolant gamma activity during the IFA-650.4 LOCA simulation test [23].

A.2. IFA-650.9

The Halden IFA-650.9 LOCA test was conducted in April 2009, using a test rodlet with an average fuel burnup of 89.9 MWd(kgU)$^{-1}$ that had been re-fabricated from a sibling sample to test rodlet IFA-650.4. Hence, the design and pre-irradiation conditions were nearly identical for these two rodlets. The main difference between them was the axial position from which they had been sampled; see section 2.1.2.

From Table 2, it is clear that the IFA-650.9 rodlet was tested at much higher power and reached significantly higher temperatures than its sibling IFA-650.4. Fig. 47 presents temperature measurements from eight different thermocouples, the positions of which are defined in Table 9. In contrast to its sibling IFA-650.4, the IFA-650.9 rodlet had cladding thermocouples attached at both ends of its ac-

tive length. The test rig was also equipped with heater thermocouples at three different axial positions.

Table 9: Thermocouple (TC) positions in the IFA-650.9 LOCA simulation test. The axial position z refers to the height above the bottom of the fuel pellet column.

TC	Position and measured property	z [mm]
TCC1	Cladding surface (lower part of active length)	100
TCC2	Cladding surface (upper part of active length)	415
TCC3	Cladding surface (upper part of active length)	415
TCH1	Heater surface (lower part)	100
TCH2	Heater surface (mid position)	200
TCH3	Heater surface (upper part)	380
TIA	Coolant inlet	-
TOA	Coolant outlet	-

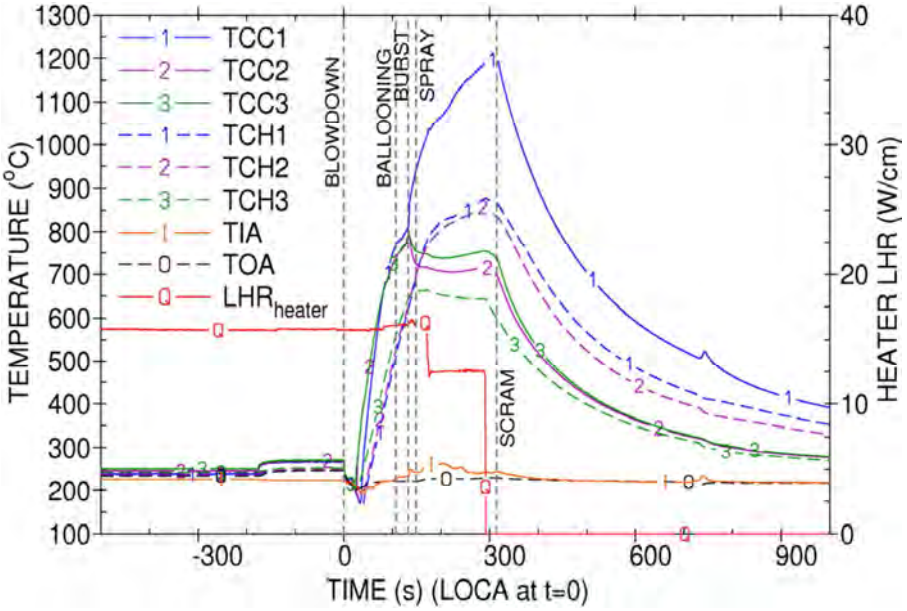

Fig. 47: Measured temperatures during the IFA-650.9 LOCA simulation test [25]. See Table 9 for definition of the thermocouples listed in the legend.

From Fig. 47, it is evident that the cladding temperature at the upper part of the IFA-650.9 rodlet started to decrease significantly after cladding rupture, which occurred at t = 133 s. As with the IFA-650.4 test, this is clear evidence of axial fuel relocation, which emptied the cladding tube at the upper thermocouple location (TCC2 and TCC3). At the same time, the cladding temperature at the bottom of the rodlet (TCC1) started to increase as a result of fuel accumulation in the ballooned cladding at this position. To keep the cladding temperature at the balloon below the planned peak temperature of 1200 °C after fuel relocation, the linear power of the electrical heater was reduced from 1.60 to 1.25 kWm^{-1} at t = 168 s.

Since this did not help much, the heater was completely switched off at t = 290 s. The reactor was scrammed at t = 316 s.

Water spraying was started at t = 149 s, but the first spray water just filled the pipeline and did not reach the test rig [25]. The first real water injection occurred during the second water spraying, which took place at t = 175 s. Water was then periodically injected by 0.5 s long spraying pulses every 20 seconds, in order to feed the cladding metal-water reactions. No spray was used after reactor scram.

Fig. 48 presents the recorded internal gas pressure in the upper plenum, rod elongation and the gamma activity in the pipeline to the blowdown tank. From these recordings, it is clear that the cladding ruptured at t = 133 s. It is interesting to note that the evolution of the plenum gas pressure is much different from that observed in the sibling test rod IFA-650.4; confer Fig. 46. Instead of an instantaneous pressure drop after cladding rupture, the plenum pressure decreases slowly towards the external (rig) pressure. This suggests that the axial gas flow between the upper plenum and the cladding breach at the bottom part of the rodlet was restricted.

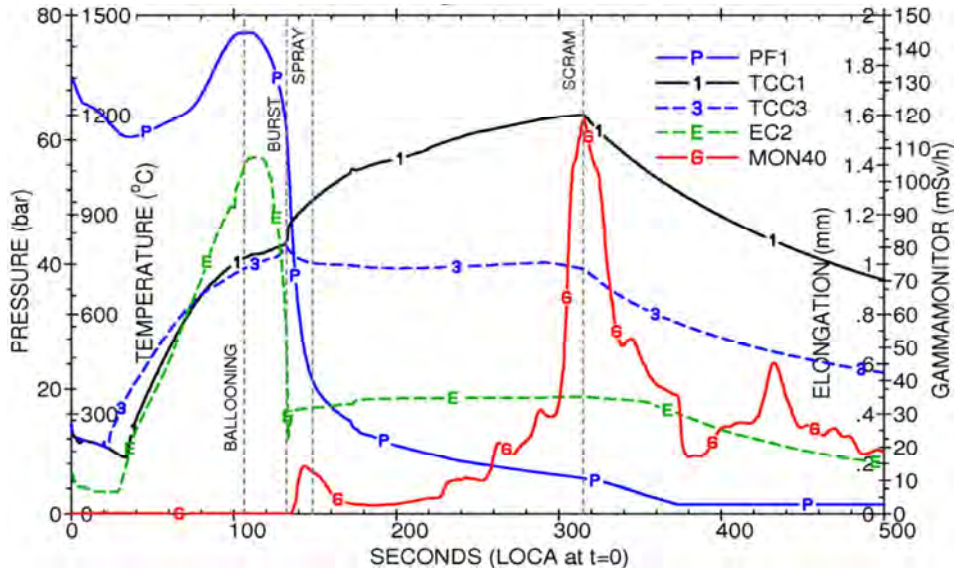

Fig. 48: Measured plenum gas pressure (PF1), rod elongation (EC2), and coolant gamma activity (MON40) during the IFA-650.9 LOCA simulation test [25].

The entire pressure flask was gamma scanned 35–40 days after the test, after which it was sent to the hot cell laboratory for further examinations. These included visual inspection, cladding profilometry, neutron radiography, cladding hydrogen analyses and ceramographic and metallographic examinations. No epoxy was used to stabilize the fuel fragments during transport. From comparisons between the results from gamma scan and neutron radiography, it is obvious that significant relocation of the fuel fragments occurred during transport.

Results from post irradiation investigations of the IFA-650.9 rodlet are presented in [48], and selected data from the investigations are compared with our calculated results in section 4.2.2. A large primary balloon was found at the bottom part of the rodlet, where the rodlet was broken into two pieces by a guillotine-type break. The rodlet also had a secondary, smaller, balloon at its axial midplane. With regard to fuel fragmentation and axial relocation, the gamma scan showed that about 120–130 mm of the fuel pellet column was missing from the upper third of the rodlet, but that a 25 mm long section of the fuel pellet column remained at the very top. The missing fuel had relocated axially to the balloons, and some of it had been expelled through the cladding breach and accumulated at the bottom of the pressure flask. Ceramography revealed extensive fragmentation and pulverization of the fuel. The pulverization had occurred predominantly at the outer third of the pellet radius [48]. The fuel fragment size distribution was not measured.

A.3. IFA-650.10

The tenth experiment in the Halden IFA-650 LOCA test series was done in May 2010 on a test rodlet with an average fuel burnup of 61.0 MWd(kgU)$^{-1}$. The rodlet was re-fabricated from a 17×17 PWR fuel rod that had been pre-irradiated for five reactor cycles with a fairly typical power history; see section 2.1.2.

From Table 2, it is clear that the IFA-650.10 rodlet was tested at moderate power and reached a peak cladding temperature just above 1100 K. Fig. 49 presents temperature measurements from eight different thermocouples, the positions of which are defined in Table 10. In similarity with the IFA-650.4 rodlet, the IFA-650.10 rodlet had a cladding thermocouple attached to the upper gas plenum. Fig. 50 is a close-up, showing the measured temperatures during the spraying phase. Also included in Fig. 50 is the spray sequence: the spraying was done in 0.5 s long pulses every 20 seconds, beginning 12 s after cladding rupture and terminating when the reactor was scrammed.

Table 10: Thermocouple (TC) positions in the IFA-650.10 LOCA simulation test. The axial position z refers to the height above the bottom of the fuel pellet column.

TC	Position and measured property	z [mm]
TCC1	Cladding surface (lower part of active length)	100
TCC2	Cladding surface (upper part of active length)	366
TCC3	Cladding surface (upper part of active length)	366
TCH1	Heater surface (lower part)	100
TCH2	Heater surface (mid position)	200
TPLE	Gas plenum (plenum axial midplane)	675
TIA	Coolant inlet (average signal from two TCs)	-
TOA	Coolant outlet	-

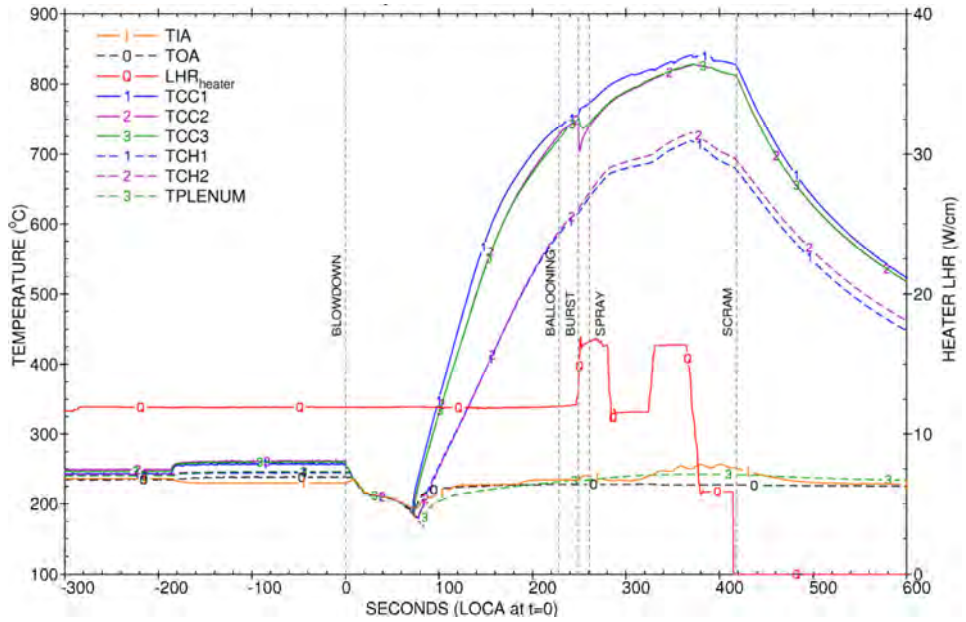

Fig. 49: Measured temperatures during the IFA-650.10 LOCA simulation test [26]. See Table 10 for definition of the thermocouples listed in the legend.

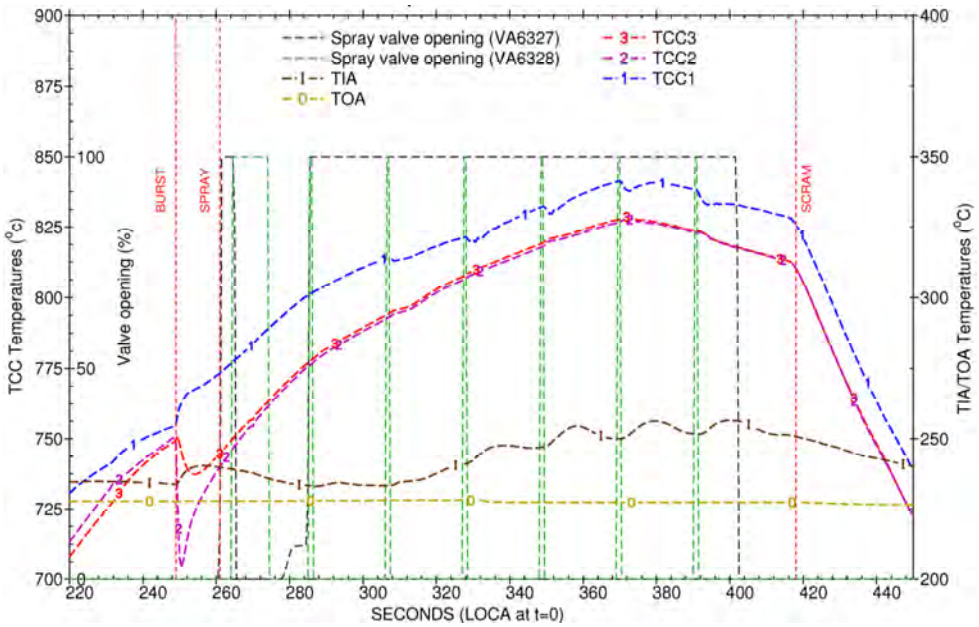

Fig. 50: Measured temperatures during the phase with spraying [26]. See Table 10 for definition of the thermocouples listed in the legend.

A fairly small balloon formed just above the axial midplane of the IFA-650.10 rodlet, and the cladding failed in the ballooned region 249 seconds after start of blowdown. From Fig. 50, it is evident that the cladding temperature in the upper part of the rodlet (TCC2 and TCC3) dropped temporarily just after cladding rup-

ture. This is attributed to cooling from the rod internal gas, which flowed from the relatively cool gas plenum towards the cladding breach. From Fig. 51, it is clear that the gas pressure in the plenum dropped instantaneously after cladding rupture, suggesting that the axial gas flow was unrestricted inside the test rodlet.

Following cladding rupture, water was periodically injected into the test rig by 0.5 s long spraying pulses every 20 seconds, in order to feed the cladding metal-water reactions. No spray was used after reactor scram. The water was sprayed through three nozzles, distributed 120° apart along the cladding circumference about 50 mm above the top of the fuel pellet column; see Fig. 1. It is clear from Fig. 50 that the spraying had no obvious effect on the cladding temperature in the upper part of the rodlet (TCC2 and TCC3). This is strange, since the spraying nozzles were just some 100 mm above the aforementioned thermocouples. On the other hand, the cladding temperature in the bottom part of the rodlet (TCC1) dropped temporarily by a few kelvin for each spraying pulse. This temperature response is expected, as the steam generated by the spray will flow past the thermocouple on its way to the blowdown line at the bottom of the test rig [26].

From Fig. 50, it is also clear that the coolant outlet temperature, which was measured by a thermocouple 356 mm above the electrical heater, remained close to the Halden reactor moderator temperature. The coolant inlet temperature, which was measured by two thermocouples at the bottom of the test rig, was on the other hand affected by the spraying: the temperature was increased by each spray, as superheated steam flowed past the inlet thermocouples on its way to the blowdown tank. The same response was observed for the coolant inlet temperature in Halden IFA-650 test 9, but not in test 4; compare Fig. 45 and Fig. 47.

It should be remarked that the heater power was adjusted to constant values of 1.2, 1.6 and 0.6 kWm^{-1} during the test; see Fig. 49. The power was changed in order to reach the target peak cladding temperature, which was 850 °C (1123 K) for the IFA-650.10 test.

The IFA-650.10 rodlet was gamma scanned less than 10 days after the test, after which it was sent to the hot cell laboratory for further examinations. These included visual inspection, cladding profilometry, neutron radiography, cladding hydrogen analyses and ceramographic and metallographic examinations. No epoxy was used to stabilize the fuel fragments during transport.

Results from post irradiation investigations of the IFA-650.10 rodlet are presented in [49], and selected data from the investigations are compared with our calculated results in section 4.2.3. In summary, the rodlet was bent after the test, but the cladding distension was small. A cladding breach was found just above the axial midplane of the rodlet, where a small balloon had formed. A slight quantity of dispersed fuel material was found at the bottom of the test rig.

The gamma scan showed no evidence of long range axial fuel relocation. Neutron radiography revealed that some fuel was missing from the upper part of the balloon, which confirms that axial fuel relocation into the balloon from higher elevations did not occur in this test. Fuel fragmentation into a mixture of large and small fragments was observed in the central part of the rodlet, but not towards the ends [49]. The fuel fragment size distribution was not measured.

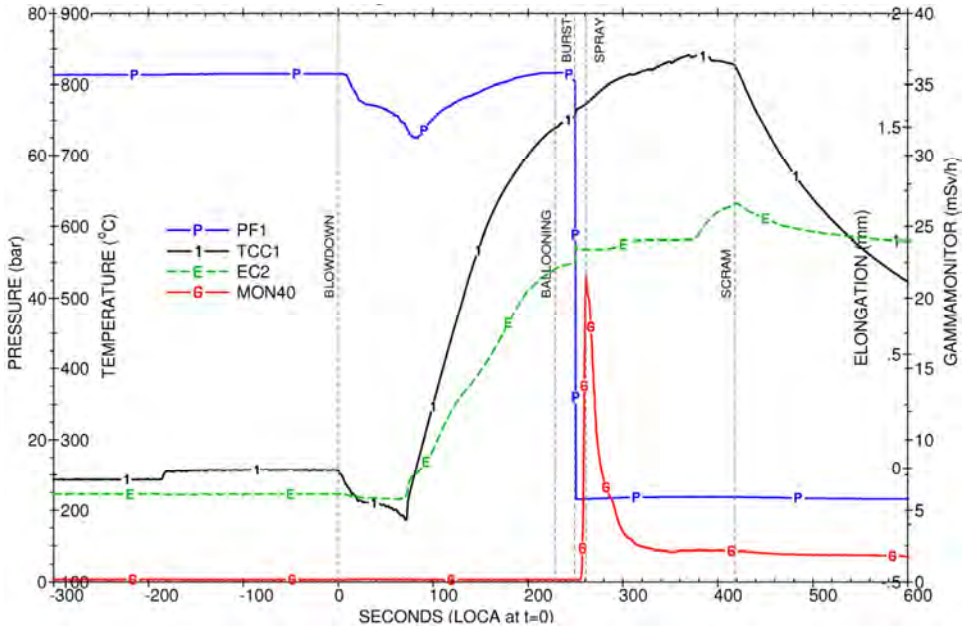

Fig. 51: Measured plenum gas pressure (PF1), rod elongation (EC2), and coolant gamma activity (MON40) during the IFA-650.10 LOCA simulation test [26].

A.4. IFA-650.14

The Halden IFA-650.14 LOCA test was done in October 2013 on a test rodlet with an average fuel burnup of 70.8 MWd(kgU)$^{-1}$. The rodlet was re-fabricated from a BWR fuel rod of Westinghouse SVEA-96 design that had been pre-irradiated for seven reactor cycles in the Leibstadt reactor, Switzerland. The linear heat generation rate for the sampled segment was around 10 kWm^{-1} during the last three cycles; see Fig. 3.

The properties of the sampled fuel rod segment (AEB072-J9-J) are well documented [29, 30]. It should be remarked that the sampled segment coincided with the fourth spacer grid in the fuel assembly [29]. The spacer grid position corresponds to the span from 220 to 245 mm along the active length of the IFA-650.14 rodlet after refabrication. In addition to the unconventional sampling, the IFA-650.14 rodlet differed from other rodlets in this report also by having a lower fill gas pressure and a much smaller fission gas plenum; see Table 1. The plenum was made small to better control the ballooning of the cladding tube and to make it possible to terminate the test before cladding rupture.

The IFA-650.14 rodlet was tested at low power, and fairly low cladding temperatures were reached during the test; see Table 2. The intention was to interrupt the ballooning process before cladding rupture occurred, with the aim to investigate if axial fuel relocation occurs before cladding rupture or as a consequence of the axial pressure gradient induced by the rupture. Fig. 52 presents temperature measurements from six different thermocouples, the positions of which are defined in Table 11. There were two additional thermocouples, but they were identified as faulty [28]. No water spraying was used in the IFA-650.14 LOCA test.

Table 11: Thermocouple (TC) positions in the IFA-650.14 LOCA simulation test. The axial position z refers to the height above the bottom of the fuel pellet column.

TC	Position and measured property	z [mm]
TCC1	Cladding surface (lower part of active length)	100
TCC2	Cladding surface (upper part of active length)	300
TCH1	Heater surface (lower part)	100
TCH2	Heater surface (mid position)	200
TIA	Coolant inlet (average signal from two TCs)	-
TOA	Coolant outlet	-

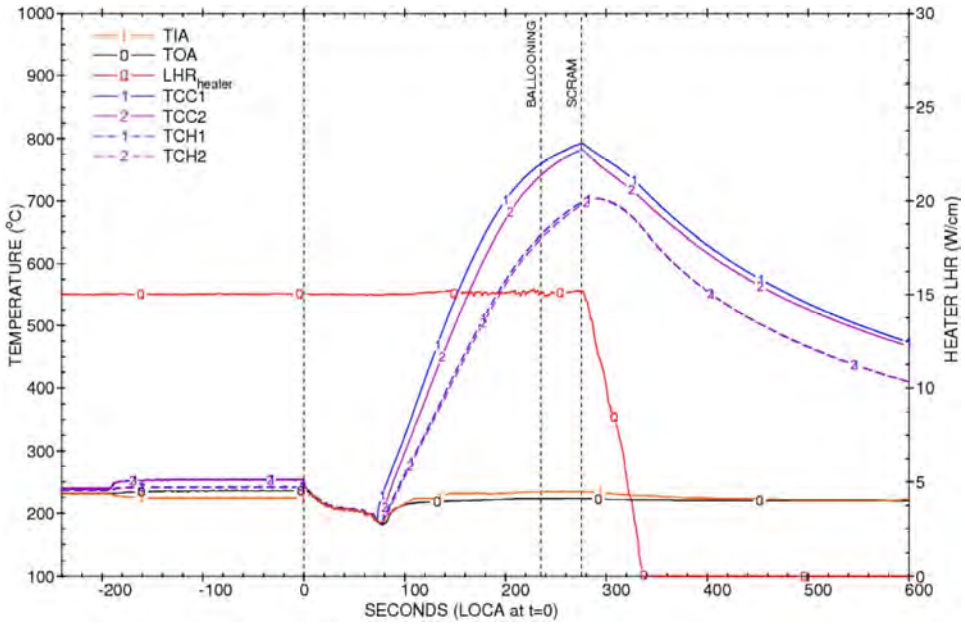

Fig. 52: Measured temperatures during the IFA-650.14 LOCA simulation test [28]. See Table 11 for definition of the thermocouples listed in the legend.

From Fig. 52, it is clear that both the cladding and the heater temperatures were fairly uniform throughout the test. Notwithstanding the uniform temperatures, a primary balloon formed just above the axial midplane of the rodlet, and two

smaller balloons formed just above this position. The cladding distension minima between the balloons coincide with the position of the fourth spacer grid in the mother fuel assembly [41].

The measured evolution of the plenum gas pressure is shown in Fig. 53. The increase in rod free volume caused by cladding distension during the test had a large impact on the gas pressure, since the plenum volume was made exceptionally small in the IFA-650.14 test rodlet. The plenum pressure reached a peak value of 7.16 MPa at t = 235 s, after which it started to decrease as a result of cladding distension. The reactor was scrammed and the electrical heater was switched off at t = 275 s. The plenum gas pressure had then dropped to 74 % of its peak value, and it continued to drop as the rodlet was slowly cooled; see Fig. 53. The cladding tube did not fail during the test [28].

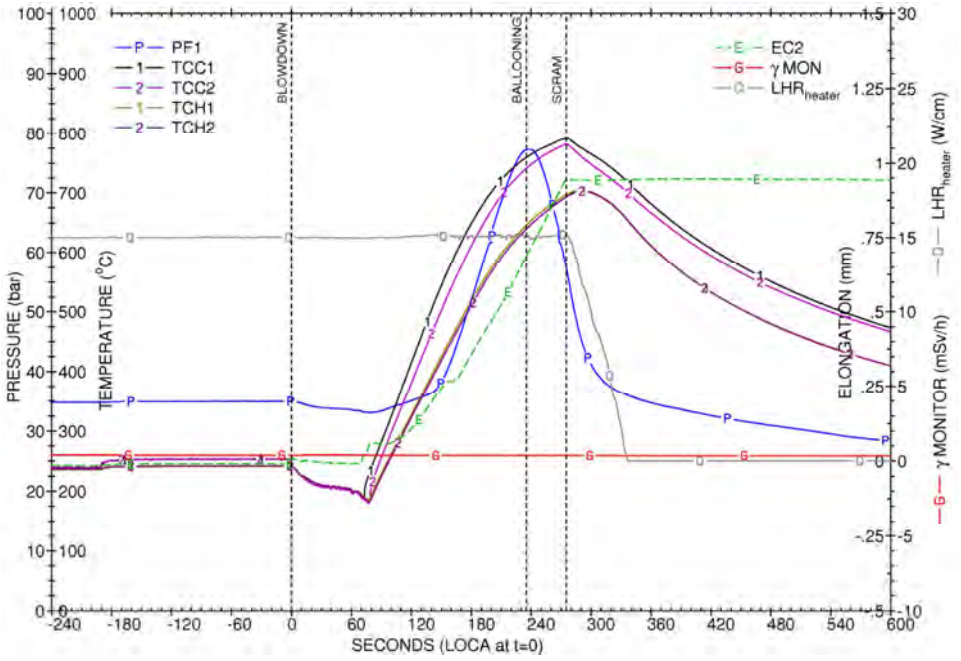

Fig. 53: Measured plenum gas pressure (PF1), rod elongation (EC2), and coolant gamma activity (MON40) during the IFA-650.14 LOCA simulation test [28].

The IFA-650.14 rodlet was gamma scanned about 20 days after the test, and then sent to the hot cell laboratory for further examinations. These included visual inspection, cladding profilometry, neutron radiography and metallographic examinations. In addition, the rodlet was punctured for gas analyses and the fuel fragment size distribution was determined by sifting [41]. Selected data from the investigations are compared with our calculated results in section 4.2.4.

The gamma scan and neutron radiography showed that axial fuel relocation had occurred, and that about 10 mm of the fuel pellet column was missing from the upper part of the rodlet. However, similar to the IFA-650.9 rodlet, a 35 mm long section (“plug”) of the fuel pellet column remained at the very top [41].

The gas analysis revealed that the amount of gas in the rod free volume had increased from 1.56×10^{-3} to 4.72×10^{-3} mole during the test, as a result of transient fission gas release from the fuel. The transient fission gas release fraction was estimated to 18 % [41].

The rodlet was defueled by cutting it near the ballooned region and at the ends of the fuel stack. The two parts were then shaken to dislodge the fragmented fuel. About 75 % of the fuel mass could be collected for sifting in this way, but the more or less intact fuel pellets in the upper end of the fuel column remained in the cladding tube. The fuel fragment size distribution was determined by sifting the collected fuel fragments through a standard system of six sieves with decreasing grit size (4.0–0.125 mm). Only 0.6 weight% of the collected fragments were found to be smaller than 0.25 mm [41].

Appendix B:
The NRC-Studsvik LOCA test 192

The NRC-Studsvik LOCA simulation test number 192 was conducted in February 2011 on a PWR-type test rodlet with an estimated rod average burnup of 78 $MWd(kgU)^{-1}$. The rodlet had a 300 mm long active part, which was sampled from the middle section of a full-length mother fuel rod that had been operated for four reactor cycles in a twin-unit power plant, USA. The design and pre-test conditions of the rodlet are given in Table 3, and the pre-irradiation history in the two PWR units is shown in Fig. 5.

The test was initiated by heating the rodlet to a nominal temperature of 573 K and maintaining this temperature for about 15 minutes to achieve thermal equilibrium. During this hold time, the rod internal pressure was also adjusted to 8.2 MPa by gas supply through the upper pressure line; see Fig. 4. This gas line was closed when the desired gas pressure was reached, and remained closed during the test. The rodlet was surrounded by flowing steam at atmospheric pressure. The upward mass flow of steam through the quartz tube was 1.8×10^{-4} kgs^{-1}.

The furnace power was increased, such that a constant heating rate of 5 Ks^{-1} was maintained from 573 K to the target peak cladding temperature of 1433 K. The cladding was held at this target temperature for five seconds, after which the temperature was decreased to 1073 K at a rate of -3 Ks^{-1}. The rodlet was then quenched by rapidly filling the quartz tube with room temperature water. The measured histories of cladding temperature and rod internal gas pressure are shown in Fig. 54. It should be remarked that the true peak cladding temperature is higher than the maximum temperature recorded by the thermocouple, which is attached 50 mm above the axial midplane of the test rodlet in order not to affect cladding ballooning and burst. The true peak cladding temperature for test 192 is estimated to be 1446 K, based on the analysis presented in Appendix D.

The internal pressure measurements suggest that the cladding failed 81 s after the heating started. The cladding temperature at time of failure was 981 K (estimated true peak value; the measured thermocouple value was 974 K) and the rod internal pressure was around 8.1 MPa. As shown in Fig. 54, the depressurization of the failed rodlet was fairly slow. More precisely, the upper pressure gauge recorded a 50 % reduction in pressure (relative to 8.1 MPa) after 13 s, and the corresponding time for the lower pressure gauge was 15 s [3, 35].

The test rodlet ballooned slightly above its axial midplane. The rupture opening was 9.0 mm wide and 22.7 mm long, and 68 g of fuel was lost during the LOCA simulation test. This corresponds to about 42 % of the total fuel inventory. An additional 16 g of fuel mass was released during the subsequent bend test and

shaking of the broken rod. The measured size distribution of all recoverable fuel fragments (71.4 g) from the rodlet is presented in Table 12. It is clear that much of the fuel had pulverized into fuel fragments smaller than 0.25 mm. Results from post-test cladding profilometry are presented together with calculated results in section 4.3 of the report.

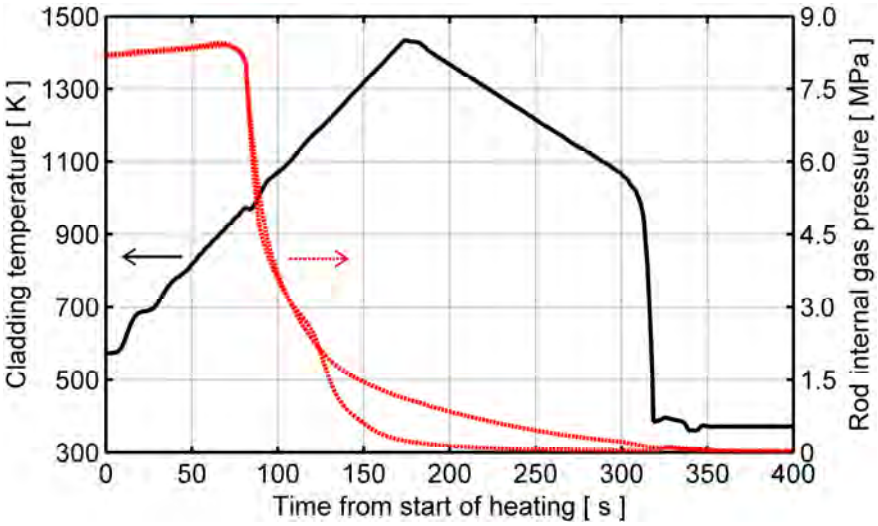

Fig. 54: Measured cladding temperature (solid black line) and rod internal pressure (dashed red lines) during the NRC-Studsvik LOCA test 192 [35]. Gas pressure data from both the upper and lower pressure transducer are shown.

Table 12: Size distribution of fuel fragments recovered from the NRC-Studsvik-192 test rodlet after simulated LOCA test, bend test and shaking to dislodge fuel fragments [3].

Fragment size class [mm]:	**Fuel mass [g]:**	**% of total mass:**
< 0.125	22.6	31.7
0.125 – 0.250	8.0	11.2
0.250 – 0.500	9.1	12.7
0.500 – 1.000	10.2	14.3
1.000 – 2.000	13.3	18.6
2.000 – 4.000	8.2	11.5
> 4.000	0.0	0.0
Total	71.4	100.0

Appendix C: Thermal-hydraulic boundary conditions for Halden IFA-650 LOCA tests

C.1. Heat transfer modes observed in the tests

With regard to clad-to-coolant heat transfer, each test in the Halden IFA-650 series can be divided into three consecutive phases. These phases are easily identified from the measured difference in temperature between the cladding tube and heater surfaces, as exemplified by Fig. 55. The three phases are:

1. Initial phase with steady-state heat transfer and cooling by natural circulation of liquid water at approximately 7 MPa and 520 K. The water flows up between the fuel rodlet and the surrounding heater, and down between the heater and the wall of the pressure flask; see Fig. 1. Since the heater is cooled from both sides, it has a slightly lower surface temperature than the fuel rodlet, as shown in Fig. 55. The cooling is fairly efficient, and the rodlet/heater surface temperatures are only slightly higher than the coolant temperature, since the rodlet/heater power levels are low.
2. Blow-down phase with rapidly decreasing pressure and outflow of coolant from the pressure flask. Both the fuel rodlet and the heater are efficiently cooled by the rapid flow, and the temperature difference between the cladding and heater surfaces are negligible, as shown in Fig. 55. The surface temperatures are in fact very close to the saturation temperature of the coolant as it flashes to steam. The saturation temperature, and hence the surface temperatures, can be calculated directly from the measured pressure evolution in the test rig. Most of the IFA-650 tests have been done by evacuating the test rig through blowdown lines from the bottom part of the pressure flask (referred to as one-sided blowdown in Halden test reports), but some tests, for example IFA-650.9, have been done by evacuating the test rig at both ends (two-sided blowdown). This leads to a much shorter blowdown phase; the typical duration is 60–80 s for one-sided blowdown and 25–35 s for two-sided blowdown. The end of the blowdown phase is easily identified by the sudden increase in cladding and heater surface temperature. Also the temperature difference between the cladding and heater increases rapidly at end of the blowdown phase, as shown in Fig. 55.
3. “Dry” phase with superheated steam in the gap between the fuel rod and the heater. The steam is at nearly stagnant conditions, and much of the heat removal from the test rodlet is by radiation to the surrounding heater. In most tests, small amounts of water are periodically sprayed into the rig to maintain a sufficient amount of steam for cladding oxidation during this phase. The influence of spraying on measured cladding, heater and coolant temperatures is

reported to be weak [26], but no quantitative information on this issue is provided. As remarked in section A.3, Appendix A, the spraying obviously leads to downward axial flow of steam through the heated section, which should provide some cooling. When the reactor is scrammed and the electrical heater is switched off, temperatures start to decrease. Since spraying is not used after reactor scram, the cooling rate is fairly low.

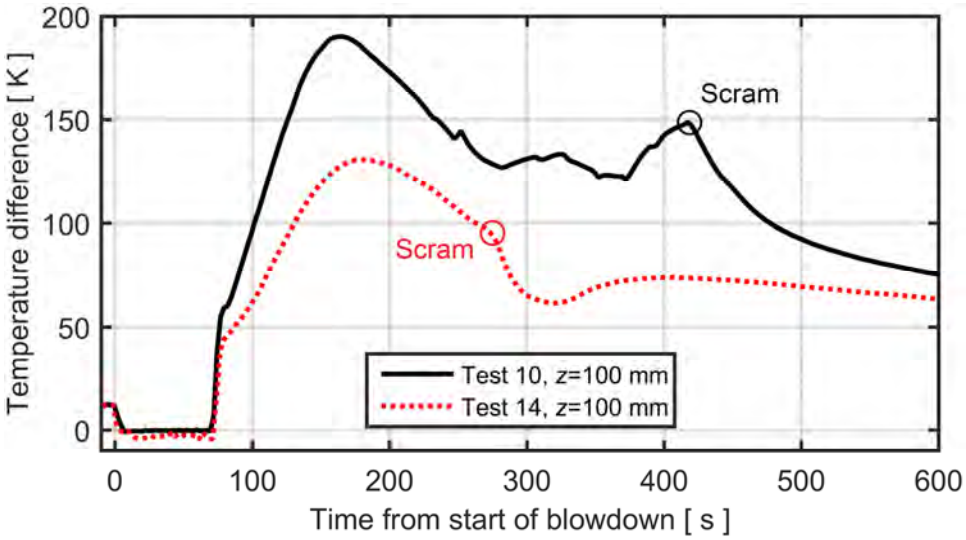

Fig. 55: Measured temperature difference between cladding and heater surfaces versus time for lower part of the fuel rodlets in Halden IFA-650 tests 10 and 14. A circle indicates the time of reactor scram, leading to a sudden drop in fuel rod heat generation.

C.2. Modelling of thermal-hydraulic boundary conditions

All analyses with our extended version of FRAPTRAN-1.5 in this report were done using the 'heat' option for the fuel rod thermal-hydraulic boundary conditions [18]. With this option, the boundary conditions must be supplied as input to FRAPTRAN in the form of time histories for coolant pressure, coolant bulk temperature and clad-to-coolant heat transfer coefficient. The coolant pressure is supposed to be uniform, while the coolant bulk temperature and clad-to-coolant heat transfer coefficient may, if needed, be defined with axial variations along the fuel rod. In practice, the latter is done by defining independent time histories for a sufficient number of axial segments along the coolant channel [18]. The 'heat' option is intended primarily to facilitate the use of FRAPTRAN for thermal-mechanical fuel rod calculations in a post-processing step to analyses with thermal-hydraulic system codes, such as RELAP, TRACE, CATHARE and ATHLET [69]. The system code then provides the required time histories as input to FRAPTRAN.

In our analyses of the Halden IFA-650 LOCA tests, the thermal-hydraulic boundary conditions were derived from temperatures and pressures measured in different parts of the test rig. More precisely, the coolant pressure history used in our

analyses with FRAPTRAN was for each test taken as the average of the measured inlet and outlet rig pressures. Time histories for the coolant bulk temperature at specific axial positions were taken as the measured *heater* temperatures at these positions. This means that the water/steam between the fuel rodlet and the heater was considered as a medium for heat transport, but not as a heat sink. The approach is believed to be justified for the conditions during the dry phase of the test, when the gap between the rodlet and the heater is filled with stagnant and superheated steam.

The heat transfer coefficient supplied as thermal-hydraulic boundary conditions to FRAPTRAN for the dry (post-blowdown) phase of the test thus refers to the clad-to-heater heat transfer. This heat transfer is in our analyses assumed to be dominated by steam conduction and convection at low temperature and by radiation at high temperature. More precisely, the clad-to-heater heat transfer coefficient is assumed to have the form

$$h(z,t) \;=\; h_{cc}(z) \;+\; h_r(z,t)\ , \tag{2}$$

where h_{cc} is the contribution from conduction and convection, and h_r is the contribution from radiation. The latter follows from Stefan-Boltzmann's law [70], and can be written

$$h_r \;=\; \varepsilon\sigma\left(T_c^2 + T_h^2\right)\left(T_c + T_h\right)\ . \tag{3}$$

Here, T_c and T_h are the surface temperatures of the cladding and heater, respectively, σ is the Stefan-Boltzmann constant (5.6704×10^{-8} $Wm^{-2}K^{-4}$), and ε is an effective surface emissivity. It is given by

$$\varepsilon \;=\; \varepsilon_c\varepsilon_h R_h\left(\varepsilon_c R_c + \varepsilon_h R_h - \varepsilon_c\varepsilon_h R_c\right)^{-1}\ , \tag{4}$$

where ε_c and ε_h are the surface emissivities of the cladding and heater, respectively, and R_c and R_h are the radii of the two cylindrical surfaces.

From eq. (3), it is clear that the radiative heat transfer coefficient depends on the cladding surface temperature, which is an unknown variable in the computational analyses. This problem can be overcome in different ways, e.g. by use of iterative procedures or by using past time step values in the computations. In the work presented here, we make the simplifying approximation $T_c \approx T_h$, which inserted into eq. (3) results in

$$h_r \;\approx\; 4\varepsilon\sigma T_h^3 \tag{5}$$

for the contribution from radiative heat transfer, and

$$h(z,t) \;\approx\; h_{cc}(z) \;+\; 4\varepsilon\sigma T_h^3(z,t) \tag{6}$$

for the total heat transfer coefficient in eq. (2). The approximation $T_c \approx T_h$ is justified by the fact that the cladding temperature is usually no more than 150 K higher than the heater temperature in the considered IFA-650 tests; see Fig. 55 and Appendix A. The approximation may lead to an underestimation of the radia-

tive heat transfer, but this is in our analyses compensated for by using fairly high values for the effective surface emissivity in eq. (6). The typical surface emissivity of oxidized zirconium alloy cladding (ε_c) is reported to be about 0.6 [71]. In our analyses of the IFA-650 tests, we used $\varepsilon = 0.60$ for the BWR rodlet (test 14) and $\varepsilon = 0.75$ for the PWR fuel rodlets (tests 4, 9 and 10). These values were found empirically, such that a good match was obtained between calculated and measured cladding surface temperatures.

Also the heat transfer contribution from conduction and convection, i.e. parameter h_{cc} in eq. (6), was empirically fitted so that the calculated evolution of cladding surface temperature matched the measured one. The best-estimate values for h_{cc} ranged from 25 to 100 W(m^{2}K)$^{-1}$. Different values for h_{cc} were used for each test, and when appropriate, different values were also used for the lower, middle and upper part of the rodlet in some tests. More precisely, in our analyses with FRAPTRAN, the coolant channel was divided into three axial segments (lower, middle and upper). For each of these three segments, the evolution of the clad-to-heater heat transfer coefficient was calculated through eq. (6), using values for h_{cc} and measured temperature histories from the heater thermocouples defined in Table 13. It should be remarked that we used eq. (6) only for the dry phase of the test: For the initial, pre-blowdown phase, we used a constant clad-to-heater heat transfer coefficient of 4.7 kW(m^{2}K)$^{-1}$, and for the blowdown phase, we used a constant value of 20 kW(m^{2}K)$^{-1}$. These values were used for all tests and for all axial positions of the test rodlets. Examples of the estimated evolution of h are shown in Fig. 56.

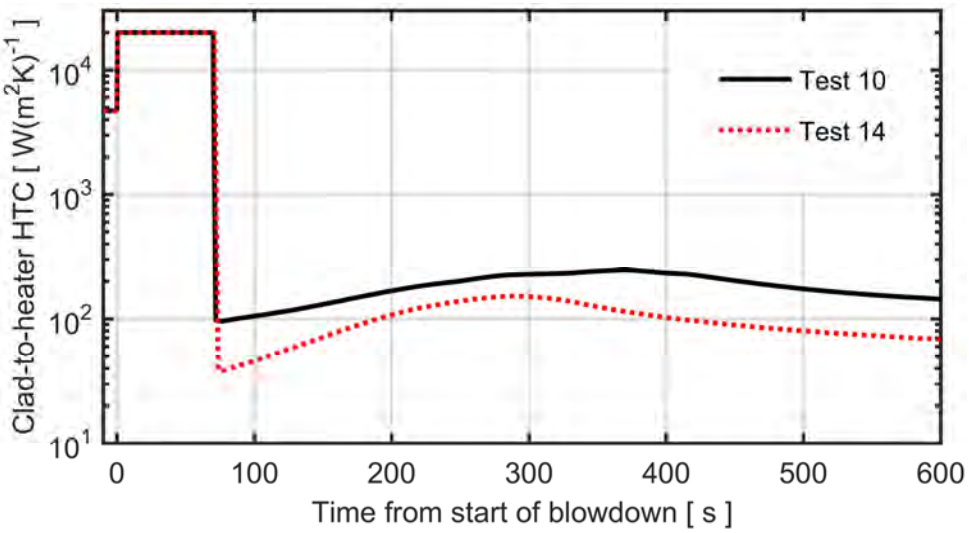

Fig. 56: Estimated clad-to-heater heat transfer coefficients for the lower part of the rodlet in Halden IFA-650 tests 10 and 14; see also Fig. 55 and Table 13.

Table 13: Heater thermocouple data used for definition of coolant bulk temperature and clad-to-coolant heat transfer coefficients in analyses of the IFA-650 tests. Values applied for the fitting constants ε and h_{cc} in eq. (6) are also given.

Parameter:		650.4	650.9	650.10	650.14
Effective emissivity, ε	[-]	0.75	0.75	0.75	0.60
Upper part of the rod:					
Heater thermocouple ID	[-]	TCH2	TCH3	TCH1	TCH2
Thermocouple elevation	[mm]	380	380	100	200
Best-estimate h_{cc}	[$W(m^2K)^{-1}$]	50	70	100	40
Middle part of the rod:					
Heater thermocouple ID	[-]	TCH1	TCH2	TCH2	TCH2
Thermocouple elevation	[mm]	205	200	200	200
Best-estimate h_{cc}	[$W(m^2K)^{-1}$]	75	50	50	30
Lower part of the rod:					
Heater thermocouple ID	[-]	TCH1	TCH1	TCH1	TCH1
Thermocouple elevation	[mm]	205	100	100	100
Best-estimate h_{cc}	[$W(m^2K)^{-1}$]	75	30	80	25

Finally, it should be remarked that we have used h_{cc} in eq. (6) as a constant fitting parameter that controls the clad-to-heater heat transfer at low temperature. In reality, however, h_{cc} is expected to change over time. This can be understood by partitioning h_{cc} into contributions from convection (h_{cv}) and conduction (h_{cd})

$$h_{cc} = h_{cv} + h_{cd} = h_{cv} + \lambda_s / w_g \,, \qquad (7)$$

where λ_s is the thermal conductivity of the superheated steam and w_g is the width of the gap between the rodlet and the heater. At a pressure of 0.3 MPa, which is the typical rig pressure during the dry phase of the Halden IFA-650 tests, λ_s increases from about 0.05 to 0.10 $W(mK)^{-1}$ as the steam temperature goes from 700 to 1100 K. The initial gap between the rodlet and the heater is about 5 mm wide, which means that h_{cd} in eq. (7) increases from less than 10 to 20 $W(m^2K)^{-1}$ during a test by the heating alone. It increases even more as the rodlet balloons and the gap between the rodlet and the heater closes. However, at high temperature, h_{cc} and h_{cd} are much smaller than h_r, which means that the variation is of little practical significance; confer Fig. 56.

Appendix D:
Boundary conditions for the NRC-Studsvik LOCA test 192

D.1. Axial variation of cladding temperature

The NRC-Studsvik LOCA simulation tests were carried out with external heating, using an infrared clamshell furnace that surrounded the test section. As explained in section 2.2.1, the power supplied to the furnace was controlled to produce a pre-determined temperature history for the cladding tube in the central part of the rodlet. A single thermocouple, attached to the rodlet by a metal clamp about 50 mm above its axial midplane, was used to control the furnace.

The heated section of the furnace was only 267 mm long [72], and commissioning tests on un-irradiated rodlets that were equipped with several thermocouples along their active length showed that there were significant axial gradients in cladding temperature towards the ends of the rodlet, and post-test measurements of the cladding oxide layer thickness corroborated this conclusion [32]. The temperature difference between the midplane and the ends of the rodlet increases in proportion to the rod average temperature: Before the furnace is switched on, when the rodlet is heated by the flowing steam alone, the cladding temperature is uniform and equal to 373 K. When the furnace operates at high power, the flowing steam is superheated, which means that the cladding temperature distribution is slightly skewed towards the upper end of the rodlet. The axial peak position is reported to be about 10–20 mm above the axial midplane [32].

An evaluation of the axial temperature distribution and some recommendations for modelling it are given in [72], but here, we will take a different approach. Based on the data presented in [32], we assume that the axial variation in cladding temperature can be written

$$T_c(z) \;=\; T_{cp} \;+\; \Delta T_c(z, T_{cp}), \tag{8}$$

where T_{cp} is the axial peak temperature and ΔT_c is a correction term that defines the temperature drop towards the ends of the rodlet. More precisely, we use the relation

$$\Delta T_c(z, T_{cp}) \;=\; \frac{(T_{cp} - 373)}{1100}\left(0.1\,(z - 0.16) \;-\; 0.01\,(z - 0.16)^2 \right), \tag{9}$$

where z (m) is the axial position with regard to the bottom end of the fuel pellet column. Equation (10) is an empirical fit to the data presented in [32]. It is plotted in Fig. 57 for four different values of T_{cp} in the range from 573 to 1473 K.

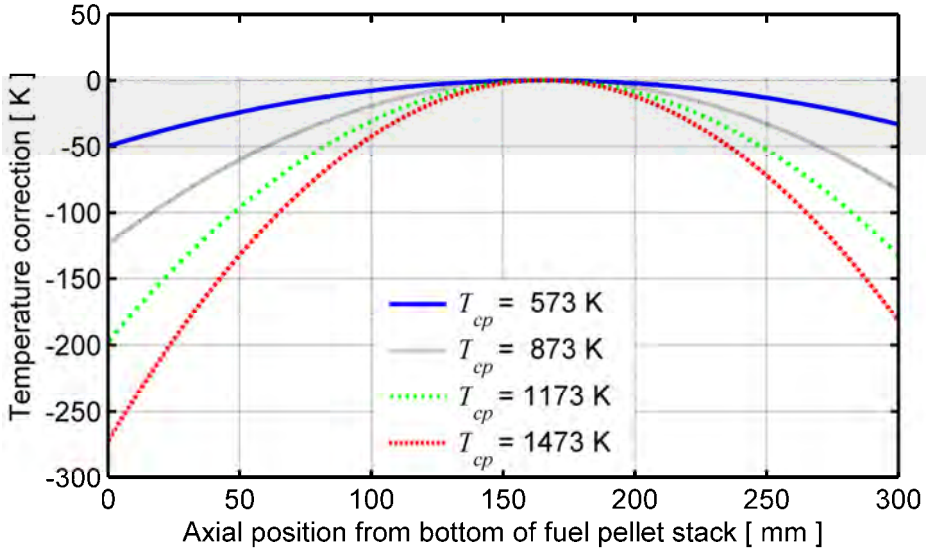

Fig. 57: Temperature correction defined by eq. (11).

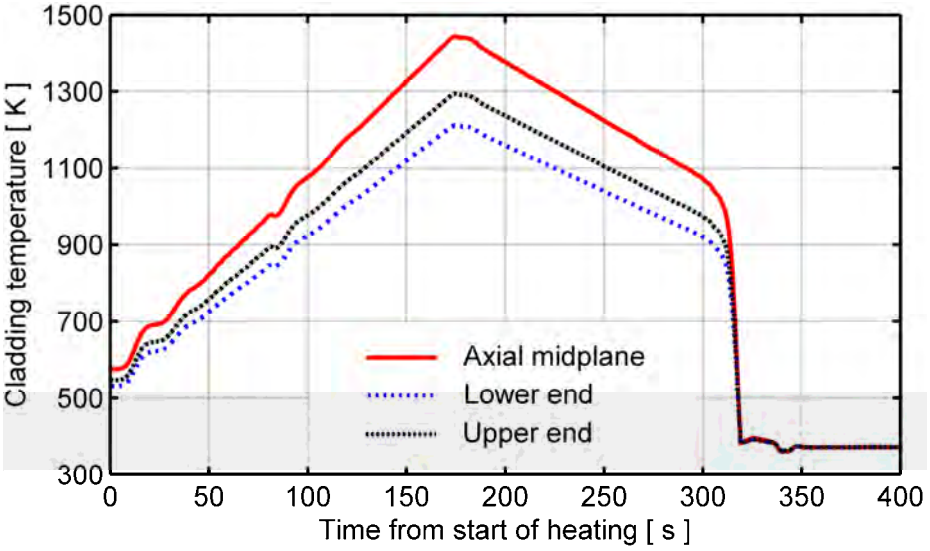

Fig. 58: Time histories for the cladding outer surface temperature at three axial positions of the rodlet, based on measured thermocouple data and the assumed axial temperature distribution defined by eq. (12).

It is clear from Fig. 57 that the temperature correction is close to zero at z = 165 mm, which is assumed to be the axial position where the peak cladding temperature, T_{cp}, is reached. The temperature drop is more significant towards the lower end (z = 0) than towards the upper end (z = 300 mm) of the rodlet. Hence, the temperature correction in eq. (13) reproduces the most important characteristics of the test rig [32], but it does not account for the observation that the axial temperature gradient is steeper during heating than under stationary temperature conditions [72]. Time histories for the cladding outer surface temperature at three dif-

ferent axial positions of the rodlet, based on the measured thermocouple data and the assumed axial temperature distribution, are shown in Fig. 58.

D.2. Gas temperature in the rodlet and connected systems

As already mentioned in section 2.2.1, the NRC-Studsvik LOCA test rodlets were connected to pressure transducers at both ends; see Fig. 4. The transducers were located outside the test section, and connected to the rodlet by pressure lines with fairly large volume; see Table 14. The gas within these pressure lines is fairly close to room temperature; some heating is expected from the nearby furnace and steam generator; see Fig. 4.

Table 14: Gas volumes and assumed gas temperatures for the NRC-Studsvik-192 LOCA test rodlet [72]. Here, $T_c(t,z=0.0)$ and $T_c(t,z=0.3)$ denote the cladding temperature at the lower and upper ends of the rodlet's active part.

Gas cavity:	Volume [cm^3]:	Temperature [K]:
Upper pressure line	6.27	298
Upper adapter	1.81	373
Upper end plug	0.49	$T_c(\,t,\,z=0.3\,)$
Rodlet upper gas plenum	1.00	$T_c(\,t,\,z=0.3\,)$
Lower end plug	0.49	$T_c(\,t,\,z=0.0\,)$
Lower adapter	1.68	373
Lower pressure line	0.84	298
Total	12.58	$T_{eg}(\,t\,)$; see below.

Since the FRAPTRAN-1.5 computer program does not have the capability to model all the partial volumes listed in Table 14, we consider a single gas plenum, having a volume of 12.58 cm^3 and an equivalent gas temperature defined by

$$T_{eg}(t) \;=\; V_{Tot} \Big/ \sum_{i=1}^{7} \frac{V_i}{T_i(t)} \,. \qquad (14)$$

Here, V_{Tot} = 12.58 cm^3 is the total gas volume, while V_i and T_i are the seven partial gas volumes and temperatures listed in Table 14. Equation (15) follows from the assumption of a uniform gas pressure within the rodlet and the connected pressure lines. From Fig. 54 in Appendix B, it follows that this assumption is reasonable up to t = 125 s. The equivalent gas temperature, T_{eg}, is plotted versus time in Fig. 59. It is clear that the temperature variation caused by the time dependent temperature of the gas within the fuel rod plenum and end plugs is moderate. In our calculations with FRAPTRAN-QT-1.5, T_{eg} is used as input for the plenum gas temperature; see section 3.3.

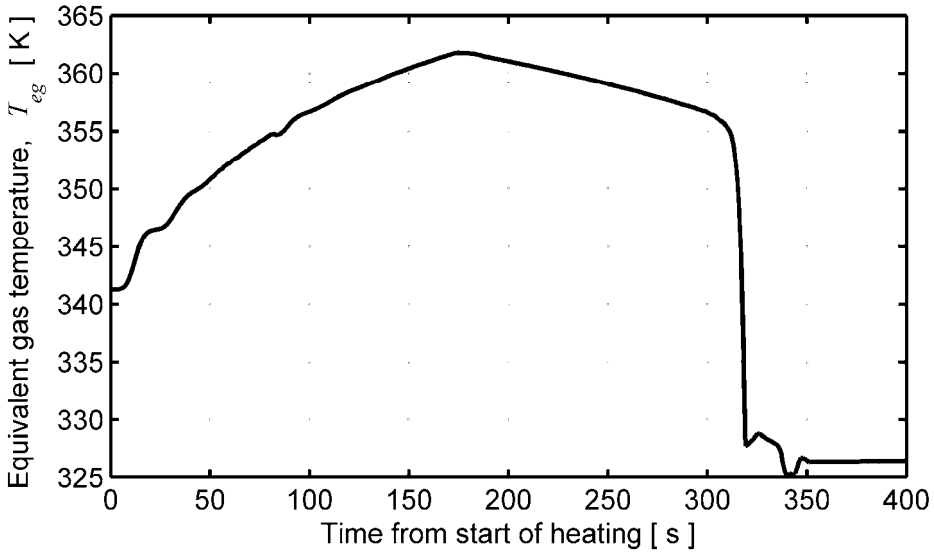

Fig. 59: Equivalent temperature of the total internal gas inventory of the NRC-Studsvik-192 LOCA test rodlet; see eq. (16).

2017:12

The Swedish Radiation Safety Authority has a comprehensive responsibility to ensure that society is safe from the effects of radiation. The Authority works to achieve radiation safety in a number of areas: nuclear power, medical care as well as commercial products and services. The Authority also works to achieve protection from natural radiation and to increase the level of radiation safety internationally.

The Swedish Radiation Safety Authority works proactively and preventively to protect people and the environment from the harmful effects of radiation, now and in the future. The Authority issues regulations and supervises compliance, while also supporting research, providing training and information, and issuing advice. Often, activities involving radiation require licences issued by the Authority. The Swedish Radiation Safety Authority maintains emergency preparedness around the clock with the aim of limiting the aftermath of radiation accidents and the unintentional spreading of radioactive substances. The Authority participates in international co-operation in order to promote radiation safety and finances projects aiming to raise the level of radiation safety in certain Eastern European countries.

The Authority reports to the Ministry of the Environment and has around 300 employees with competencies in the fields of engineering, natural and behavioural sciences, law, economics and communications. We have received quality, environmental and working environment certification.

Strålsäkerhetsmyndigheten
Swedish Radiation Safety Authority

SE-171 16 Stockholm
Solna strandväg 96

Tel: +46 8 799 40 00
Fax: +46 8 799 40 10

E-mail: registrator@ssm.se
Web: stralsakerhetsmyndigheten.se

Arkitektkopia AB, Bromma, 2017